UNIVERSITY OF WOLLONGONG AUSTRALIA

DISTRIBUTION OF LIPIDS IN THE HUMAN LENS AND THE AFFECT OF AGEING

Jo Ann Seng

Supervisors:

Assoc. Prof. Todd W. Mitchell

Dr. Jessica R. Nealon

Prof. Stephen J. Blanksby

This thesis is presented as part of the requirement for the conferral of the degree:

Doctor of Philosophy

The University of Wollongong

School of Chemistry

August 2018

Abstract

The lens is a transparent, biconvex structure located between the iris and the vitreous humour. It is bathed by aqueous humour anterior to the lens, which plays a role in nutrient transport into the lens as it is avascular. The outermost layer of the lens consists of a single layer of epithelial cells. These cells elongate and differentiate into lenticular fibres which are laid down in concentric layers to form the mass of the lens. Mature fibre cells lose all their organelles to maintain lens transparency, thus there is no lipid or protein turnover in the lens nucleus. The lens is first formed *in utero* and continues to grow throughout a human's lifespan. The lens formed before birth is referred to as the lens core, where the cells that were laid down immediately after birth (infantile nucleus) are referred to as the inner region. Tissue formed during childhood years make up the first layers of lens cortex outside the nucleus, while cells laid down after middle age are referred to as the outer region. The formation of the barrier between the inner cortex and nucleus at middle age reduces the diffusion of antioxidants and water into the nucleus, as a consequence of the occlusion of membrane pores. Alterations to the membrane lipid composition has the ability to alter the water permeability of aquaporin-0 and also render the membrane more adhesive to α-crystallins, which may reduce water permeability and also cause greater pore occlusion. As a consequence, the lens is more susceptible to protein precipitation and oxidation, leading to age-related nuclear cataract. Experimental evidence suggests that the lipid profile of the lens core changes dramatically around the age of 40, coinciding with the formation of the barrier region. It has been observed that lens sphingomyelin and dihydrosphingomyelin form an annular distribution within the barrier region in an adult lens, while ceramide and dihydroceramide levels that were negligible in the core of young lenses have a sharp increase in abundance after the age of 40. These studies indicate that the change in lipid profile may be related the barrier formation with middle age.

In this thesis, methods to optimise mass spectrometric imaging of human lens tissue were developed. It was found that sublimation of matrix was the fastest way to apply a layer of homogenous matrix that was optimal for matrix-assisted laser desorption ionisation (MALDI) imaging. Sublimation conditions were fined tuned for 2-Mercaptobenzothiazole to be used as the matrix in positive ion mode and 2,5-diaminonapthalene to be used as the matrix in negative ion mode.

Following the development of MALDI imaging of human lenses, the distribution of lens lipids was investigated. Many recently identified sphingolipids and also complex glycosphingolipids were mapped for the first time in the adult human lens. It was observed that certain sphingolipids only localise in certain regions of the lens. For example, sulfatides were only observed in the cortex and not the nucleus. In contrast, ceramides and dihydrolactosylceramides were localised to the lens nucleus. The difference in distribution for each lipid class raises questions as to the role of these lipids within the human lens. Distribution images of glycerophospholipids were also obtained in this study. Most phospholipid classes were present in the cortex except for lysohosphatidylethanolamine. Phosphatidic acid species which has only been recently detected in the lens were imaged for the first time. They were found to be distributed around the cortex of the lens. Combining these data, the spatial information for most of the lipids identified to-date in the human lens were obtained.

Lipids were also quantified in each region of the lens over the human lifespan. It was revealed that the lipid composition is different in each lens region, for example, glycerophospholipids were found to have a higher abundance in the lens cortex, while sphingolipids were found to have a higher abundance in the lens nucleus. Some lipid classes did not show significant changes with age whilst of those that did, glycerophospholipids decreased in concentration with age and sphingolipids increased in concentration with age. There is a sudden increase in ceramide and dihydroceramide levels in the nucleus after the age of 40 as previously observed, however this change also occurs in the cortex. It was also identified that age-related alterations in lipid abundances are most prevalent in the barrier region of the human lens.

In conclusion, this thesis has developed a method for the imaging of lens lipids and studied the distribution and abundance of a range of lipid classes in different regions of the lens. Middle age appears to be a key transition point for changes in lipid composition, with major changes to the lipid composition occurring around this time in all regions of the lens. This coincides with previously reported macroscopic changes occurring at approximately age 40. The alterations to the majority of lipid classes in the barrier also suggest that the barrier region is more prone to age-related effects compared to other regions. The lens is a unique model which allows us to study the effect of ageing on lipid composition and the change in lipid composition of long-lived and newer fibre cells.

Acknowledgments

To my supervisors, Assoc. Prof. Todd Mitchell, Dr. Jessica Nealon and Prof. Stephen Blanksby, thank you for all your patience, supervision and guidance over the years. None of these could be achieved without your continuous support and time, especially when we are in different countries and time zones.

I would also like to thank the Australian government for the International Postgraduate Research Scholarship and University of Wollongong for the University Postgraduate Award scholarship.

Thanks to Mr. Michael Melcher of Institute of Applied Statistics and Computing, University of Natural Resources and Life Sciences Vienna for the statistical analysis done in Chapter 5.

To the people of MSURFF, especially Monica, thank you for making my honours and PhD years fun and enjoyable. It was friendship that I have gained the most out of all the years I have spent in UOW. Special thanks to Michael Friedrich for sharing his valuable knowledge and experience in lens dissection and Sarah Hancock for giving me advices on statistical analysis.

Finally, I would like to thank my parents, siblings and family for their endless support and understanding during difficult times. Dear Jayee and Jayneth, your arrivals have been the biggest motivation for me to complete this thesis. I wanted you to know that even though it is tough to juggle between being a mother and a student, nothing can stop us from becoming who we want to be.

Dear Jimmy, thank you for believing in me. Your endless love and support are what kept me going throughout the years.

Certification

I, Jo Ann Seng, declare that this thesis submitted in fulfilment of the requirements for the conferral of the degree Doctor of Philosophy, from the University of Wollongong, is wholly my own work unless otherwise referenced or acknowledged. This document has not been submitted for qualifications at any other academic institution.

Jo Ann Seng

30th August 2018

List of Names or Abbreviations

BHT	butylated hydroxytoluene
Cer	ceramide
CerP	ceramide-1-phosphate
CID	collision-induced dissociation
d18:0	sphinganine
d18:1	sphingosine
DAN	1,5-diaminonapthalene
DESI	desorption electrospray ionisation
DHB	2,5-dihydroxybenzoic acid
DHCerP	dihydroceramide phosphate
DHGM1	dihydromonosialotetrahexosylganglioside
DHGM3	dihydromonosialodihexosylganglioside
DHLacCer	dihydrolactosylceramides
DHSialyl-Le^x	dihydrosialyl Lewis acid
DHSM	dihydrosphingomyelin
DHSM3	dihydrolactosyl ceramide sulfates
DHST	dihydrosulfatides
DHTriHexCer	dihydrotrihexosylceramide
GAM	generalised additive models
GP	glycerophospholipid
LacCer	lactosylceramide
LPE	lysophosphatidylethanolamine
LSM	lysosphingomyelin
MALDI-MS	matrix assisted laser desorption ionisation mass spectrometry
MBT	2-mercaptobenzothiazole
MS	mass spectrometry

MSI	mass spectrometry imaging
MTBE	methyl-tert-butyl ether
OCT	optimal cutting temperature
PA	phosphatidic acid
PC	phosphatidylcholine
PE	phosphatidylethanolamine
PG	phosphatidylglycerol
PI	phosphatidylinositol
PS	phosphatidylserine
SL	sphingolipid
SM	sphingomyelin
SM3	lactosyl ceramide sulfates
ST	sulfatide
TFA	trifluoroacetic acid
TLC	thin-layer chromatogtraphy

Table of Contents

List of Tables

List of Figures

Chapter 1: Introduction

1.1 The Lens

The human eye enables vision through the detection and transduction of light. It has two regions: an optical region which gathers and focuses light to form an image; and a neural region (retina) where the image is then converted into an electrical signal for the primary visual cortex to interpret. The lens is a transparent tissue located in the anterior chamber of the eye, between the iris and the vitreous body. It is enclosed within an elastic capsule and is suspended by zonular fibres that extend from the ciliary body. As an avascular structure, the lens must obtain nutrients from the aqueous humour that bathes the anterior surface of the lens.[1, 2] The lens develops continuously throughout a person's life beginning at the embryonic phase. Its development starts from the epithelium that consists of a layer of cuboidal cells. Posterior epithelial cells in the lens vesicle elongate and form primary fibre cells, which are arranged in tightly packed concentric layers (Figure 1.1).[3, 4] These primary lens fibre cells are the shortest mature fibres in the lens.[5]

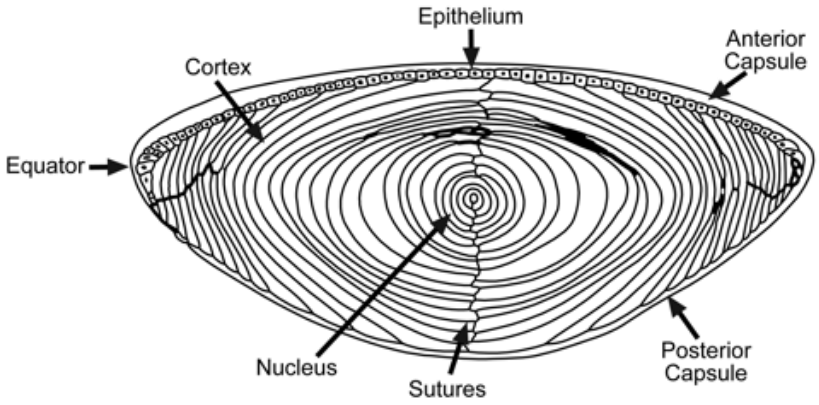

Figure 1.1: A transverse section of the human lens. Figure taken from Harding (2002).[2]

The differentiation of anterior epithelium fibre cells at the lens equator is followed by a subsequent loss of nuclei and other intracellular organelles.[6, 7] This process maintains lens transparency and prevents light scattering. Epithelial cells at the germinative zone elongate and differentiate to stack on top of pre-existing fibre cells, known as secondary fibre cells.[7] Fibre cells are never lost or replaced from the lens, thus it grows in size throughout a person's life.[5] The lens at birth, which consists of the primary cells in the centre is known as the nucleus; while the cortex refers to cells that are laid down thereafter.

The lens fibre cells are interconnected by gap junctions and an anterior layer of single cuboidal cells at the lens surface known as epithelial cells.[8] These gap junctions allow metabolic co-operation of small molecules through the intercellular diffusion of ions, metabolites and water.[8] They are formed by a family of integral membrane channel-forming proteins called connexins.[8, 9] The transport properties in the lens differs in three zones. The epithelial cells express most of the active transport proteins in the lens, where the mature fibers, which lack organelles express membrane transporters for nutrients and antioxidants that are needed for homeostasis.[9] The differentiating fibers, which still have organelles, have different membrane transporters than the epithelium.[9] Early study of the lens microcirculation system found that the lens current densities at the surface of a free-standing lens were surprisingly large and were not directed across the lens.[10] In fact, they were inward in the region of either the anterior or posterior pole and outward at the equator (as shown in Figure 1.2).[11] This is the most dramatic physiological property of a normal lens and is believed to maintain the lens clarity.[10]

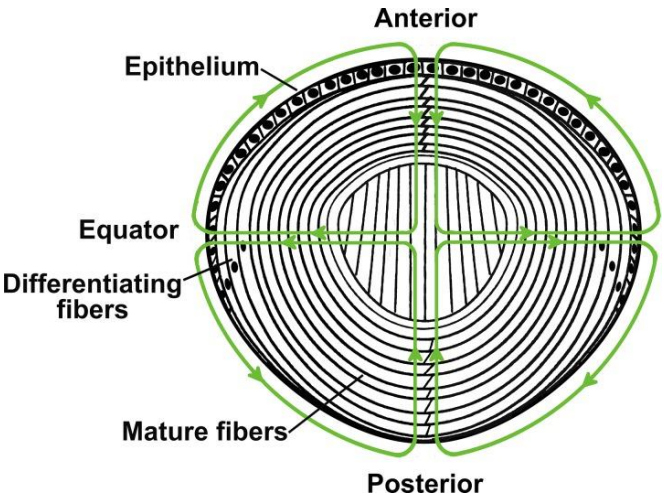

Figure 1.2: Cross section of a mouse lens. The circulation of ions and fluid (depicted in green) follows the pattern indicated by the arrowheads: ions and fluid enter extracellular spaces of the lens at the anterior and posterior poles and they exit across epithelial cell membranes at the equator.[11]

In this thesis, lenses are discussed based on the dissected four regions, which are the outer, barrier, inner and core (Figure 1.3). Anatomically, the cortex region includes the outer and the barrier region, whereas the nucleus includes the inner and core regions. The outer region solely contains the cortex cells, which is comprised of both fibre cells and epithelial cells. These cells are still metabolically active. The barrier refers

to the region within the inner boundary of the cortex, which corresponds to lens fibre cells that were laid down during childhood years.[12-14] This region develops into a functional barrier to the lens nucleus around the age of 40 as described by Sweeney and Truscott[14] as opposed to the anatomical barrier, which is described by Donaldson and Lim.[15, 16] Changes to the protein and lipid composition in the barrier with age have been implicated in the development of age-related nuclear cataract.[14] The formation of a barrier retards the diffusion of antioxidants from the cortex into the lens centre, leaving it prone to oxidative modification.[17] The core is sectioned so that it only contains *in utero* nuclear cells, thus this region can be used for true age-related comparisons. The inner region is comprised of the remaining nuclear fibre cells but may also contain some early cortical cells laid down shortly after birth.

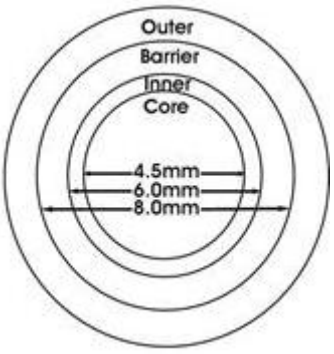

Figure 1.3: Illustration of the four regions of human lens obtained by dissection.[18]

Energy production in the lens is dependent on anaerobic glycolysis, as the lens loses most of its organelles, including mitochondria, during differentiation.[3] The mature fibre cells in the lens centre therefore undergo little or no metabolic activity.[19-21] Most of the lipids in the lens are membrane lipids, which function as channels for diffusion.[8] Therefore, the lens nuclear cells rely on the efficient transport of gluthatione from the outer cortex and epithelium via diffusion through pores.[14]

1.2 Lens Membrane

Biological cellular membranes are composed of lipids, proteins and carbohydrates. They serve as selective barriers that regulate the entry and exit of substances into and out of the cell and provide an active surface for biochemical reactions to occur. Membrane proteins have many roles, they may function as ion channels or pumps that control the exchange of solutes; or act as energy transducers, enzymes or receptors for

transmembrane signalling.[22, 23] Phospholipids, glycolipids and cholesterol are the main lipids forming the membrane bilayer. These lipids function as signalling molecules, anchors for membrane proteins, and create a semi-permeable bilayer that preserves electrochemical gradients.[22-24]

Figure 1.4 shows the differences between the fluid mosaic model as proposed in 1972 by Singer and Nicholson,[25] and the lens membrane proposed by Borchman *et al.* in 2010.[26] Transmembrane proteins in the typical membrane float in a fluid bilayer of phospholipids and glycolipids, with a low abundance of cholesterol packing in between the phospholipids to facilitate order in the membrane.[26] Phospholipids in the typical membrane are of a variety of classes, head groups and fatty acyl chains, and the degree of unsaturation of the fatty acyl chain is a key factor in regulating membrane fluidity.

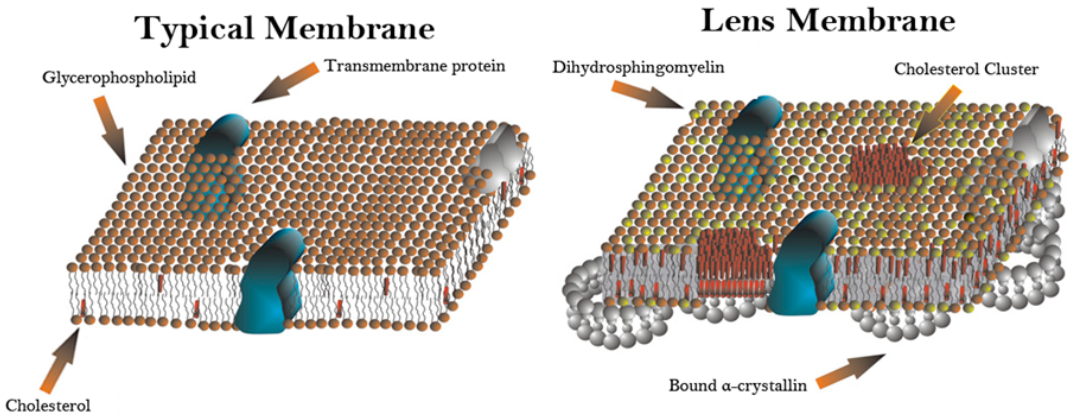

Figure 1.4: A comparison of the typical membrane proposed by Singer and Nicholson and lens membrane proposed by Borchman.[26]

The human lens membrane has a unique lipid profile compared to other mammalian lenses and other human tissues.[27] The human lens has one of the most saturated and ordered membranes in the human body owing to the lipids that are present.[26] It has the highest abundance of dihydrosphingomyelin (DHSM), comprising 47% of total human lens phospholipid, and 72% of total sphingolipid (SL) in the human lens.[27-29] This is in contrast to other animal lenses where DHSM is less than 3% of total phospholipid.[27] It is suggested that humans have adapted to the higher SL content in order to maintain membrane stability over our extended lifespan.[26, 30] Other long-lived animals, such as camels, rarely develop cataract in old age, despite living in adverse conditions. It has been shown that camel lenses are comprised of 77% SL.[30] In addition to the high abundance of DHSM, human lens membranes also contain a high level of cholesterol. The molar ratio of

cholesterol to phospholipid in the human lens ranges from 2-6 in comparison to the plasma membrane which is about 0.52-0.70.[31-34] In fact, there is enough cholesterol in a human lens membrane to aggregate and form pure cholesterol domains.[35, 36] Cholesterol domains are pure bilayers of cholesterol, which differ from lipid rafts that consist of laterally associated sphingolipids with cholesterol filling the space between the sphingolipids.[36] Moreover, lipid rafts are involved in signalling,[33, 37, 38] while no such role has been identified for cholesterol domains. In the raft regions of the lens, cholesterol preferably associates with DHSM as it is more abundant than SM and has a stronger binding affinity to cholesterol.[39]

The high abundance of cholesterol and DHSM in the lens membrane may be essential for maintaining lens function. The highly saturated and stable DHSM may prevent oxidation in the lens membrane.[39] Studies have also shown that the inhibition of cholesterol synthesis in animal lens causes cataract[40] and cholesterol clusters were absent in cataractous human lens.[33]

1.3 Lens Lipids

Besides cholesterol, the main component of the lens membrane are phospholipids. Phospholipids contain a hydrophilic headgroup, which interacts with the cytoplasm or the extracellular environment and two fatty acyl chains which contribute to the hydrophobic region of a membrane lipid bilayer.[41] Different head groups and the length and degree of unsaturation of the fatty acyl chain can affect physical properties such as membrane fluidity.[41] Similarly to lens proteins, lens membrane lipids do not turn over[42, 43] and therefore, need to be able to resist oxidation and degradation throughout a human's lifespan.[43]

1.3.1 Fatty Acids

Fatty acids are carboxylic acids with a long hydrocarbon chain. They are the major building blocks of complex lipids found in membranes. Fatty acids are mostly esterified to phospholipids, cholesterol esters and sphingolipids. In the lens, systemic fatty acids are transported into fibre cells by albumin in the aqueous humour.[44-46] Fatty acids can vary in the number of carbons in the chain, and the number, position and stereochemistry of the double bonds. The two most abundant fatty acyl chains in the human lens are palmitic and nervonic acid.[27, 32]

The stereochemistry of the double bonds is often described first, with *cis* (*Z*) representing both substituents

on the same side of the bond, in comparison to the *trans* (*E*) conformation where the substituents are located on opposite sides. Generally, fatty acids are described by i) the hydrocarbon chain length; ii) the number of double bonds; iii) the location of the double bonds and iv) the stereochemistry of their double bonds.[47, 48] The nomenclature of fatty acids is illustrated in Figure 1.5. For example, a 24-carbon fatty acyl chain with a *cis* configuration at the 15th carbon is named as FA 24:1(15*Z*). If the position and stereochemistry of the double bond is unknown, as is the case with conventional mass spectrometry, then this lipid is described as 24:1. When present in a molecular lipid, *e.g.* DHSM with a 24:1 fatty acyl chain it is written as SM(d18:1/**24:1**), where 1 is the number of double bonds present in the fatty acyl chain.

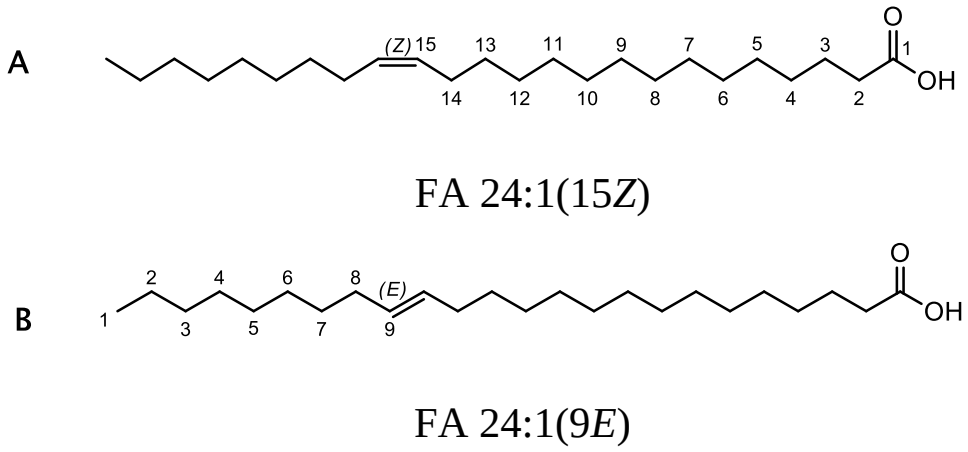

Figure 1.5: Structural differences between cis and trans geometry of nervonic acid (common name), also known as 15-tetracosenoic acid (systematic name). (A) is FA 24:1(15Z) as for cis configuration, the numbering shows the location of the double bond from the terminal -COOH group. (B) is FA 24:1(9E) as for trans configuration the numbering shows the location of the double bond from the terminal methyl group.

1.3.2 Lens Glycerophospholipids

Glycerophospholipids (GPs) consist of a 3-carbon glycerol backbone with two fatty acids at the *sn-1* and *sn-2* positions and a phosphate head group attached at the *sn*-3 position (Figure 1.7). There are four main classes of GP present in the human lens: phosphatidylcholine (PC), phosphatidylethanolamine (PE), phosphatidylserine (PS) and phosphatidic acid (PA) as shown in Figure 1.7.[27] GPs are named according to the fatty acyl chains and the head group, for example: phosphatidylcholine with 16:0 and 18:1 fatty acyl chains attached at the *sn-1* and *sn-2* positions respectively, is named PC (16:0/18:1).[47, 48] In most tandem mass spectrometry experiments sn-position cannot be determined, therefore it is written as PC (16:0/18:1). In addition to the ester linkage of fatty acyl chains to the glycerol backbone, they can be also bound via an

1-*O*-alkyl ether or 1-*O*-alkenyl ether linkage at the *sn-1* position (Figure 1.6). In the human lens, two thirds of phosphatidylethanolamine and phosphatidylserine are 1-*O*-alkyl ether-linked.[27, 29, 49]

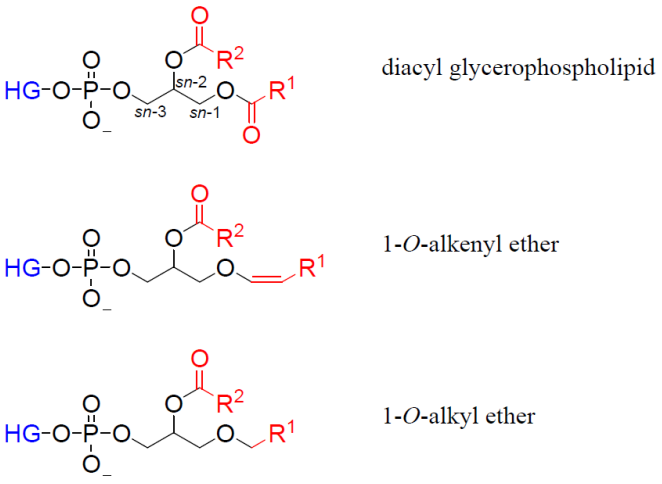

Figure 1.6: The general structure of glycerophospholipids. HG: head group; R^1 acyl chain at the sn-1 position; R^2 acyl chain at the sn-2 position; sn: stereospecific numbering.

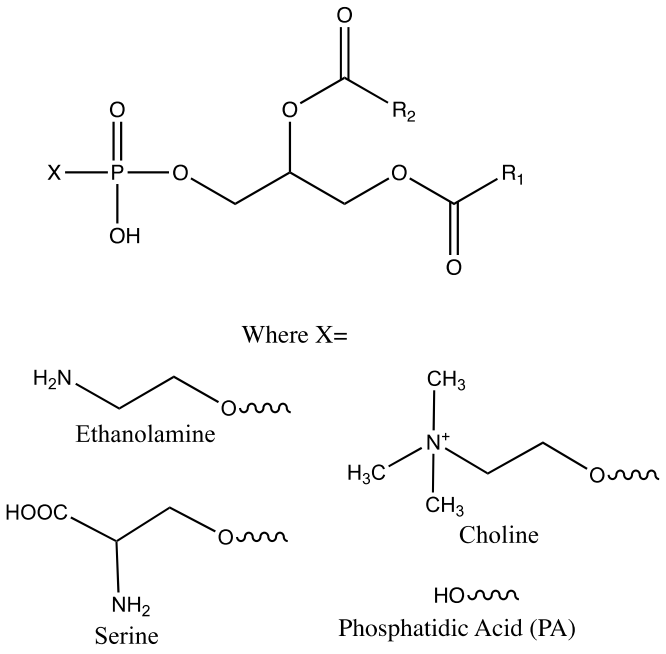

Figure 1.7: A schematic illustration of glycerophospholipids. R1 and R2 represent the fatty acyl chains at the sn-1 and sn-2 positions, respectively. X corresponds to the headgroup moiety linked via an ester linkage at the sn-3 position. The abbreviation of phospholipid class is shown in brackets.

Phosphatidylcholine is the most abundant GP in animals lenses, which accounts for 31-46% of total phospholipids in rat, chicken, sheep, cow, and pig.[27] On the other hand, PC only accounts for 11% of the total human lens phospholipidome.[27] The most abundant GP in the human lens is phosphatidylethanolamine,[27, 29, 50] the majority of which are 1-*O*-alkyl ether-linked.[27, 49] These ether-linked phospholipids are believed to be associated with lens transparency, as the inhibition of their synthesis causes cataract in mice.[51] Lyso-derivatives of GPs that possess only the sn-1 fatty acyl chain are also observed.[27, 49]

1.3.3 Lens Sphingolipids

The main lipid classes present in the human lens belong to the sphingolipid family. These lipid classes contain either a sphinganine (d18:0) backbone, or the unsaturated sphingosine (d18:1) backbone with 18 carbons and a *trans* double bond at the 4 position (see Figure 1.8).[52] The "d" stands for "dihydroxy", referring to the two hydroxyl groups present on the sphingoid backbones. Derivatives of the sphingosine backbones such as SM, ceramide (Cer) and ceramide-1-phosphate (CerP) have also been detected and quantified in older human lenses.[53] SM contains a phosphocholine head group esterified to the sphingoid base. Examples of these structures are shown in Figure 1.8. The same names apply to those with the sphinganine backbone but with a prefix of "dihydro-", which is abbreviated by "DH". For example, ceramides with a sphinganine backbone can be referred as dihydroceramides, or DHCer.[49, 54] The CerP or dihydroceramide phosphate (DHCerP) contain an extra phosphate group when compared to Cer or DHCer. Fatty acids are attached via an amide linkage at the 2nd carbon of the backbone, and the nomenclature used is similar to that used for GP. In the human lens, most of the sphingolipids are comprised of a sphinganine backbone with either a 16:0 or a 24:1 fatty acyl chain.[12, 30, 55] For example, a SM with a 16:0 fatty acyl chain will be named SM (**d18:1**/16:0) whereas a DHSM with a 16 carbon saturated fatty acyl chain will be represented by SM (**d18:0**/16:0).

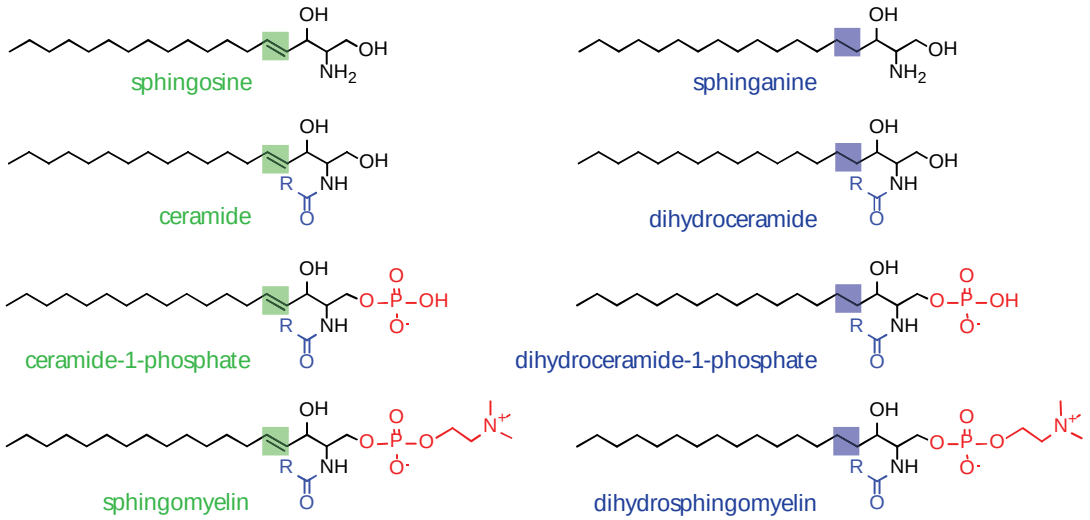

Figure 1.8: The structures of the sphingosine and sphinganine backbone and their derivatives. The two sphingoid backbones differ in the presence of trans-double bond between the 4th and 5th carbons. CerP and DHCerP contain an extra phosphate group in comparison with Cer and DHCer. A phosphocholine moiety is esterified at the sphingoid backbone for both SM and DHSM. Fatty acids are attached via an amide bond at the 2nd carbon.

As shown in Figure 1.8 the *de novo* synthesis of SLs begins with the condensation of palmitoyl coenzyme A and serine, catalysed by serine palmitoyltransferase. The synthetic pathway of DHSM still remains unclear despite it being the most abundant SL in the lens. It is proposed by Michel *et al.* that it may be synthesised from DHCer through an unknown enzyme.[56] However, a recent review by Merill has suggested that DHSM is synthesised from DHCer by sphingomyelin synthase.[57] Other dihydroglycosphingolipids such as dihydrolactosylceramides (DHLacCer) may also be synthesised from DHCer, while glycosphingolipids, SM and CerP are derived from Cer.[58, 59] A detailed description of sphingolipid synthesis is beyond the scope of this thesis however, further information regarding the synthetic pathways can be found in Futerman *et al.*[59]

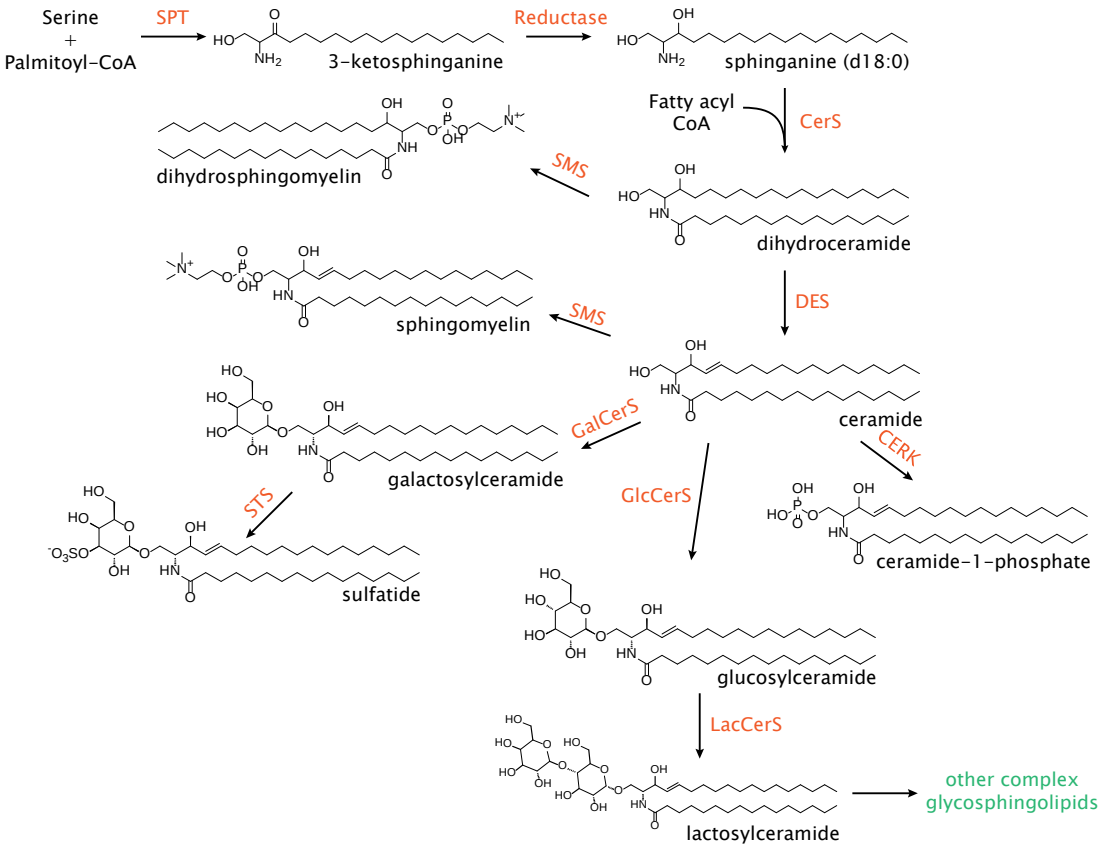

Figure 1.9: The de novo synthetic pathway of SLs through to lactosylceramide and sulfatide. The enzymes involved in each step are shown in orange. SPT: serine palmitoyltransferase; CerS: ceramide synthase; SMS: sphingomyelin synthase; DES: dihydroceramide desaturase; GalCerS: galactosylceramide synthase; GlcCerS: glucosylceramide synthase; CERK: ceramide kinase; STS: sulfatide synthase; LacCerS: lactosylceramide synthase.

1.3.4 Lens Glycosphingolipids & Other Complex Gangliosides

Glycosphingolipids (GSLs) refer to lipids containing either a sphingoid or ceramide moiety with one or more monosaccharide groups attached to the 1-hydroxyl position via a β-glycosidic linkage. The identification of this class of lipid in normal[60-62] and cataractous[55, 62, 63] human lenses has previously been reported. They can be subdivided into categories of neutral GSLs and acidic GSLs, depending on the properties of the groups that are attached to the lipid. For example, neutral GSLs are those with sugar groups attached, whereas acidic GSLs may have sialic acid or sulfate ester groups bound to them. Ariga *et al.* (1994) demonstrated that in cataractous lenses, the majority of GSLs contain the sphinganine backbone and the fatty acyl chain 16:0, 24:0 and 24:1, which follow the compositional trends of fatty acyl chains observed in other sphingolipid classes.[55] Although the major fatty acyl chains in GSLs have been identified, they are not correlated with any specific, individual subcategory of GSLs. One such example is sulfatide (ST), which

is shown in Figure 1.10.

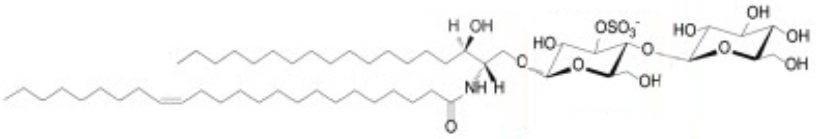

Figure 1.10: The structure of SM3 (d18:1/24:1). It contains two sulfate head groups and a ceramide backbone with a 24:1 fatty acyl chain attached to the amide.

We have recently developed methods to detect these low abundant species in the lens using mass spectrometry (MS). Direct coupling of ambient ionisation mass spectrometry techniques with thin-layer chromatogtraphy (TLC) has enabled the direct analysis of TLC plates without further sample preparation. These advances have been made possible by the development of desorption electrospray ionisation (DESI) by the Cooks group in 2004.[64] In brief, DESI operates in the ambient environment by spraying charged micro-droplets from an emitter towards the sample surface, where analytes are desorbed into the gas phase and ionised, then extracted into the mass spectrometer for analysis.[65]

Our previous work has illustrated that TLC-DESI-MS is a promising method to obtain qualitative data on the lens sphingolipidome.[66] By combining TLC with DESI-MS, faint spots on the TLC plate or incomplete separation can be resolved by precise mass spectrometric analysis. With this technique, 30 species of SLs from 11 different classes were identified in a lipid extract from a 20 year-old human lens. The classes not only include DHSM, SM, Cer, DHCer, DHLacCer, CerP and DHCerP that have previously been reported;[26, 28, 67-69] but also several novel classes of lipids such as lactosyl ceramide sulfates (SM3), dihydrolactosyl ceramide sulfates (DHSM3), sulfatides (ST) and dihydrosulfatides (DHST).[66] Although these lipids were found at very low abundance in the lens,[26] the structures of each molecule were able to be elucidated by collision-induced dissociation (CID). A negative ion mass spectrum obtained from the DHSM3 region of a TLC plate is shown in Figure 1.11(A). Like other SLs in the lens, the two most abundant analogues of DHSM3 contain a 16:0 or 24:1 fatty amide chain. The lipid structure is characterised by CID, which is shown in Figure 1.11B.

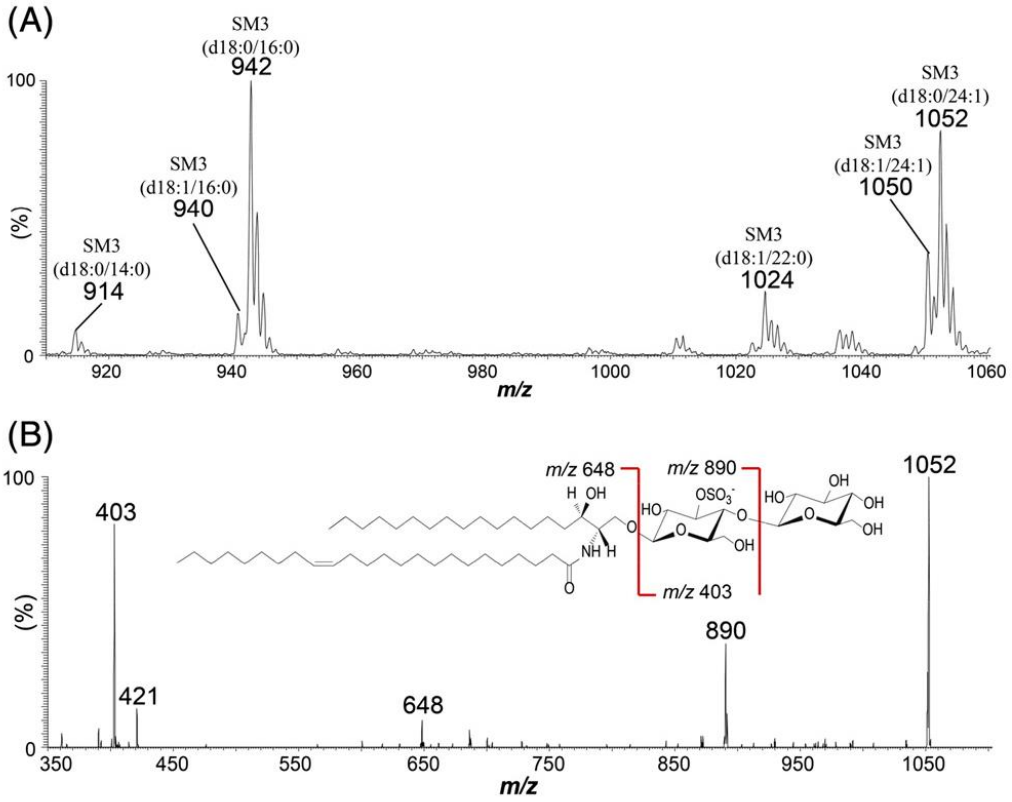

Figure 1.11: (A) Negative ion mass spectrum of a 20-year old human lens lipid extract DHSM3 region. (B) CID spectrum of SM3 (d18:0/24:1) at m/z 1052 with its proposed structure.[66]

Although this lipid class is proposed to be less than 1% of the total human lens lipidome,[28] GSLs are known to be essential for the differentiation and maturation of lens fibre cells.[70] GSLs are often located at the exocytoplasmic leaflet of cell membranes, where their sugar moieties interact with other biomolecules in cellular differentiation and transformation.[71] They are also involved in signal transduction in conjunction with lipid rafts.[72] The physicochemical properties of lipid rafts in normal and cataractous lenses appear to be different, thus it is important to further elucidate the composition of these lipids in particular regions of the human lens.[33] An increase in GSL abundance has also been observed with age and cataract,[61, 62, 73] and is proposed to influence cell-to-cell interactions that initiate cataractogenesis.[60]

1.4 Age-related Changes in the Lens

Accommodation is the process whereby the lens adjusts its curvature to focus light upon the retina to observe near objects. Age is the major factor for the lens to lose its ability to accommodate. The lens is exposed to cumulative effects of oxidation, radiation and post-translational modifications with ageing, such

that proteins and other biomolecules in the lens are modified, leading to visual impairment.[74] Previous work has also shown that there is a massive increase in lens stiffness with age, particularly in the nuclear region.[75]

1.4.1 Changes in Proteins

As there is no protein turnover in the human lens nucleus,[42] these long-lived proteins are exposed to factors that can cause undesirable modifications that may lead to protein aggregation.[76] The damaged proteins become insoluble and thus precipitate, causing opacification of the lens. The lens contains an abundance of α-crystallins, which act as chaperones, binding to proteins as they denature to maintain their solubility.[76, 77] This process is essential for maintaining the transparency of the lens. With age, more α-crystallins sequester the denatured protein to form high molecular weight complexes, causing free α-crystallins to decrease.[77] The depletion of chaperones causes the accumulation of denatured protein in the lens nucleus, which results in stiffening of the lens.[77] α-crystallins binding to lens membrane proteins may lead to the formation of a barrier that reduces the diffusion of antioxidants into the lens centre, leaving the proteins and lipids vulnerable to oxidation and consequently cataract.[78]

Aquaporin-0 is the most abundant integral membrane protein in fibre cells, which is responsible for water transport through its core.[79] The association between aquaporin-0 and membrane phospholipids was observed in sheep lenses using X-ray crystallography.[80] Lipids were found to form a one-molecule wide shell around the protein.[80] Mutations in aquaporin-0 may prevent proper interactions between this protein and its surrounding lipids that could affect the folding and integration of membrane proteins into a bilayer.[81]

In summary, the changes in lens proteins causes a reduction in the diffusion of water from the cortex to the lens nucleus as well as accumulation of high molecular weight aggregates and insoluble proteins. Consequently, the lens undergoes a gradual reduction in transparency, increase in stiffness and an increase in the scattering and aberration of light waves as well as a degradation of the optical quality of the eye which may lead to the onset of cataract.[82]

1.4.2 Changes in Lipids

The long lifespan of lipids in the lens membrane is likely to result in cumulative photo- and/or chemical oxidation despite the hypoxic environment in the lens.[83] The association between lipid oxidation and lens

transparency with age suggests that lipid oxidation may initiate cataractogenesis.[29, 84] More than 40% of phospholipids in the lens are degraded throughout a human's lifespan, even more in the case of cataract, forming deleterious oxidation products.[29, 68] The insertion of hydrophilic moieties into acyl chains as a result of oxidation can disrupt lipid-lipid interactions, causing structural abnormalities in the membrane.[85]

Analysis of the lens lipid composition has revealed that the abundance of phospholipids and SLs in the lens nucleus changes as we age.[53] GPs are abundant in the nucleus of young lenses, but decrease with age until 40 years and then plateau at very low levels (Figure 1.12).[53] Figure 1.12A shows that PC is reduced by approximately 75% by the age of 40 while Figure 1.12B shows that PS is reduced by 85% over the same period.[53] PE, which is the second most abundant GP class in the lens, showed a similar trend with a 50-fold decrease in Figure 1.12C.[53] Hughes *et al.* identified and quantified lysophosphatidylethanolamine (LPE), the most abundant GP class in the human lens nucleus. This lipid class showed a gradual decline in concentration with age.[53] Other microscopic and macroscopic changes to the lens also occur around 40-50 years of age. For example, presbyopia normally occurs around the age of 50.[86, 87] This dramatic change in the membrane lipid composition may contribute to increased binding of crystallins and blockage of membrane pores in the lens, which could in turn disrupt intracellular transport promoting oxidation.[18]

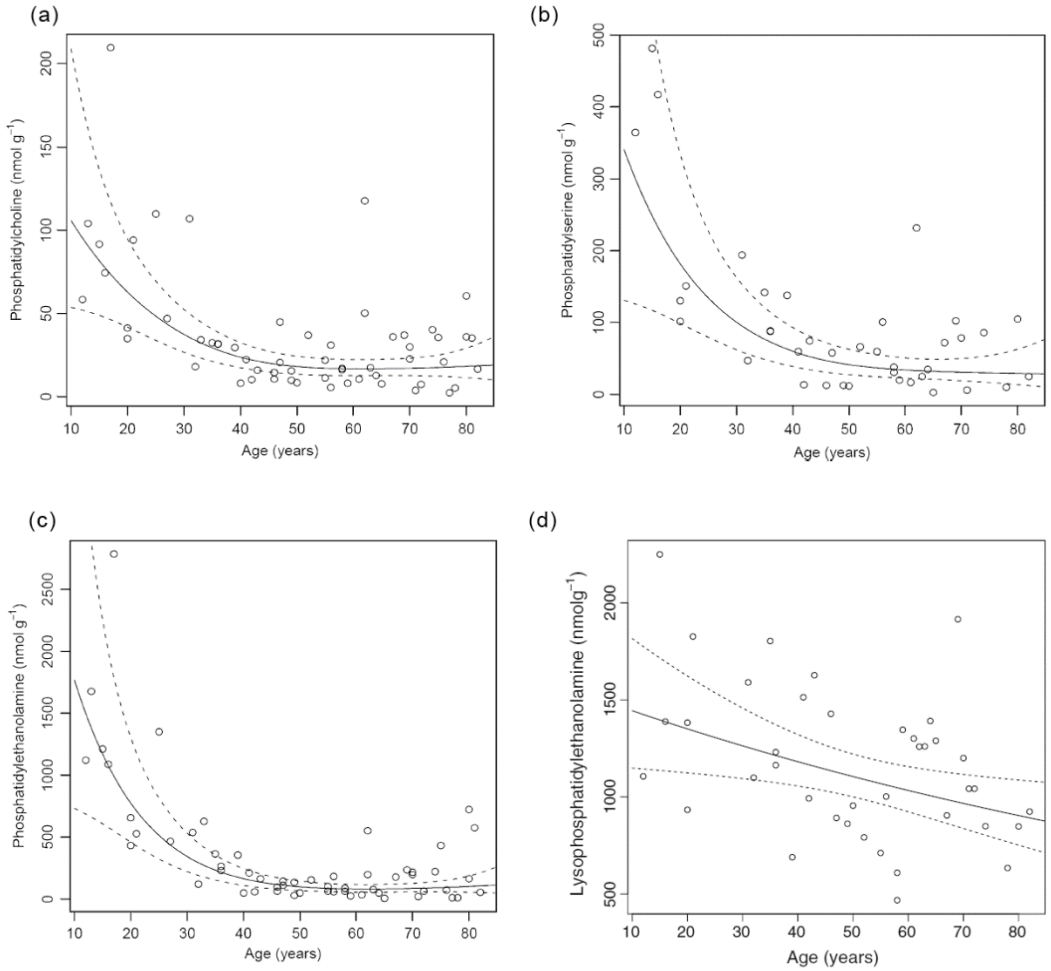

Figure 1.12: Total concentration of (a) PC; (b) PS; (c) PE and (d) LPE present in the human lens nuclei from young to old lens.[53] The solid line is a generalised additive model fit; the dashed lines provide a 95% confidence band.

To date, glycosphingolipids identified in the human lens include DHLacCer, DHSM3, DHST[55, 66, 67, 88] and other complex glycosphingolipids such as gangliosides which have a sialic acid moiety attached.[55, 60, 62] These GSLs were identified using whole lens lipid extracts and were not quantified except for the gangliosides. More recently, DHSM3 and DHST were identified in a whole lens homogenate, however, they were not quantified.[47] Therefore, their distribution and concentration in the different regions of the lens remain unknown. Although the literature identifies the age of 40 as an age of transition in the lens nucleus,[53] the reason for the increase of DHCer and Cer in the lens nucleus remains unknown. Therefore an investigation of age-related changes of these GSLs is crucial to determine if they contribute to the

increase in ceramides. It is also essential to study the changes of lipid composition in different regions of the lens such as the barrier and outer cortical regions, as these regions comprised of newer fibre cells that were synthesised post-natally.

1.5 Mass Spectrometry Imaging

Mass spectrometry imaging (MSI) has emerged as a complementary tool to study the distribution of specific biomolecules in tissue. MSI now allows for specificity in spatial localisation of anatomical structures, cells, stains and even biomolecules like lipids and proteins without labelling.[89] MSI contains a number of different ionisation techniques whereby each technique requires a unique process to preserve the corresponding sample. Matrix assisted laser desorption ionisation mass spectrometry (MALDI-MS) is the most popular ionisation technique for MSI due to its capability to image a wide range of molecular weights and molecular species.[90] However, its requirement of a matrix for proper ionisation and production of only singly-charged ions often limits its applicability to large proteins. There are also other varieties of MALDI-MSI such as scanning microprobe MALDI (SMALDI),[91] infrared (IR)-matrix assisted laser desorption ESI (MALDESI)[92] and surface-assisted laser desorption/ionisation (SALDI). [93] However, none of these techniques have been used for studying the occular lens and will not be discussed further.

MALDI-MS has been widely used in understanding the cellular components of the eye. It has been applied to study the structure and function of normal ocular tissue, the molecular changes that are associated with the ageing eye and in pathological processes that lead to diseases of the eye, such as cataract and macular degeneration.[89] These studies include the imaging of proteins and lipids in the retina,[94-99] optic nerves[97, 100, 101] and lens.[12, 69, 102-104]

In brief, in MALDI-MSI, thin tissue is mounted on a target, then coated with matrix before being analysed using a MALDI source. In the source, a laser is rastered across the tissue surface while mass spectra are collected at each sampling location. MALDI images are then obtained by plotting the intensity of an observed ion as a function of its sampling location. More details of MALDI-MSI can be found in Chapter 2.

On the other hand, DESI-MS was first reported for visualisation of brain lipids by Ifa *et al.* in 2012.[105] The typical set up for DESI analysis is shown in Figure 1.3. In DESI, a pneumatically assisted electrospray is

directed at the surface of interest, causing charged droplets to impinge the surface.[106] Analytes are then dissolved, generating secondary droplets that scatter off the surface and ionise for MS-analysis.[64, 107] The advantage of DESI-MS over other methods of MSI are its ability to directly analyse surfaces under ambient conditions with minimal sample preparation and allowing the soft ionisation of biomolecules such as lipids and proteins at the same time.[108] The spatial resolution of DESI is largely determined by the spray droplet diameter which is typically around 200-500 μm.[107]

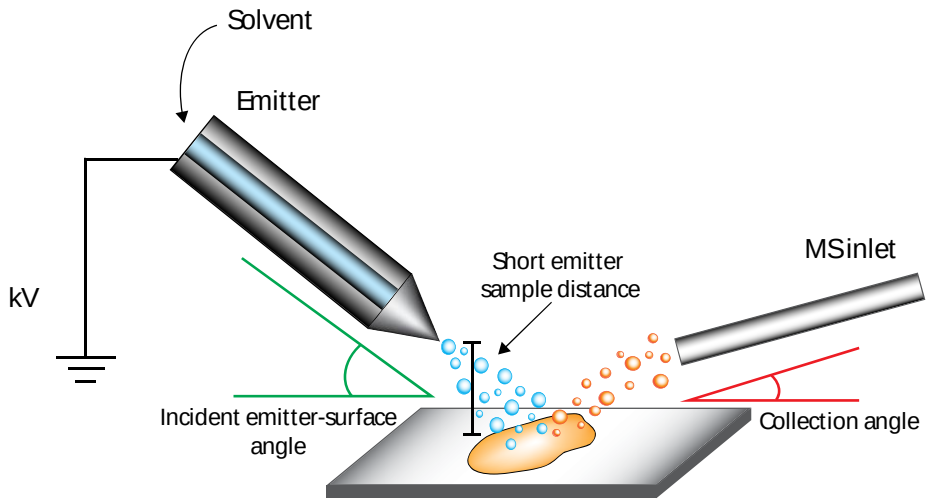

Figure 1.13: Typical experimental set up for DESI.

1.5.1 Lens Protein Imaging

The distribution of α-crystallins in the bovine lens were originally mapped using MALDI-MS by Han *et al.*[109] Traditionally, immunohistochemistry is the preferred technique to profile protein distribution in a tissue. However, this technique requires antibodies to detect specific proteins and is usually limited to one protein at a time. This study highlighted the advantage of using MSI over an antibody-based strategy for mapping multiple post-translational truncations to a single protein. By using MALDI-MS, they were able to image bovine lens α-crystallins in its multiple forms in a single experiment.[109] Further studies of crystallin imaging using animal lenses from rabbit and rodents were aimed at improving the spatial resolution,[110] developing methods to map β- and γ-crystallins[111, 112] and to investigate the changes to crystallins in age-related cataract.[113] Human lens mapping of β- and γ-crystallin peptides were also studied in ageing and cataractous lenses.[114-117] Grey and colleagues have developed a method to spatially map the age-related changes of human lens α-crystallins using MALDI-MS.[114] The results showed that intact α-

crystallins (1-173) are most abundant in the cortex and also present in the nucleus of 7- and 29-year-old lenses (Figure 1.14). However, in 51- and 75-year-old lenses, intact α-crystallins were not detected in the lens nucleus. Application of this spatially resolved proteomic technique improves our understanding of lens protein modifications with age.

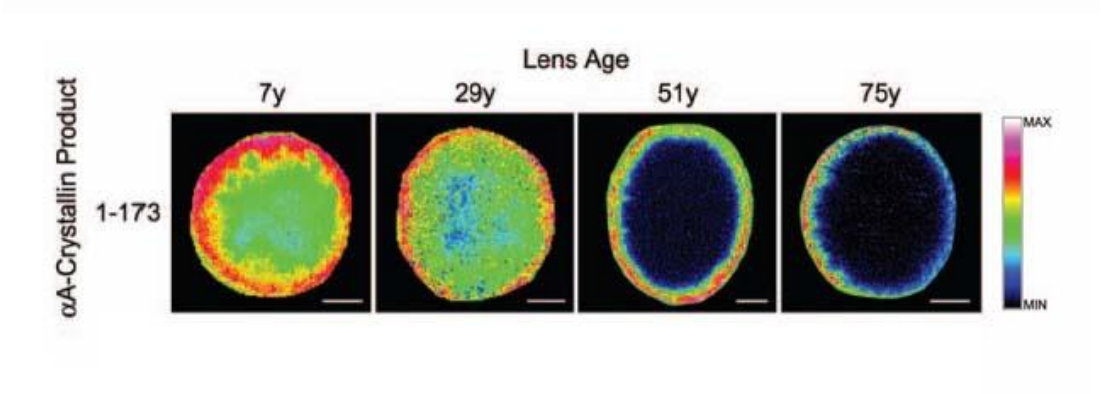

Figure 1.14: MALDI tissue images of intact αA-crystallin (1-173) with age in equatorial human lens sections.[1]

1.5.2 Lens Lipid Imaging

Lens lipid imaging has been performed previously by DESI-MS and MALDI-MS. Ellis *et al.* used DESI-MS to study the distribution of a wide range of lipids including CerP, PE, PS, LPE and cholesterol for the first time in the human lens.[67] These images are shown in Figure 1.15. However, as the lens fibre cells are arranged in a tightly compacted structure, a strong acid needs to be added in the spray solvent in order to disrupt the physical structure of the tissue.[67] This may compromise the spatial distribution of lens lipids. Although DESI-MS was able to provide distribution images of the lipids, its resolution of ~200μm is significantly lower than what standard MALDI-MS can provide (~50-100μm).

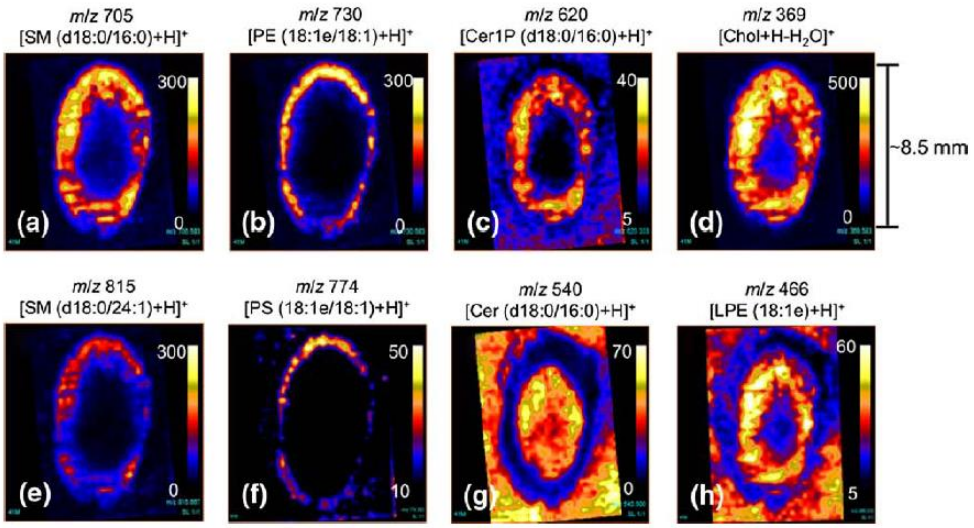

Figure 1.15: DESI images of a 41-year old human lens showing the distribution of (a) SM (d18:0/16:0); (b) PE (18:1e/18:1); (c) CerP (d18:0/16:0); (d) Cholesterol; (e) SM (d18:0/24:1); (f) PS (18:1e/18:1); (g) Cer (d18:0/16:0); (h) LPE (18:1e) by Ellis et al.[67]

Lens lipid imaging has also been performed using MALDI-MS in human[12, 118] and porcine[69, 103] lenses. The initial MALDI-MSI analysis of porcine lens detected seven species of SM and two species of CerP.[69] A further MALDI-MSI study of porcine lenses also imaged PC, PE, PA using exact mass measurements.[103] Deeley *et al.* utilised MALDI-MSI to identify changes in the distribution of sphingolipids such as Cer and DHSM in the human lens with age (as shown previously in Figure 1.11).[12] Nevertheless, the analysis was only performed in positive ion mode and only SM, DHSM, Cer and DHCer were analysed. More recently, a MALDI-MSI study on lens ageing provided the first insight into lysosphingomyelin (LSM) and DHLacCer distribution in the human lens.[118] Moreover, data from this study suggests that lysolipids could be an indicator of human lens ageing.[118]

Changes in the distribution of SLs with age has been demonstrated using imaging mass spectrometry (Figure 1.16).[12] With age, it was observed that DHCer increased in relative abundance in the lens nucleus while DHSM formed a dense annular distribution in the barrier region of an older lens.[12] It was hypothesised that the increase in DHCer levels in the lens nucleus was a result of DHSM degradation, as they are structurally related. However, quantitative data suggests that DHSM abundance remains unchanged in the lens nucleus with age (Figure 1.17A),[53] while DHCer levels increase approximately 1000-fold (Figure 1.17B). The mechanism that leads to the increase in Cer and DHCer with age is currently unknown. As

there is no enzymatic activity in the nucleus in order to synthesise these molecules,[42, 43] it has been postulated that the breakdown of other sphingolipid classes may contribute to the formation of Cer and DHCer observed with age. Furthermore, although the abundance of DHSM remains unchanged in the lens nucleus with age, quantitative data has shown that there is an increase in DHSM in the barrier region, which is consistent with results obtained from lens imaging (Figure 1.16).[12]

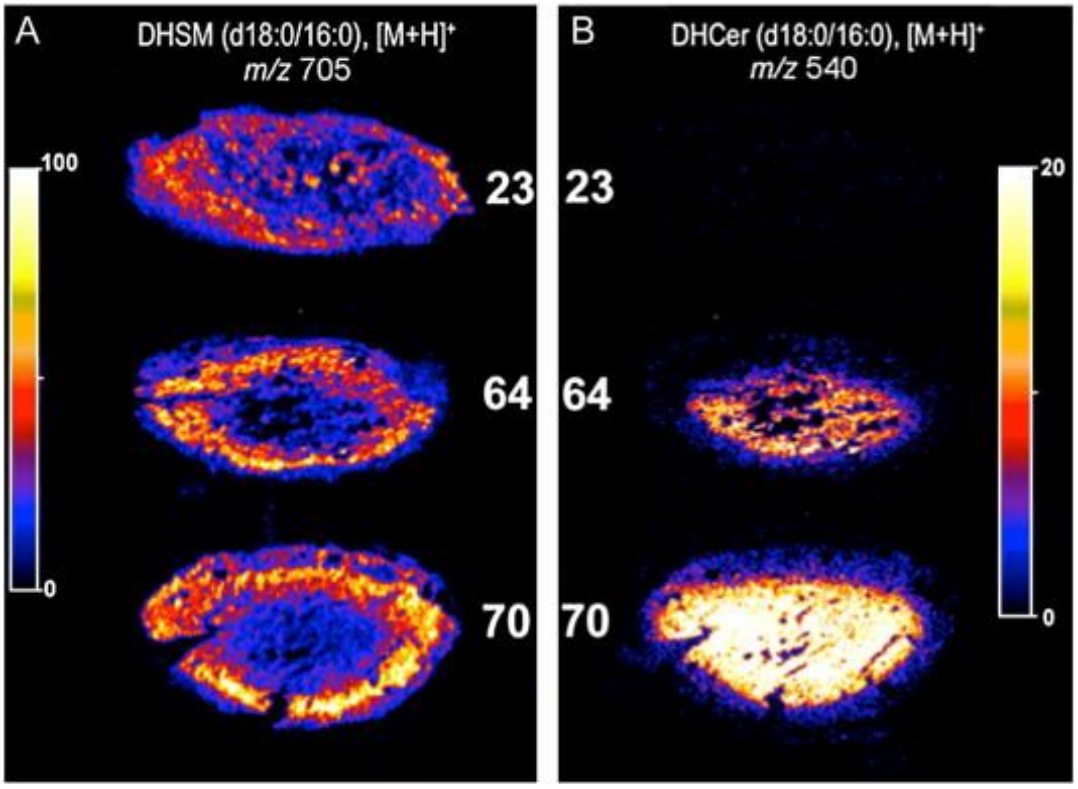

Figure 1.16: The changes in distribution for SM (d18:0/16:0) and Cer (d18:0/16:0) in a 23-, 64- and 70-year old lenses generated by imaging mass spectrometry.[12]

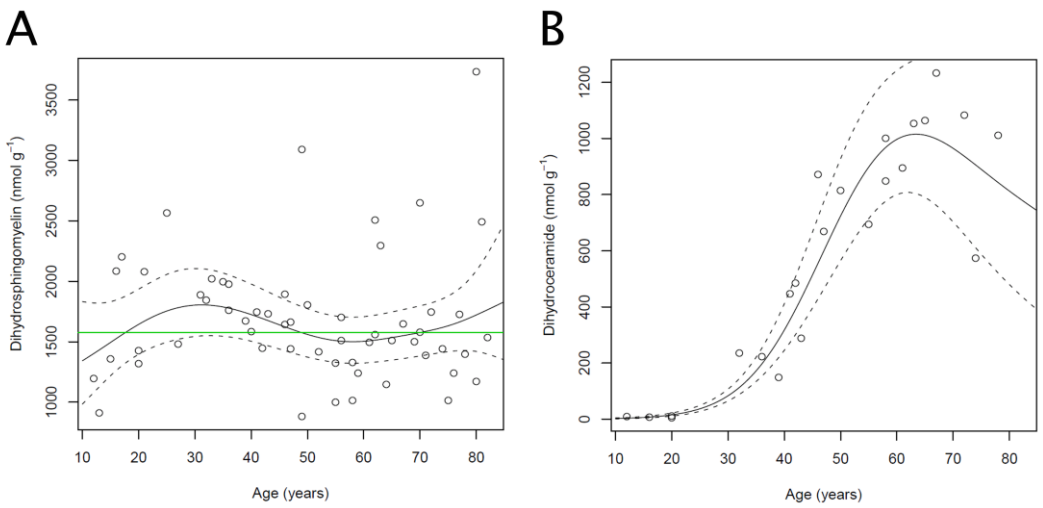

Figure 1.17: Total (A) DHSM and (B) DHCer present in individual human lens nuclei of different ages.[53] *It is observed that DHSM level is constant from lenses of young to old ages. In contrast, the abundance of DHCer increases about a thousand-fold in the older lenses compared to the young ones. The solid line is a generalised additive model fit; the dashed lines provide a 95% confidence band.*

Together, these MSI studies have given greater insight into the lipid changes that occur with age. However, the spatial distribution of many lens sphingolipids, e.g., DHSM3 and DHST and complex GSL such as gangliosides are yet to be determined. A more thorough imaging study containing the spatial distribution of these lipids is essential to understand the lens composition in different regions of the lens.

1.6 Summary

Although some of these glycosphingolipids have been identified and quantified in the lens, most studies have used whole lens extracts for identification and quantification. The lack of spatial distribution and also their abundance in each region of the lens are missing pieces of information, which are essential to elucidate the whole sphingolipidome of the lens. The mechanisms underlying the sudden increase in DHCer in the lens nucleus after the age of 40 remain unanswered.

1.7 Aims

Therefore, the aims of this PhD project were to determine:

- the distribution of each SL and GP class in the human lens,

- changes to these distributions with age,
- the quantitative alterations to lens lipids in the nucleus, cortex and barrier with age,
- if complex glycosphingolipid degradation in the nucleus is the source of DHCer accumulation with age.

1.8 References

1. Zlokovic, B. V.; Mackic, J. B.; McComb, J. G.; Kaplowitz, N.; Weiss, M. H.; Kannan, R., Blood-to-lens Transport of Reduced Glutathione in an In Situ Perfused Guinea-pig Eye. *Experimental Eye Research* **1994,** *59* (4), 487-496.

2. Harding, J. J., Viewing molecular mechanisms of ageing through a lens. *Ageing Research Reviews* **2002,** *1* (3), 465-479.

3. Harding, J. J., *Cataract: Biochemistry, Epidemiology and Pharmacology*. Chapman & Hall: London: 1991.

4. Lovicu, F. J.; McAvoy, J. W., Growth factor regulation of lens development. *Developmental Biology* **2005,** *280* (1), 1-14.

5. Augusteyn, R. C., On the growth and internal structure of the human lens. *Experimental Eye Research* **2010,** *90* (6), 643-654.

6. Berman, E. R., *Biochemistry of the Eye*. Plenum Press: New York: 1991.

7. Bassnett, S., Lens Organelle Degradation. *Experimental Eye Research* **2002,** *74* (1), 1-6.

8. Goodenough, D. A., The crystalline lens. A system networked by gap junctional intercellular communication. *Seminars in Cell Biology* **1992,** *3* (1), 49-58.

9. Mathias, R. T.; White, T. W.; Gong, X., Lens gap junctions in growth, differentiation, and homeostasis. *Physiological reviews* **2010,** *90* (1), 179-206.

10. Mathias, R. T.; Rae, J. L.; Baldo, G. J., Physiological properties of the normal lens. *Physiological Reviews* **1997,** *77* (1), 21-50.

11. Gao, J.; Minogue, P. J.; Beyer, E. C.; Mathias, R. T.; Berthoud, V. M., Disruption of the lens circulation causes calcium accumulation and precipitates in connexin mutant mice. *American Journal of Physiology-Cell Physiology* **2018,** *314* (4), C492-C503.

12. Deeley, J. M.; Hankin, J. A.; Friedrich, M. G.; Murphy, R. C.; Truscott, R. J. W.; Mitchell, T. W.; Blanksby, S. J., Sphingolipid distribution changes with age in the human lens. *Journal of Lipid Research* **2010,** *51* (9), 2753-2760.

13. Moffat, B. A.; Landman, K. A.; Truscott, R. J. W.; Sweeney, M. H. J.; Pope, J. M., Age-related Changes in the Kinetics of Water Transport in Normal Human Lenses. *Experimental Eye Research* **1999,** *69* (6), 663-669.

14. Sweeney, M. H. J.; Truscott, R. J. W., An Impediment to Glutathione Diffusion in Older Normal Human Lenses: a Possible Precondition for Nuclear Cataract. *Experimental Eye Research* **1998,** *67* (5), 587-595.

15. Donaldson, P.; Lim, J., Membrane transporters: new roles in lens cataract. In *Ocular Transporters in Ophthalmic Diseases and Drug Delivery*, JF, R.; J, T.-T.; CJ, B., Eds. Humana Press Inc.: Totowa, NJ, 2008; pp 89-110.

16. Lim, J. C.; Walker, K. L.; Sherwin, T.; Schey, K. L.; Donaldson, P. J., Confocal Microscopy Reveals Zones of Membrane Remodeling in the Outer Cortex of the Human Lens. *Investigative Ophthalmology & Visual Science* **2009,** *50* (9), 4304-4310.

17. Korlimbinis, A.; Berry, Y.; Thibault, D.; Schey, K. L.; Truscott, R. J. W., Protein aging: Truncation of aquaporin 0 in human lens regions is a continuous age-dependent process. *Experimental eye research* **2009,** *88* (5), 966-973.

18. Friedrich, M. G.; Truscott, R. J. W., Large-Scale Binding of α-Crystallin to Cell Membranes of Aged Normal Human Lenses: A Phenomenon That Can Be Induced by Mild Thermal Stress. *Investigative Ophthalmology & Visual Science* **2010,** *51* (10), 5145-5152.

19. Dovrat, A.; Scharf, J.; Gershon, D., Glyceraldehyde 3-phosphate dehydrogenase activity in rat and human lenses and the fate of enzyme molecules in the aging lens. *Mechanisms of Ageing and Development* **1984,** *28* (2-3), 187-191.

20. Scharf, J.; Dovrat, A.; Gershon, D., Defective superoxide-dismutase molecules accumulate with age in human lenses. *Graefe's Archive for Clinical and Experimental Ophthalmology* **1987,** *225* (2), 133-136.

21. Zhu, X.; Korlimbinis, A.; Truscott, R. J., Age-Dependent Denaturation of Enzymes in the Human Lens: A Paradigm for Organismic Aging? *Rejuvenation Research* **2010,** *13* (5), 1-8.

22. Hite, R.; Gonen, T.; Harrison, S., Interactions of lipids with aquaporin-0 and other membrane proteins. *European Journal of Physiology* **2008,** *456*, 651-661.

23. Palsdottir, H.; Hunte, C., Lipids in membrane protein structures. *Biochimica et Biophysica Acta* **2004,** *1666*, 2-18.

24. Eyster, K., The membrane and lipids as integral participants in signal transduction: lipid signal transduction for the non-lipid biochemist. *Advances in Physiology Education* **2007,** *31*, 5-16.

25. Singer, S. J.; Nicholas, G. L., The fluid mosaic model of the structure of cell membranes. *Science* **1972,** *175*, 720-721.

26. Borchman, D.; Yappert, M. C., Lipids and the ocular lens. *Journal of Lipid Research* **2010,** *51*, 2473-2488.

27. Deeley, J. M.; Mitchell, T. W.; Xiaojia, W.; Korth, J.; Nealon, J. R.; Blanksby, S. J.; Truscott, R. J. W., Human lens lipids differ markedly from those of commonly used experimental animals. *Biochimica et Biophysica Acta* **2008,** *1781* (6-7), 288-298.

28. Borchman, D.; Byrdwell, W. C.; Yappert, M. C., Regional and age-dependent differences in the phospholipid composition of human lens membranes. *Investigative Ophthalmology & Visual Science* **1994,** *35* (11), 3938-3942.

29. Huang, L.; Grami, V.; Marrero, Y.; Tang, D.; Yappert, M. C.; Rasi, V.; Borchman, D., Human lens phospholipid changes with age and cataract. *Investigative Ophthalmology & Visual Science* **2005,** *46* (5), 1682-1689.

30. Borchman, D.; Yappert, M. C.; Afzal, M., Lens lipids and maximum lifespan. *Experimental Eye Research* **2004,** *79* (6), 761-768.

31. Cotlier, E.; Obara, Y.; Toffness, B., Cholestrol and phospholipids in protein fractions of human lens and senile cataract. *Biochimica et Biophysica Acta* **1978,** *530* (2), 267-278.

32. Zelenka, P. S., Lens lipids. *Current Eye Research* **1984,** *3* (11), 1337-1359.

33. Rujoi, M.; Jin, J.; Borchman, D.; Tang, D.; Yappert, M. C., Isolation and lipid chracterization of cholesterol-enriched fractions in cortical and nuclear human lens fibres. *Investigative Ophthalmology & Visual Science* **2003,** *44* (4), 1634-1642.

34. Ji, S.-R.; Wu, Y.; Sui, S.-f., Cholesterol is an important factor affecting the membrane insertion of β-amyloid peptide (Aβ1–40), which may potentially inhibit the fibril formation. *Journal of Biological Chemistry* **2002,** *277* (8), 6273-6279.

35. Jacob, R. F.; Cenedella, R. J.; Mason, R. P., Direct evidence for immiscible cholestrol domains in human ocular lens fibre cell plasma membranes. *Journal of Biological Chemistry* **1999,** *274* (44), 31613-31618.

36. Borchman, D.; Yappert, M. C., Lipids and the ocular lens. *Journal of Lipid Research* **2010**.

37. Simons, K.; Derek, T., Lipid rafts and signal transduction. *Nature Reviews. Molecular cell biology* **2000,** *1*, 31-39.

38. Brown, D.; London, E., Functions of lipid rafts in biological membranes. *Annual Review of Cell and Developmental Biology* **1998,** *14*, 111-136.

39. Epand, R. M., Cholesterol in bilayers of sphongomyelin or dihydrosphingomyelin at concentrations found in ocular lens membrane. *Biophysical journal* **2003,** *84* (5), 3102-3110.

40. Cenedella, R. J., Apparent coordination of plasma membrane component synthesis in the lens. *Investigative Ophthalmology & Visual Science* **1993,** *34* (7), 2186-2194.

41. Harding, J., *Biochemistry of the Eye*. Taylor & Francis: 1998.

42. Lynnerup, N.; Kjeldsen, H.; Heegaard, S.; Jacobsen, C.; Heinemeier, J., Radiocarbon Dating of the Human Eye Lens Crystallines Reveal Proteins without Carbon Turnover throughout Life. *PLOS ONE* **2008,** *3* (1), e1529.

43. Hughes, J. R.; Levchenko, V. A.; Blanksby, S. J.; Mitchell, T. W.; Williams, A.; Truscott, R. J. W., No turnover in lens lipids for the entire human lifespan. *eLife* **2015,** *4*, e06003.

44. Sabah, J. R.; Davidson, H.; McConkey, E. N.; Takemoto, L., In vivo passage of albumin from the aqueous humor into the lens. *Molecular Vision* **2004,** *10*, 254.

45. Sabah, J.; McConkey, E.; Welti, R.; Albin, K.; Takemoto, L. J., Role of albumin as a fatty acid carrier for biosynthesis of lens lipids. *Experimental Eye Research* **2005,** *80* (1), 31-36.

46. Sabah, J. R.; Schultz, B. D.; Brown, Z. W.; Nguyen, A. T.; Reddan, J.; Takemoto, L. J., Transcytotic Passage of Albumin through Lens Epithelial Cells. *Investigative Ophthalmology & Visual Science* **2007,** *48* (3), 1237-1244.

47. Fahy, E.; Subramaniam, S.; Brown, H. A.; Glass, C. K.; Merrill, A. H.; Murphy, R. C.; Raetz, C. R. H.; Russell, D. W.; Seyama, Y.; Shaw, W.; Shimizu, T.; Spener, F.; van Meer, G.; VanNieuwenhze, M. S.; White, S. H.; Witztum, J. L.; Dennis, E. A., A comprehensive classification system for lipids. *Journal of Lipid Research* **2005,** *46* (5), 839-862.

48. Fahy, E.; Subramaniam, S.; Murphy, R. C.; Nishijima, M.; Raetz, C. R. H.; Shimizu, T.; Spener, F.; van Meer, G.; Wakelam, M. J. O.; Dennis, E. A., Update of the LIPID MAPS comprehensive classification system for lipids. *Journal of Lipid Research* **2009,** *50* (Supplement), S9-S14.

49. Estrada, R.; Puppato, A.; Borchman, D.; Yappert, M. C., Reevaluation of the phospholipid composition in membranes of adult human lenses by 31P NMR and MALDI MS. *Biochimica et Biophysica Acta (BBA) - Biomembranes* **2010,** *1798* (3), 303-311.

50. Borchmann, D.; Byrdwell, W. C.; Yappert, M. C., Regional and age-dependent differences in the phospholipid composition of human lens membranes. *Investigative Ophthalmology & Visual Science* **1994,** *35* (11), 3938-3942.

51. Rodemer, C.; Thai, T.-P.; Brugger, B.; Kaercher, T.; Werner, H.; Nave, K.-A.; Wieland, F.; Gorgas, K.; Just, W. W., Inactivation of ether lipid biosynthesis causes male infertility, defects in eye development and optic nerve hypoplasia in mice. *Human Molecular Genetics* **2003,** *12* (15), 1881-1895.

52. Merrill, A. H.; Stokes, T. H.; Momin, A.; Park, H.; Portz, B. J.; Kelly, S.; Wang, E.; Sullards, M. C.; Wang, M. D., Sphingolipidomics: a valuable tool for understanding the roles of sphingolipids in biology and disease. *Journal of Lipid Research* **2009,** *50* (Supplement), S97-S102.

53. Hughes, J. R.; Deeley, J. M.; Blanksby, S. J.; Leisch, F.; Ellis, S. R.; Truscott, R. J. W.; Mitchell, T. W., Instability of the cellular lipidome with age. *AGE* **2012,** *34* (4), 935-947.

54. Byrdwell, W. C.; Borchman, D.; Porter, R. A.; Taylor, K. G.; Yappert, M. C., Separation and characterization of the unknown phospholipid in human lens membranes. *Investigative Ophthalmology & Visual Science* **1994,** *35* (13), 4333-43.

55. Ariga, T.; Tao, R. V.; Lee, B. C.; Yamawaki, M.; Yoshino, H.; Scarsdale, N. J.; Kasama, T.; Kushi, Y.; Yu, R. K., Glycolipid composition of human cataractous lenses. Characterisation of Lewisx glycolipids. *Journal of Biological Chemistry* **1994,** *269* (4), 2667-2675.

56. Michel, C.; van Echten-Deckert, G.; Rother, J.; Sandhoff, K.; Wang, E.; Merrill, A. H., Characterisation of Ceramide Synthesis. *Journal of Biological Chemistry* **1997,** *272* (36), 22432-22437.

57. Merrill, A. H., Sphingolipid and Glycosphingolipid Metabolic Pathways in the Era of Sphingolipidomics. *Chemistry Review* **2011,** *111* (10), 6387-6422.

58. Merrill, A. H., De Novo Sphingolipid Biosynthesis: A Necessary, but Dangerous, Pathway. *Journal of Biological Chemistry* **2002,** *277* (29), 25843-25846.

59. Futerman, A. H.; Riezman, H., The ins and outs of sphingolipid synthesis. *Trends in Cell Biology* **2005,** *15* (6), 312-318.

60. Ogiso, M.; Komoto, M.; Okinaga, T.; Koyota, S.; Hoshi, M., Age-related changes in ganglioside composition in human lens. *Experimental Eye Research* **1995,** *60* (3), 317-323.

61. Sarkar, C. P.; Cenedella, R. J., Gangliosides in normal and cataractous lenses of several species. *Biochimica et Biophysica Acta (BBA) - Lipids and Lipid Metabolism* **1982,** *711* (3), 503-508.

62. Ogiso, M.; Saito, N.; Sudo, K.; Kubo, H.; Hirano, S.; Komoto, M., Increase in lens gangliosides due to aging and cataract progression in human senile cataract. *Investigative Ophthalmology & Visual Science* **1990,** *31* (10), 2171-9.

63. Ogiso, M.; Okinaga, T.; Ohta, M.; Komoto, M.; Hoshi, M., Identification and synthetic pathway of sialyl-Lewisx-containing neolacto-series gangliosides in lens tissues. l. Characterisation of gangliosides in human senile cataractous lens. *Biochimica et Biophysica Acta (BBA) - Lipids and Lipid Metabolism* **1995,** *1256* (2), 166-174.

64. Takáts, Z.; Wiseman, J. M.; Gologan, B.; Cooks, R. G., Mass Spectrometry Sampling Under Ambient Conditions with Desorption Electrospray Ionisation. *Science* **2004,** *306* (5695), 471-473.

65. Blatherwick, E. Q.; Van Berkel, G. J.; Pickup, K.; Johansson, M. K.; Beaudoin, M.-E.; Cole, R. O.; Day, J. M.; Iverson, S.; Wilson, I. D.; Scrivens, J. H.; Weston, D. J., Utility of spatially-resolved atmospheric pressure surface sampling and ionisation techniques as alternatives to mass spectrometric imaging (MSI) in drug metabolism. *Xenobiotica* **2011,** *41* (8), 720-734.

66. Seng, J. A.; Ellis, S. R.; Hughes, J. R.; Maccarone, A. T.; Truscott, R. J. W.; Blanksby, S. J.; Mitchell, T. W., Characterisation of sphingolipids in the human lens by thin layer chromatography–desorption electrospray ionisation mass spectrometry. *Biochimica et Biophysica Acta (BBA) - Molecular and Cell Biology of Lipids* **2014,** *1841* (9), 1285-1291.

67. Ellis, S. R.; Wu, C.; Deeley, J. M.; Zhu, X.; Truscott, R. J. W.; Panhuis, M.; Cooks, R. G.; Mitchell, T. W.; Blanksby, S. J., Imaging of Human Lens Lipids by Desorption Electrospray Ionisation Mass Spectrometry. *Journal of American Society of Mass Spectrometry* **2010,** *21*, 2095-2104.

68. Hughes, J.; Deeley, J.; Blanksby, S.; Leisch, F.; Ellis, S.; Truscott, R.; Mitchell, T., Instability of the cellular lipidome with age. *AGE* **2011,** *In Press*.

69. Vidová, V.; Pól, J.; Volný, M.; Novák, P.; Havlíček, V.; Wiedmer, S. K.; Holopainen, J. M., Visualizing spatial lipid distribution in porcine lens by MALDI imaging high-resolution mass spectrometry. *Journal of Lipid Research* **2010,** *51* (8), 2295-2302.

70. Ogiso, M., Implication of glycolipids in lens fiber development. *Acta Biochimica Polonica* **1998,** *45* (2), 501-507.

71. Iwamori, M., A new turning point in glycosphingolipid research. *Human Cell* **2005,** *18* (3), 117-133.

72. Simons, K.; Ikonen, E., Functional rafts in cell membranes. *Nature* **1997,** *387* (6633), 569-572.

73. Ogiso, M.; Saito, N.; Sudo, K.; Kubo, H.; Hirano, S.; Komoto, M., Increase in lens gangliosides due to aging and cataract progression in human senile cataract. *Investigative Ophthalmology & Visual Science* **1990,** *31* (10), 2171-2179.

74. Bron, A. J.; Koretz, J.; Maraini, G.; Harding, J. J., The Ageing Lens. *Ophthalmologica* **2000,** *214* (1), 86-86-104.

75. Heys, K. R.; Cram, S. L.; Truscott, R. J., Massive increase in the stiffness of the human lens nucleus with age: the basis for presbyopia? *Molecular Vision* **2004,** *16* (10), 956-963.

76. Bloemendal, H.; de Jong, W.; Jaenicke, R.; Lubsen, N. H.; Slingsby, C.; Tardieu, A., Ageing and vision: structure, stability and function of lens crystallins. *Progress in Biophysics and Molecular Biology* **2004,** *86* (3), 407-485.

77. Heys, K. R.; Friedrich, M. G.; Truscott, R. J. W., Presbyopia and heat: changes associated with aging of the human lens suggest a functional role for the small heat shock protein, α-crystallin, in maintaining lens flexibility. *Aging Cell* **2007,** *6* (6), 807-815.

78. Boyle, D. L.; Takemoto, L., EM immunolocalization of α-crystallins: Association with the plasma membrane from normal and cataractous human lenses. *Current Eye Research* **1996,** *15* (5), 577-582.

79. Gonen, T.; Cheng, Y.; Kistler, J.; Walz, T., Aquaporin-0 Membrane Junctions Form Upon Proteolytic Cleavage. *Journal of Molecular Biology* **2004,** *342* (4), 1337-1345.

80. Gonen, T.; Cheng, Y.; Sliz, P.; Hiroaki, Y.; Fujiyoshi, Y.; Harrison, S. C.; Walz, T., Lipid-protein interactions in double-layered two-dimensional AQP0 crystals. *Nature* **2005,** *438* (7068), 633.

81. Okamura, T.; Miyoshi, I.; Takahashi, K.; Mototani, Y.; Ishigaki, S.; Kon, Y.; Kasai, N., Bilateral congenital cataracts result from a gain-of-function mutation in the gene for aquaporin-0 in mice. *Genomics* **2003,** *81* (4), 361-368.

82. Pescosolido, N.; Barbato, A.; Giannotti, R.; Komaiha, C.; Lenarduzzi, F., Age-related changes in the kinetics of human lenses: prevention of the cataract. *International Journal of Ophthalmology* **2016,** *9* (10), 1506-1517.

83. Barbazetto, I. A.; Liang, J.; Chang, S.; Zheng, L.; Spector, A.; Dillon, J. P., Oxygen tension in the rabbit lens and vitreous before and after vitrectomy. *Experimental Eye Research* **2004,** *78* (5), 917-924.

84. Babizhayev, M. A.; Deyev, A. I.; Linberg, L. F., Lipid peroxidation as a possible cause of cataract. *Mechanisms of Ageing and Development* **1988,** *44* (1), 69-89.

85. Borchman, D.; Lamba, O.; Salmassi, S.; Lou, M.; Cecilia Yappert, M., The dual effect of oxidation on lipid bilayer structure. *Lipids* **1992,** *27* (4), 261-265.

86. McGinty, S. J.; Truscott, R. J. W., Presbyopia: the first stage of nuclear cataract? *Opthalmic Research* **2006,** *38* (3), 137.

87. Truscott, R. J., Presbyobia. Emerging from a blur towards understanding of the molecular basis for this most common eye condition. *Experimental Eye Research* **2009,** *88* (2), 241-247.

88. Ogiso, M.; Irie, A.; Kubo, H.; Komoto, M.; Matsuno, T.; Koide, Y.; Hoshi, M., Characterisation of Neutral Glycosphingolipids in Human Cataractous Lens. *Journal of Biological Chemistry* **1993,** *268*, 13242-13247.

89. Grey, A. C., MALDI imaging of the eye: Mapping lipid, protein and metabolite distributions in aging and ocular disease. *International Journal of Mass Spectrometry* **2016,** *401*, 31-38.

90. Buchberger, A. R.; DeLaney, K.; Johnson, J.; Li, L., Mass Spectrometry Imaging: A Review of Emerging Advancements and Future Insights. *Analytical Chemistry* **2018,** *90* (1), 240-265.

91. Khalil, S. M.; Römpp, A.; Pretzel, J.; Becker, K.; Spengler, B., Phospholipid Topography of Whole-Body Sections of the Anopheles stephensi Mosquito, Characterized by High-Resolution Atmospheric-Pressure Scanning Microprobe Matrix-Assisted Laser Desorption/Ionization Mass Spectrometry Imaging. *Analytical Chemistry* **2015,** *87* (22), 11309-11316.

92. Nazari, M.; Muddiman, D. C., Polarity switching mass spectrometry imaging of healthy and cancerous hen ovarian tissue sections by infrared matrix-assisted laser desorption electrospray ionization (IR-MALDESI). *The Analyst* **2016,** *141* (2), 595-605.

93. Phan, N. T. N.; Mohammadi, A. S.; Dowlatshahi Pour, M.; Ewing, A. G., Laser Desorption Ionization Mass Spectrometry Imaging of Drosophila Brain Using Matrix Sublimation versus Modification with Nanoparticles. *Analytical Chemistry* **2016,** *88* (3), 1734-1741.

94. Hayasaka, T.; Goto-Inoue, N.; Sugiura, Y.; Zaima, N.; Nakanish, H.; Ohishi, K.; Nakanish, S.; Naito, T.; Taguchi, R.; Setou, M., Matrix-assisted laser desorption/ionization quadrupole ion trap time-of-flight (MALDI-QIT-TOF)-based imaging mass spectrometry reveals a layered distribution of phospholipid molecular species in the mouse retina. *Rapid Communications in Mass Spectrometry* **2008,** *22* (21), 3415-3426.

95. Hayasaka, T.; Goto-Inoue, N.; Zaima, N.; Shrivas, K.; Kashiwagi, Y.; Yamamoto, M.; Nakamoto, M.; Setou, M., Imaging Mass Spectrometry with Silver Nanoparticles Reveals the Distribution of Fatty Acids in Mouse Retinal Sections. *Journal of the American Society for Mass Spectrometry* **2010,** *21* (8), 1446-1454.

96. Roy, M. C.; Nakanishi, H.; Takahashi, K.; Nakanishi, S.; Kajihara, S.; Hayasaka, T.; Setou, M.; Ogawa, K.; Taguchi, R.; Naito, T., Salamander retina phospholipids and their localization by MALDI imaging mass spectrometry at cellular size resolution. *Journal of Lipid Research* **2011,** *52* (3), 463-470.

97. Berry, K. A. Z.; Gordon, W. C.; Murphy, R. C.; Bazan, N. G., Spatial organization of lipids in the human retina and optic nerve by MALDI imaging mass spectrometry. *Journal of Lipid Research* **2014,** *55* (3), 504-515.

98. Sun, N.; Ly, A.; Meding, S.; Witting, M.; Hauck, S. M.; Ueffing, M.; Schmitt-Kopplin, P.; Aichler, M.; Walch, A., High-resolution metabolite imaging of light and dark treated retina using MALDI-FTICR mass spectrometry. *Proteomics* **2014,** *14* (7-8), 913-923.

99. Anderson, D. M. G.; Ablonczy, Z.; Koutalos, Y.; Spraggins, J.; Crouch, R. K.; Caprioli, R. M.; Schey, K. L., High Resolution MALDI Imaging Mass Spectrometry of Retinal Tissue Lipids. *Journal of the American Society for Mass Spectrometry* **2014,** *25* (8), 1394-1403.

100. Anderson, D. M. G.; Spraggins, J. M.; Rose, K. L.; Schey, K. L., High Spatial Resolution Imaging Mass Spectrometry of Human Optic Nerve Lipids and Proteins. *Journal of the American Society for Mass Spectrometry* **2015,** *26* (6), 940-947.

101. Anderson, D. M. G.; Mills, D.; Spraggins, J.; Lambert, W. S.; Calkins, D. J.; Schey, K. L., High-resolution matrix-assisted laser desorption ionization-imaging mass spectrometry of lipids in rodent optic nerve tissue. *Molecular vision* **2013,** *19*, 581-92.

102. Rujoi, M.; Estrada, R.; Yappert, M. C., In situ MALDI-TOF MS regional analysis of neutral phospholipids in lens tissue. *Analytical Chemistry* **2004,** *76* (6), 1657-1663.

103. Pol, J.; Vidova, V.; Hyotylainen, T.; Volny, M.; Novak, P.; Strohalm, M.; Kostiainen, R.; Havlicek, V.; Wiedmer, S. K.; Holopainen, J. M., Spatial Distribution of Glycerophospholipids in the Ocular Lens. *Plos One* **2011,** *6* (4).

104. Le, C. H.; Han, J.; Borchers, C. H., Dithranol as a MALDI Matrix for Tissue Imaging of Lipids by Fourier Transform Ion Cyclotron Resonance Mass Spectrometry. *Analytical Chemistry* **2012,** *84* (19), 8391-8398.

105. Ifa, D. R.; Wiseman, J. M.; Song, Q.; Cooks, R. G., Development of capabilities for imaging mass spectrometry under ambient conditions with desorption electrospray ionization (DESI). *International Journal of Mass Spectrometry* **2007,** *259* (1), 8-15.

106. Venter, A.; Sojka, P. E.; Cooks, R. G., Droplet dynamics and ionization mechanisms in desorption electrospray ionization mass spectrometry. *Analytical Chemistry* **2006,** *78* (24), 8549-8555.

107. Takáts, Z.; Wiseman, J. M.; Cooks, R. G., Ambient mass spectrometry using desorption electrospray ionization (DESI): instrumentation, mechanisms and applications in forensics, chemistry, and biology. *Journal of Mass Spectrometry* **2005,** *40* (10), 1261-1275.

108. Ellis, S. R.; Brown, S. H.; in het Panhuis, M.; Blanksby, S. J.; Mitchell, T. W., Surface analysis of lipids by mass spectrometry: more than just imaging. *Progress in lipid research* **2013,** *52* (4), 329-353.

109. Han, J.; Schey, K. L., MALDI tissue Imaging of ocular lens alpha-crystallin. *Investigative Ophthalmology & Visual Science* **2006,** *47* (7), 2990-2996.

110. Thibault, D. B.; Gillam, C. J.; Grey, A. C.; Han, J.; Schey, K. L., MALDI tissue profiling of integral membrane proteins from ocular tissues. *Journal of the American Society for Mass Spectrometry* **2008,** *19* (6), 814-822.

111. Schey, K. L.; Anderson, D. M.; Rose, K. L., Spatially-Directed Protein Identification from Tissue Sections by Top-Down LC-MS/MS with Electron Transfer Dissociation. *Analytical Chemistry* **2013,** *85* (14), 6767-6774.

112. Debois, D.; Bertrand, V.; Quinton, L.; De Pauw-Gillet, M.-C.; De Pauw, E., MALDI-In Source Decay Applied to Mass Spectrometry Imaging: A New Tool for Protein Identification. *Analytical Chemistry* **2010,** *82* (10), 4036-4045.

113. Stella, D. R.; Floyd, K. A.; Grey, A. C.; Renfrow, M. B.; Schey, K. L.; Barnes, S., Tissue Localization and Solubilities of alpha A-crystallin and its Numerous C-terminal Truncation Products in Pre- and Postcataractous ICR/f Rat Lenses. *Investigative Ophthalmology & Visual Science* **2010,** *51* (10), 5153-5161.

114. Grey, A. C.; Schey, K. L., Age-Related Changes in the Spatial Distribution of Human Lens alpha-Crystallin Products by MALDI Imaging Mass Spectrometry. *Investigative Ophthalmology & Visual Science* **2009,** *50* (9), 4319-4329.

115. Su, S.-P.; McArthur, J. D.; Aquilina, J. A., Localization of low molecular weight crystallin peptides in the aging human lens using a MALDI mass spectrometry imaging approach. *Experimental Eye Research* **2010,** *91* (1), 97-103.

116. Ronci, M.; Sharma, S.; Chataway, T.; Burdon, K. P.; Martin, S.; Craig, J. E.; Voelcker, N. H., MALDI-MS-Imaging of Whole Human Lens Capsule. *Journal of Proteome Research* **2011,** *10* (8), 3522-3529.

117. Ronci, M.; Sharma, S.; Martin, S.; Craig, J. E.; Voelcker, N. H., MALDI MS imaging analysis of apolipoprotein E and lysyl oxidase-like 1 in human lens capsules affected by pseudoexfoliation syndrome. *Journal of Proteomics* **2013,** *82*, 27-34.

118. Pol, J.; Faltyskova, H.; Krasny, L.; Volny, M.; Vlacil, O.; Hajduch, M.; Lemr, K.; Havlicek, V., Age-related changes in the lateral lipid distribution in a human lens described by mass spectrometry imaging. *European Journal of Mass Spectrometry* **2015,** *21* (3), 297-303.

Chapter 2: Method Development

2.1 Methods development for MALDI-Imaging

2.1.1 Background

MALDI requires the deposition of a layer of matrix, which can be any compound that can absorb the laser wavelength to allow gentle energy transfer to ionise the analytes on the tissue. The MALDI process is complex, where the matrix aids both desorption and ionisation of the molecules. The matrix plays a vital role in diluting and isolating analytes as well as acting as a mediator for energy absorption.[1] Further information about multiple models of ionisation such as photoionisation and photochemical reaction pathways have been reviewed previously in literature.[1] The laser then rasters across the tissue and the mass spectra at a defined X,Y-coordinate is translated into pixels forming an image based on ion intensity. The spatial resolution of an image is dependent on the laser beam size, the distance between each laser spot and the matrix crystal size. A modified schematic diagram of the MALDI work flow for human lens is shown in Figure 2.1.

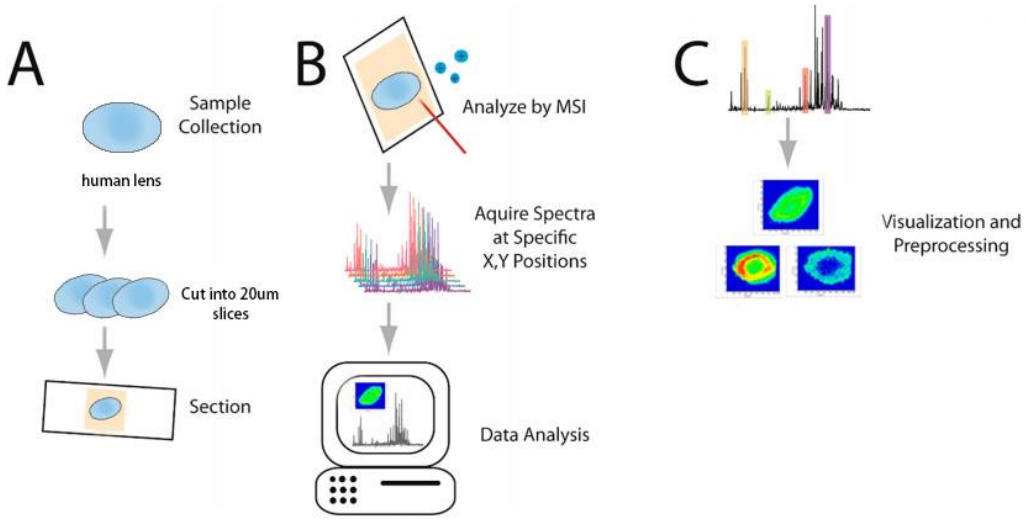

Figure 2.1: A modified schematic diagram of MALDI imaging workflow for human lens analysis. A) sample preparation; B) MS analysis; and C) data processing.[2]

Matrix deposition is an essential step during the sample preparation process to ensure molecules are extracted and desorbed efficiently and uniformly across the tissue surface.[3, 4] In wet extraction approaches, the matrix should be deposited on the tissue surface to produce a uniform layer of crystals that dissolves the analytes and facilitates the desorption or ionisation process during laser irradiation.[5] Furthermore, deposition of the matrix solution should not dissolve the analytes excessively to maintain their spatial distribution in the tissue.[6] This can be achieved by repeated steps of applying a minimal amount of matrix deposition and then drying.

Methods for matrix application have been developed to maximize ion generation and increase the spatial resolution of an image.[4, 7] These include dried droplet deposition, electrospray deposition, inkjet deposition and airbrush deposition.[6, 8] Manual aerosol spray deposition provides good homogeneity and spatial resolution of the images nevertheless, this is a manual procedure and suffers from low reproducibility.[9, 10] If the tissue is too wet during the process, large matrix crystals will be formed, resulting in the loss of spatial resolution. Alternatively, if it is too dry the matrix molecule will not be incorporated into the tissue effectively. Therefore, automated matrix deposition systems such as ImagePrep™ (Bruker Daltonics Inc.), TM Sprayer™ (HTX Technologies, LLC) and Potrait Spotter™ (Labcyte Inc.) have been developed.[4, 10, 11] The advantage of automated system is the reduction in sample-to-sample variation in matrix deposition, which leads to irreproducible mass spectral images. However, wet deposition strategies can lead to delocalisation of analytes via diffusion through droplets.[12] An alternative strategy for matrix deposition is sublimation, which will be discussed in Section 2.1.5

The aim of this chapter is to trial matrix deposition methods suitable for lens lipid imaging and optimise matrix choice for lens lipid detection.

2.1.2 Tissue preparation

Sample preparation is the key to obtaining high quality MALDI MS images. Essential factors during the preparation of a lens tissue slice include the slicing temperature, thickness of the slice, and the

consistency of the tissue and matrix deposition. The packed fibre cells in the lens are especially susceptible to damage during cutting. Careless handling may result in undesirable loss of tissue, and hence loss of chemical and spatial information.[5] To prevent this, different mounting techniques were tested. Previous studies on lens proteins have shown that a methanol[13, 14] or ethanol soft-landing technique[15] can aid in maintaining the integrity of the lens tissue. This technique is not suitable for lipids as they are more soluble in ethanol than proteins, which results in lipid delocalisation and compromised spatial resolution. In this study, tissues were thaw-mounted onto a cold glass slide using body temperature with a finger pressed on the underneath surface of the glass slide.

For MALDI-MS analysis, lenses were mounted onto a cryostat holder using a minimal amount of OCT at – 20 °C in a cryo-microtome (Leica CM 1950, Leica Biosystems, Australia). The lenses were sliced in the transverse plane to produce 20 µm thick slices and were thaw-mounted onto the glass slide. The samples were immediately stored at -20 °C until analysed. Prior to analysis, samples were dried in a desiccator for 10 minutes.

2.1.3 Mass spectrometry parameters

The samples were then analysed by an LTQ-Orbitrap XL mass spectrometer (ThermoScientific, Australia) equipped with a MALDI source. The entire surface of the human lens was examined with a raster step size of 100 µm. The laser performed 50 shots per spot with a summed spectrum collected from each spot. The mass resolution at *m/z* 400 was 33000 and the mass range acquired was *m/z* 400-2000. The instrument was externally calibrated using commercially available Calmix for LTQ-Orbitrap (Sigma Aldrich, Australia) in both ion modes. MS imaging data were visualized by ImageQuest 1.0 (ThermoScientific, Australia).

2.1.4 ImagePrep™

The automated matrix deposition system used in the current study was an ImagePrep™ system (Bruker Daltonics, Bremen) as shown in Figure 2.2.[16]

Figure 2.2: The ImagePrep™ station for matrix deposition. (Image from ImagePrep Manual)[16]

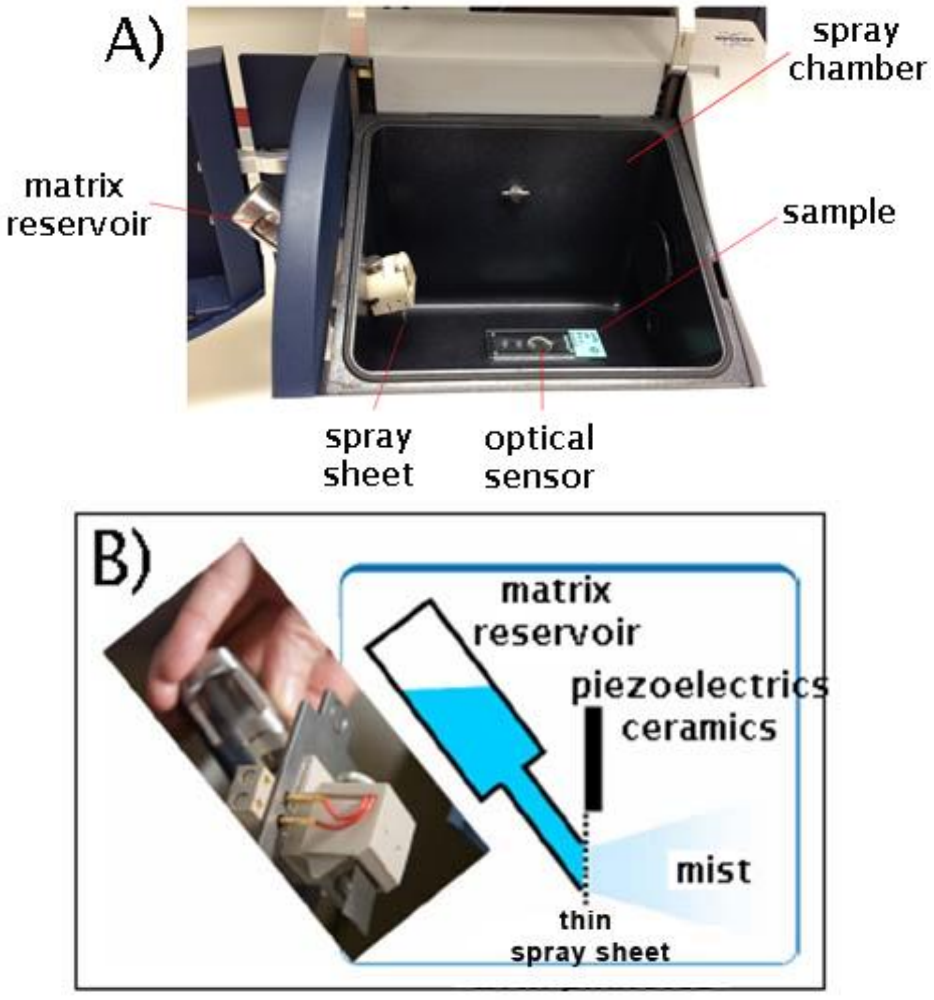

Figure 2.3: (A) The set-up of the sample prior to matrix deposition. (B) A schematic diagram of the spray head.

The ImagePrep™ device produces matrix aerosol by vibrational vaporisation. The set-up of the spray chamber is shown in

Figure *2.3*A. The matrix solution was first loaded into the matrix reservoir and upon the vibration of the thin spray sheet, a mist of matrix solution was produced through the pinholes as shown in

Figure *2.3*B. During the entire preparation process the spray chamber was filled with nitrogen to prevent sample oxidation and to obtain reproducible experimental conditions independent of the ambient humidity. The sample was placed on top of the optical sensor, without blocking its activity. The optical sensor monitors light scattered from the crystalline matrix layer to control relevant parameters such as wetness, matrix layer thickness, drying rate, deposition periods and intervals. It takes 30-100 cycles to apply a homogenous coating of matrix to a typical microscope glass slide, depending on the desired matrix thickness. Each cycle consists of three phases: i) deposition of the droplet layer; ii) incubation, which is the waiting period after each spray (no active drying with gas flow); and iii) active drying (partially/completely). Increased incubation time provides better incorporation of analytes into the matrix crystals, however it also increases the overall preparation time. The wetness of the tissue relies on the drying phase. Although a wetter tissue allows a better extraction, the spatial resolution can be sacrificed due to analyte delocalisation. These parameters can be optimised manually depending on individual sample needs.

Table 2.1: Instrument parameters for ImagePrep™.

Spray time	**Incubation time**	**Drying time**	**Total cycles**
2 s	30 s	60 s	200

Table 2.1 shows the most optimum parameters used in this experiment. A total of 200 spray cycles were applied onto a lens tissue on a glass slide with 20 mg/ml 2,5-dihydroxybenzoic acid (DHB) in 50% methanol + 0.2% trifluoroacetic acid (TFA) as the matrix solvent. The deposition time for the entire

process was approximately 90 minutes.

A snapshot of matrix post-deposition is shown in Figure 2.4A. Despite being a commonly used matrix for MALDI-MS analysis, DHB forms long and visible crystals on the tissue using this matrix deposition method, which is not suitable for imaging. This agrees with previous findings, where DHB crystals appear to be longer than other matrices and the formation of the crystals is highly dependent on the solvent evaporation rate.[17] These crystals are larger than the laser beam diameter (~60 μm), as shown in Figure 2.4B, and therefore affect the spatial resolution of the image acquired.

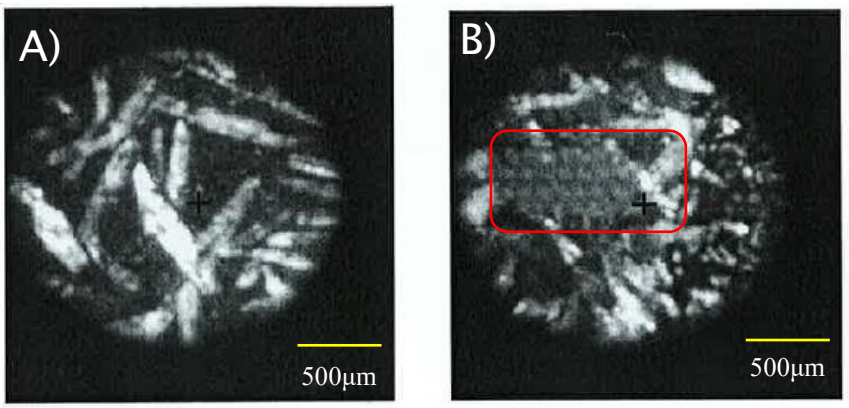

Figure 2.4: A) Snapshot of DHB crystals formed on tissue via the camera in the MALDI source. B) Snapshot of laser rastering across the tissue during MS analysis at 100 μm spatial resolution. Ablation spots are circled in red.

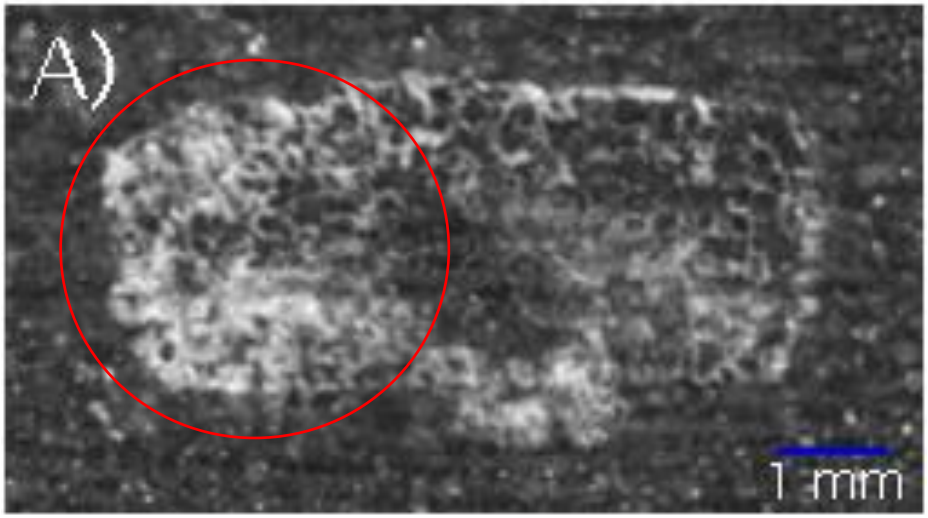

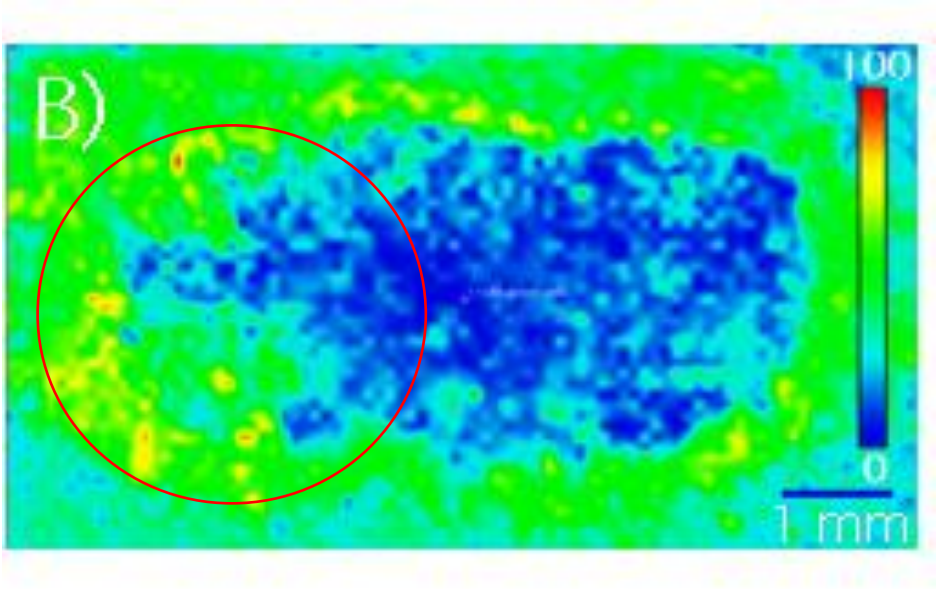

Figure 2.5: A) An optical image of a 74 year-old human lens tissue after DHB matrix deposition by ImagePrep™. The white spots in the red circle showed excessive matrix (not homogenous) deposited on the tissue. B) A total ion count diagram of the same lens tissue. The "hot spot" is shown towards the left of the image (red circle) where yellow and red dots are visible.

Moreover, the crystals formed on the tissue were not homogeneous, where larger crystals tended to form around the edges of the tissue (red circled region in Figure 2.5A). This created what is referred to as matrix "hot spots". Figure 2.5B shows that a higher total ion count is observed at the regions with an increased matrix crystal density while the areas with lesser matrix have a relatively lower total ion

count. The use of solvent also encourages analyte delocalisation, as some lipid ions were detected outside the tissue area as demonstrated in Figure 2.5B.

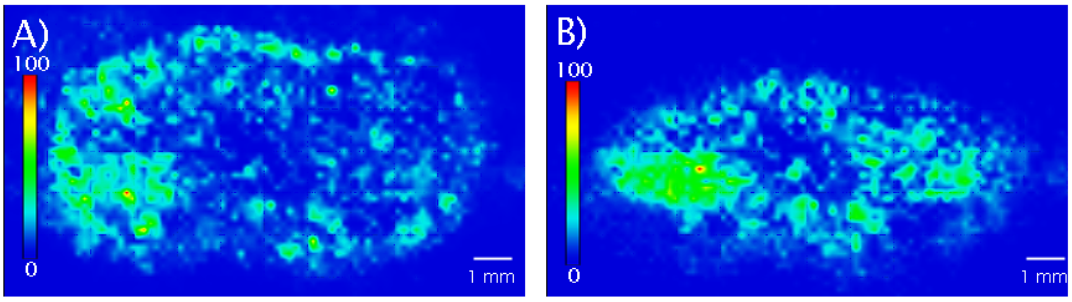

Figure 2.6: A) The distribution image of m/z 743 which corresponds to the $[M+K]^+$ ion of SM (d18:0/16:0); and B) The distribution image of m/z 578 which corresponds to the $[M+K]^+$ ion of Cer (d18:0/16:0).

The distribution image of individual lipids in the lens is also affected by these "hot spots". The distribution images for SM (d18:0/16:0) (Figure 2.6A) and Cer (d18:0/16:0), (Figure 2.6B) were obtained from the same lens slice shown in Figure 2.5. As with the total ion count, these images clearly demonstrate that the lipid ions are more abundant at "hot spots" than other areas where less matrix crystals were observed. The influence of the matrix "hot spots" cannot be neglected as they mask the real distribution and relative abundance of the lipid investigated and decrease the spatial resolution of the image. The higher abundance of the ion at the "hot spots" may be explained by better incorporation of analytes into the matrix crystals.[18] It is possible that the matrix solvent sat on the surface for a longer period to form larger crystals compared to other areas.

Several attempts to improve the Imageprep™ deposition method were performed, however, these were not successful. As this wet method requires the matrix to be in an organic solvent that is compatible with Imageprep™, other matrices with a lower solubility in methanol or acetonitrile could not be investigated. This method is not suitable for lens lipid analysis as it requires matrices that are soluble in a limited range of organic solvents, produces large crystals, and does not form a homogeneous layer of matrix and results in poor spatial resolution.

2.1.5 Sublimation

The dry methods used previously for imaging include “dusting” the dry matrix onto the tissue and sublimation, with the latter forming a more homogeneous layer of matrix.[19, 20] These solvent-free systems often form a finer layer of matrix crystals on the tissue where sensitivity and spatial resolution can be enhanced, however, the extraction of analytes may not be as efficient as a matrix solvent system.

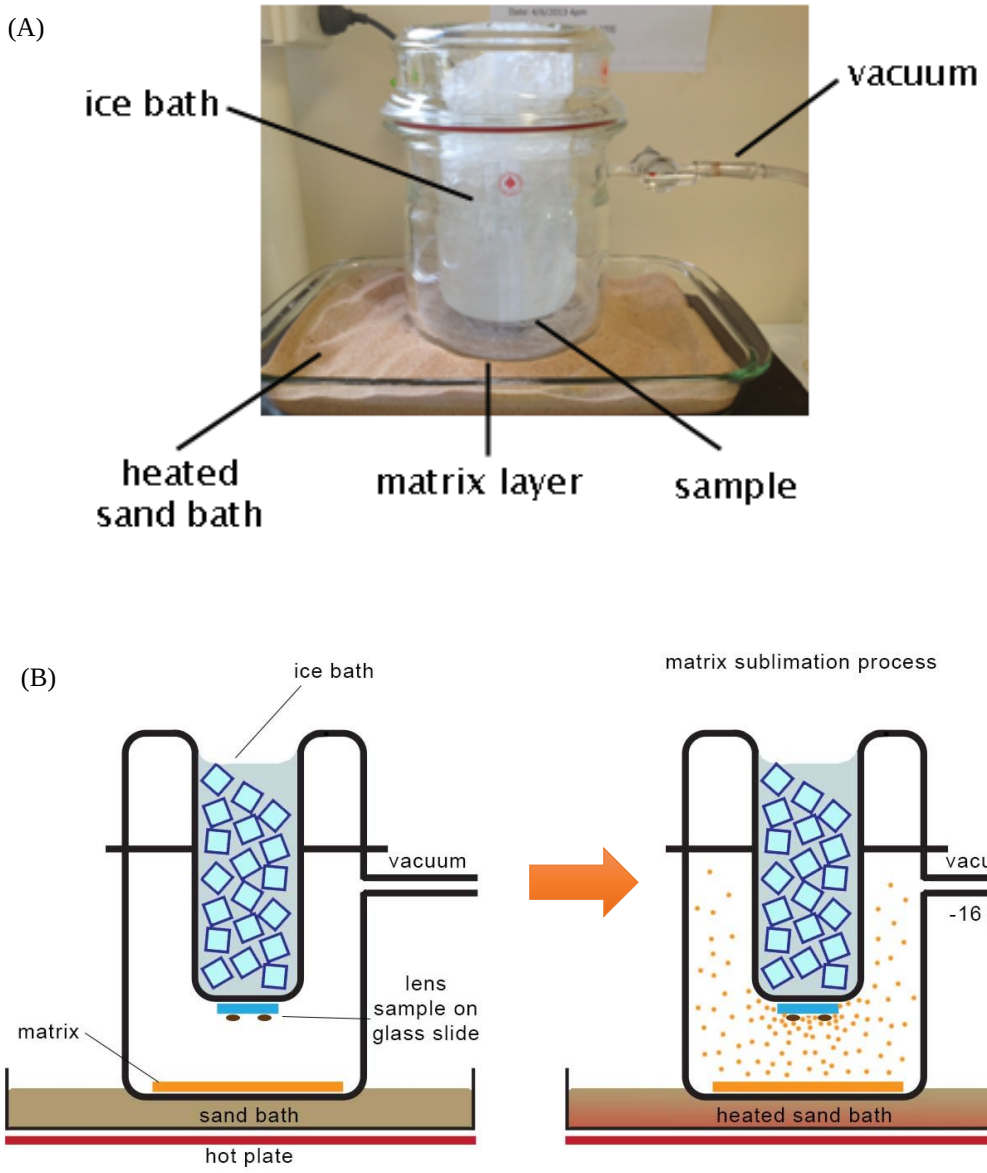

Figure 2.7: (A) The set up of a sublimation apparatus for MALDI-MS analysis sample preparation. (B) Schematic diagram of matrix sublimation process.

The set up of a sublimation apparatus for matrix deposition and a schematic diagram of the sublimation process is shown in Figure 2.7A and B, respectively. Pre-weighted glass slides with the adhered sample are fixed upside-down on a metal plate at the bottom of the inner flat surface of the glass condenser using a heat conductive tape. Matrix (100 mg) was added to the bottom section of the apparatus, dissolved with a small amount of acetone and then dried by rotating a constant nitrogen flow slowly

around the rim of the sublimator. This helped to achieve a more homogeneous layer of matrix. The two sections of the sublimator were assembled with an O-ring seal and were connected to a vacuum pump to produce a chamber pressure of –16 psi. The condenser was then filled with ice and water.

The sublimator was placed in a sand bath and the amount of matrix condensed onto the tissue was empirically determined by adjusting the temperature of the sand bath (heat applied to matrix) and time of sublimation. These were optimised based on the matrix used as the heat applied was approximately 50 ºC lower than its boiling point. A matrix layer that was too thin yielded very few ions and a matrix layer that was too thick yielded only matrix ions. After this time, the post-deposition glass slide with sample was weighed again to calculate the amount of matrix deposited. The optimised conditions, shown in Table 2.2 yield approximately 3 mg (~ 0.16 mg/cm^2) of matrix deposited on the glass slide. The time was optimised for each matrix to achieve the same amount of deposition on the sample.

Table 2.2: Sublimation conditions for different matrices.

Matrix	**Temperature (°C)**	**Time (min)**
2,5-dihydrobenzoic acid (DHB)	110	10
1,5-diaminonapthalene (DAN)	120	6
2-mercaptobenzothiazole (MBT)	115	8

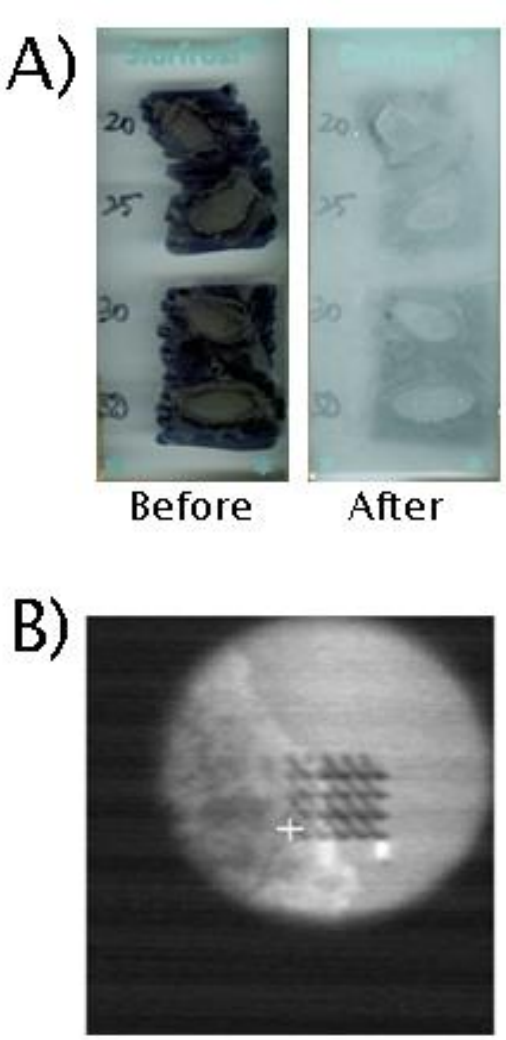

Figure 2.8: A) Glass slide with samples before (left) and after sublimation of DHB (right). B) Snapshot of laser rastering across the sublimed tissue during MS analysis at 100 µm spatial resolution.

A layer of homogeneous fine matrix crystals were deposited onto the glass slide after sublimation as shown Figure 2.8A. A magnified snapshot of the laser rastering across the sublimed tissue showed that no large crystals were formed Figure 2.8B. The crystals formed are visible as a layer of powder and are smaller than the laser beam. This is in contrast with the large crystals formed during wet matrix deposition (see Figure 2.4B) and suggests that the dry method avoids the formation of large crystals on human lens tissue and hence enables a higher spatial resolution for imaging.

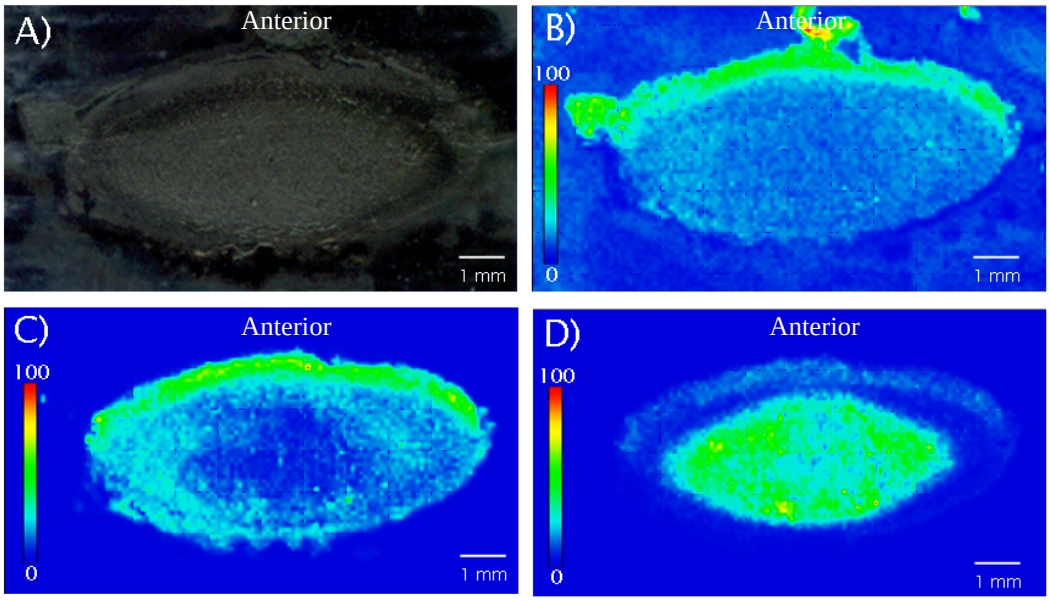

Figure 2.9: A) Optical image of a 51 year-old human lens. B) Total ion count image for the same human lens. C) The distribution image of m/z 705 which corresponds to the $[M+H]^+$ ion of SM (d18:0/16:0); and D) The distribution image of m/z 540 which corresponds to the $[M+H]^+$ ion of Cer (d18:0/16:0).

Figure 2.9A-D shows the optical image, total ion count, distribution of SM (d18:0/16:0) and Cer (d18:0/16:0) of a 51 year-old human lens tissue slice, respectively. The tissue was sliced with the iris attached during the freezing process, which is represented by the green area around the edge of the lens (anterior to the anterior lens surface) in Figure 2.9B. The total ion distribution of the lipid in the lens is homogeneous across the lens. In Figure 2.9C and D, the images of sphingomyelin and ceramide distribution are of greater spatial resolution and there are minimal matrix "hot spots" compared to the images acquired by a wet deposition method (cf. Figure 2.6).

Matrices were chosen according to the maximum number of lipid classes detected during MSI, as shown in Table 2.3. There were the least number of lipid classes detected with DHB in both modes. DAN detected the most classes of lipids in negative ion mode such as PA, PS, PE, LPE, CerP, DHCerP, ST, DHST, SM3, DHSM3, DHGM1, DHGM3 and DHSialyl-Le^X. In positive ion mode, 5 lipid classes were detected by MBT which were SM, DHSM, Cer, DHCer and DHLacCer. Therefore, MBT was used for positive ion mode and DAN was used for negative ion mode during MSI.

Table 2.3: Number of lipid classes detected in positive and negative ion mode for each matrix.

Matrix	No. of lipid class detected in positive mode	No. of lipid class detected in negative mode
2,5-dihydrobenzoic acid (DHB)	4	2
1,5-diaminonapthalene (DAN)	2	13
2-mercaptobenzothiazole (MBT)	5	2

2.1.6 Mass spectrometry parameters for MSI

The samples were analysed by an LTQ-Orbitrap XL mass spectrometer (ThermoScientific, Australia) equipped with a MALDI source. The entire surface of the human lens was examined with a raster step size of 100 µm. The laser performed 50 shots per spot with a summed spectrum collected from each spot. Mass spectra were acquired in both positive (using MBT as the matrix) and negative ion mode (using DAN as the matrix). The mass resolution at *m/z* 400 was 33000 and the mass range acquired was *m/z* 400-2000. The instrument was externally calibrated using commercially available Calmix for LTQ-Orbitrap (Sigma Aldrich, Australia) in both ion modes. MS imaging data were visualized by ImageQuest 1.0 (ThermoScientific, Australia). SM, DHSM, LacCer, Cer and DHCer were detected on lens slices in positive ion mode, with MBT as the matrix. Other classes of sphingolipids were detected in negative ion mode on adjacent lens slices using DAN. The extracted ion count of each sphingolipid was normalized to the total ion count of the spectra to obtain the abundance of the ions. Therefore, the abundance was compared within the same ion mode and same lens only.

2.1.7 Summary

In conclusion, sublimation requires a shorter preparation time (~15 mins) as compared to the ImagePrep™ method (~90 mins) and produces a more homogeneous layer of crystals. Although this is a manual process, which may not produce an identical coating of matrix each time, parameters such as temperature and time are monitored with each sample preparation to minimise inconsistency. Therefore,

samples need to be weighed before and after sublimation to ensure the same possible amount of matrix (~3 mg) is coated each time.

2.2 Method Development for Lipid Quantification (Chapter 5)

2.2.1 Lens Dissection

Sixteen lenses between the ages of 8 and 74 were dissected as described previously.[21] Trephines with diameters of 8, 6, and 4.5 mm were used to dissect lenses into the outer (>8 mm), barrier (8–6 mm), inner (6–4.5mm), and core (4.5 mm) regions, respectively (Figure 2.10).

The trephines were precooled to -20°C. Lenses were decapsulated and placed into a precooled polytetrafluoroethylene (Teflon; DuPont, Wilmington, DE) holder with a 9-mm diameter. An 8-mm trephine was used to remove the outer tissue. The resultant billet was transferred to an 8-mm polytetrafluoroethylene holder, and barrier tissue was removed with a 6-mm trephine. A cold scalpel was used to remove approximately 1 mm from each end from the cylinder (inner core), which was inserted into a 6-mm holder and refrozen. After refreezing, a 4.5-mm trephine was used to separate the core region from the inner region.

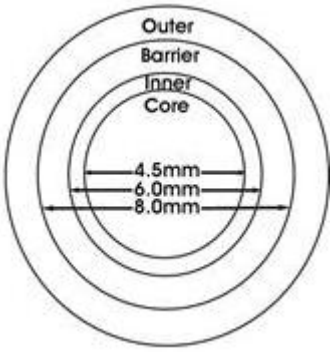

Figure 2.10: Illustration of the four regions of the lens obtained by dissection.[21]

2.2.2 Lipids quantification

A representative spreadsheet that was used for quantification is shown in Figure 2.11. The ion abundance of each lipid were obtained directly from the spectrum. The isotope distribution was

calculated from isotope models for each lipid ion. This was used to predict the ion abundance of the first, second, third, fourth and fifth isotopes. The total ion abundance including all the isotopes were summed and normalised to the concentration of the internal standard. The amount of each lipid was then divided by the weight of lens tissue to give the concentration of lipid per gram of tissue.

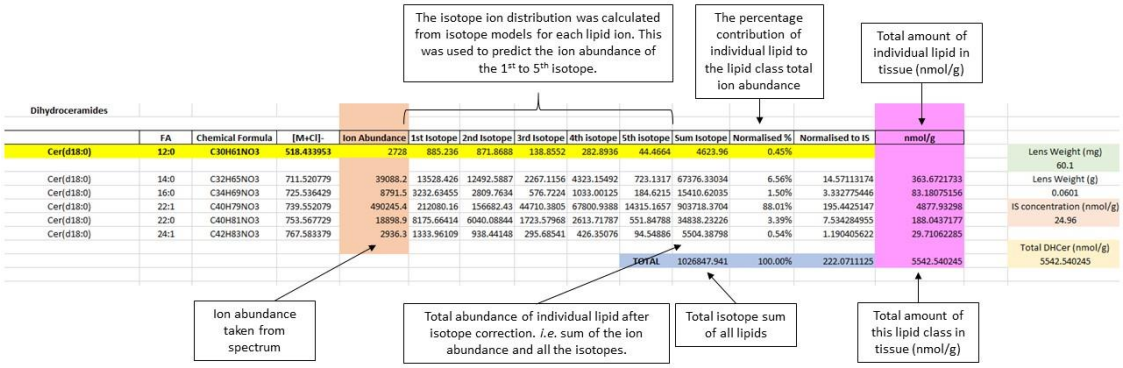

Figure 2.11: A representative spreadsheet used for quantification of lipids.

2.3 References

1. Karas, M.; Glückmann, M.; Schäfer, J., Ionization in matrix-assisted laser desorption/ionization: singly charged molecular ions are the lucky survivors. *Journal of Mass Spectrometry* **2000,** *35* (1), 1-12.

2. Buchberger, A. R.; DeLaney, K.; Johnson, J.; Li, L., Mass Spectrometry Imaging: A Review of Emerging Advancements and Future Insights. *Analytical Chemistry* **2018,** *90* (1), 240-265.

3. Amstalden van Hove, E. R.; Smith, D. F.; Heeren, R. M. A., A concise review of mass spectrometry imaging. *Journal of Chromatography A* **2010,** *1217* (25), 3946-3954.

4. Végvári, Á.; Fehniger, T. E.; Gustavsson, L.; Nilsson, A.; Andrén, P. E.; Kenne, K.; Nilsson, J.; Laurell, T.; Marko-Varga, G., Essential tactics of tissue preparation and matrix nano-spotting for successful compound imaging mass spectrometry. *Journal of Proteomics* **2010,** *73* (6), 1270-1278.

5. Vidová, V.; Pól, J.; Volný, M.; Novák, P.; Havlíček, V.; Wiedmer, S. K.; Holopainen, J. M., Visualizing spatial lipid distribution in porcine lens by MALDI imaging high-resolution mass spectrometry. *Journal of Lipid Research* **2010,** *51* (8), 2295-2302.

6. Baluya, D. L.; Garrett, T. J.; Yost, R. A., Automated MALDI Matrix Deposition Method with Inkjet Printing for Imaging Mass Spectrometry. *Analytical Chemistry* **2007,** *79* (17), 6862-6867.

7. Chaurand, P.; Norris, J. L.; Cornett, D. S.; Mobley, J. A.; Caprioli, R. M., New Developments in Profiling and Imaging of Proteins from Tissue Sections by MALDI Mass Spectrometry. *Journal of Proteome Research* **2006,** *5* (11), 2889-2900.

8. Axelsson, J.; Hoberg, A.-M.; Waterson, C.; Myatt, P.; Shield, G. L.; Varney, J.; Haddleton, D. M.; Derrick, P. J., Improved Reproducibility and Increased Signal Intensity in Matrix-assisted Laser Desorption/Ionization as a Result of Electrospray Sample Preparation. *Rapid Communications in Mass Spectrometry* **1997,** *11* (2), 209-213.

9. Murray, K. K.; Russell, D. H., Aerosol Matrix-Assisted Laser Desorption Ionization Mass Spectrometry. *Journal of the American Society for Mass Spectrometry* **1994,** *5* (1), 1-9.

10. Yamada, Y.; Hidefumi, K.; Shion, H.; Oshikata, M.; Haramaki, Y., Distribution of chloroquine in ocular tissue of pigmented rat using matrix-assisted laser desorption/ionization imaging quadrupole time-of-flight tandem mass spectrometry. *Rapid Communications in Mass Spectrometry* **2011,** *25* (11), 1600-1608.

11. Aichler, M.; Walch, A., MALDI Imaging mass spectrometry: current frontiers and perspectives in pathology research and practice. *Laboratory Investigation* **2015,** *95* (4), 422-431.

12. Dong, Y.; Li, B.; Malitsky, S.; Rogachev, I.; Aharoni, A.; Kaftan, F.; Svatoš, A.; Franceschi, P., Sample Preparation for Mass Spectrometry Imaging of Plant Tissues: A Review. *Frontiers in Plant Science* **2016,** *7* (60).

13. Grey, A. C.; Chaurand, P.; Caprioli, R. M.; Schey, K. L., MALDI Imaging Mass Spectrometry of Integral Membrane Proteins from Ocular Lens and Retinal Tissue†. *Journal of Proteome Research* **2009,** *8* (7), 3278-3283.

14. Grey, A. C.; Schey, K. L., Age-Related Changes in the Spatial Distribution of Human Lens α-Crystallin Products by MALDI Imaging Mass Spectrometry. *Investigative ophthalmology & visual science* **2009,** *50* (9), 4319-4329.

15. Han, J.; Schey, K. L., MALDI Tissue Imaging of Ocular Lens α-Crystallin. *Investigative Ophthalmology & Visual Science* **2006,** *47* (7), 2990-2996.

16. In *ImagePrep user manual*, Bruker Daltonic: 2010; Vol. Revision 3.

17. Dai, Y.; Whittal, R. M.; Li, L., Confocal Fluorescence Microscopic Imaging for Investigating the Analyte Distribution in MALDI Matrices. *Analytical Chemistry* **1996,** *68* (15), 2494-2500.

18. Le, C. H.; Han, J.; Borchers, C. H., Dithranol as a MALDI Matrix for Tissue Imaging of Lipids by Fourier Transform Ion Cyclotron Resonance Mass Spectrometry. *Analytical Chemistry* **2012,** *84* (19), 8391-8398.

19. Puolitaival, S. M.; Burnum, K. E.; Cornett, D. S.; Caprioli, R. M., Solvent-Free Matrix Dry-Coating for MALDI Imaging of Phospholipids. *Journal of the American Society for Mass Spectrometry* **2008,** *19* (6), 882-886.

20. Hankin, J. A.; Barkley, R. M.; Murphy, R. C., Sublimation as a method of matrix application for mass spectrometric imaging. *Journal of the American Society for Mass Spectrometry* **2007,** *18* (9), 1646-1652.

21. Friedrich, M. G.; Truscott, R. J. W., Large-Scale Binding of α-Crystallin to Cell Membranes of Aged Normal Human Lenses: A Phenomenon That Can Be Induced by Mild Thermal Stress. *Investigative Ophthalmology & Visual Science* **2010,** *51* (10), 5145-5152.

Chapter 3: Distribution of Sphingolipids in the Human Lens by Mass Spectrometry Imaging

Jo Ann Seng [a], Jessica R. Nealon [b,d], Stephen J. Blanksby[c], Todd W. Mitchell [b,d]*

[a] School of Chemistry, Faculty of Science, Medicine and Health, University of Wollongong, NSW 2522, Australia.

[b] School of Medicine, Faculty of Science, Medicine and Health, University of Wollongong, NSW 2522, Australia.

[c] Central Analytical Research Facility, Queensland University of Technology, Brisbane, QLD 4000, Australia.

[d] Illawarra Health and Medical Institute, University of Wollongong, NSW 2522, Australia.

[*] Correspondence to: T.W. Mitchell, School of Medicine, University of Wollongong, NSW 2522, Australia. Email: toddm@uow.edu.au

Abstract

The human lens sphingolipdome is unique in that the most abundant sphingolipids contain a saturated dihydrosphinganine backbone. Following recent data that elucidated and characterised the lens sphingolipidome, we aimed to explore the spatial distribution of these sphingolipids in the human lens. Sections of two human lenses aged 51 and 67 were analysed by matrix-assisted laser desorption ionisation imaging mass spectrometry. This study reveals the localisation of sphingolipids in different regions of the lens. This is the first study to determine the distribution of sulfatides, lactosylceramide sulfates and complex gangliosides in the adult human lens, which may be significant for future studies examining age-related changes to the lipid distribution of the human lens.

Keywords

gangliosides, glycosphingolipids, human lens, mass spectrometry imaging, lactosylceramide sulfate, lipidomics, sialyl Lewis acid, sulfatides

Highlights

- Human lens sphingolipid distribution was mapped using MALDI-MS
- First distributions of gangliosides, sulfatides, lactosylceramide sulfates were studied.
- Lipids such as ceramides and ceramide phosphates have complementary distributions.

Abbreviations

2,5-diaminonapthalene (DAN), 2-mercaptobenzathiazole (MBT), ceramide (Cer), ceramide phosphate (CerP), desorption electrospray ionisation (DESI), dihydroceramide (DHCER), dihydroceramidephosphate (DHCerP), dihydromonosialotetrahexosylganglioside (DHGM1), dihydromonosialodihexosylganglioside (DHGM3), dihydrolactosylceramide (DHLacCer), dihydrolactosylceramide sulfate (DHSM3), dihydrosialyl Lewis acid (DHSialyl-LeX), dihydrosphingomyelin (DHSM), dihydrosulfatide (DHST), lactosylceramide (LacCer), lactosylceramide sulfate (SM3), lysophosphatidylethanolamine (LPE),

lysosphingomyelin (LSM), matrix-assisted laser desorption ionisation (MALDI), mass spectrometry imaging (MSI), optimal cutting temperature (OCT), phosphatidylethanolamine (PE), phosphatidylserine (PS), sphinganine (d18:0), sphingolipid (SL), sphingomyelin (SM), sphingosine (d18:1), sulfatide (ST)

3.1 Introduction

The human lens is comprised of fibre cell layers, with the central layers formed in utero or shortly after birth (the nucleus) and concentric layers added throughout the human lifespan (the cortex).[1-4] The lens fibre cells lose their organelles and nuclei after differentiating to maintain lens transparency.[1, 3, 5] The nucleus can be divided into two sub regions; the core and the inner region. The core is formed *in utero* and the inner region is formed around the core immediately after birth.[6, 7] The cortex can be separated into two sub regions; the barrier and the outer cortex. At middle age (approximately 40-50 years), the barrier region is formed outside the inner region, which is thought to be the result of age-related modifications to proteins in the metabolically inactive nuclear region.[8, 9] Finally, the outer cortex is comprised of newly formed fibre cells that are still metabolically active.[10] Owing to its unique growth pattern, there is no membrane protein or lipid turnover in the lens nucleus.[11, 12] As a result of the lack of turnover, there are significant alterations to both protein structure and lipid composition that occur with age[2, 12-17].

The lipid profile of the human lens is different from other tissues in the human body or other animals.[13] In the human lens, lipids are mainly comprised of sphingolipid (SL) with a saturated sphinganine (d18:0) backbone.[2, 13, 18] The most abundant sphingolipid present in the lens is dihydrosphingomyelin (DHSM), which contributes approximately 72% of total sphingolipid and approximately 47% of total phospholipid.[13] This is in contrast to other animal lenses where DHSM is approximately 3% of total phospholipids.[1]

To better study lens pathologies that are associated with biochemical alterations to lens constituents, knowledge of the spatial distribution of lens lipids is essential in order to understand the difference in lipid profile in older (nuclear) and younger (cortical) fibre cells. Mass spectrometry imaging (MSI) has emerged as a complementary tool to study the distribution of specific lipids in tissue.[19-22] Matrix-assisted laser desorption ionization (MALDI) mass spectrometry has been a key technique in the success of MSI.[23] MALDI requires the deposition of a layer of matrix, which can be any compound that can absorb the laser wavelength to allow gentle energy transfer to ionise the analytes in the tissue and also aid desorption of analytes.[19, 22]

Previous MSI of human, bovine and porcine lens lipids has been performed with MALDI and desorption electrospray ionisation (DESI) mass spectrometry.[13, 24-28] The direct analysis of the porcine lens using MALDI detected only two ceramide phosphates (CerPs) and sphingomyelins (SMs).[24] Deeley *et al.* has also identified age-related changes in the distribution of ceramides (Cers), dihydroceramides (DHCers) and DHSM in adult human lens.[13] More recently, MALDI has also been used to provide the first data describing the distribution of lysosphingomyelins (LSMs) and dihydrolactosylceramides (DHLacCers) in the human lens.[29] The distribution of a wider range of lipids including CerP, phosphatidylethanolamine (PE), phosphatidylserine (PS), lysophosphatidylethanolamine (LPE) and cholesterol have been studied in the human lens using DESI.[25] However, lipids in the lens tissue cannot be desorbed by DESI without the presence of a strong acid, which causes a physical disruption to the tissue structure.[25] The physical disruption of the tissue means that the spatial distribution of lipids by DESI may be compromised. Ellis *et al.* predict that this may be a consequence of the tightly-packed laminae of fibre cells and their relatively high protein concentration in comparison with other human tissues.[25] Together, these MSI studies provide new insight into the distribution of some lipid classes in the lens.

The recent discovery of other low abundant lipid classes such as dihydrolactosylceramide sulfate (DHSM3), dihydrosulfatide (DHST), and other gangliosides,[30] and the large alterations in sphingolipid distribution with age[12] highlights the need for further understanding of sphingolipid distribution in the human lens. The aim of this study was to complete the distribution map of sphingolipids in the adult human lens, with a particular focus on the sphingolipids that have been recently identified in this unique tissue utilizing MALDI-MSI.[30]

3.2 Materials and Methods

3.2.1 Materials

The matrices 2-mercaptobenzathiazole (MBT) and 2,5-diaminonapthalene (DAN) were purchased from Sigma Aldrich (Castle Hill, Australia). Glass microscope slides for tissue mounting were purchased from

Proscitech (Townsville, Australia). The optimal cutting temperature (OCT) compound was purchased from Sakura Finetek (Torrance, USA).

3.2.2 Lenses

Human lenses were obtained from eyes donated to the NSW Lions Eye Bank at the Sydney Eye Hospital, (Sydney, Australia) within 2–6 hours of death, and were stored immediately at – 80 °C until required. All work was approved by the human research ethics committees at the University of Wollongong (HE 13/401).

3.2.3 MALDI-MS

For MALDI-MS analysis, lenses were mounted onto a cryostat holder using a minimal amount of OCT at – 20 °C in a cryo-microtome (Leica CM 1950, Leica Biosystems, Australia). The lenses were sliced in the transverse plane to produce 20 µm thick slices and were thaw-mounted onto the glass slide. The samples were immediately stored at -20 °C until analysed. Prior to analysis, samples were dried in a desiccator for 10 minutes. Matrices were then applied via sublimation at 30 mTorr and 120 °C for MBT and 112 °C for DAN. The samples were removed after 8 minutes and 6 minutes, respectively. 3 mg (~ 0.16 mg/cm^2) of matrix were applied on each sample. The samples were then analysed by an LTQ-Orbitrap XL mass spectrometer (ThermoScientific, Australia) equipped with a MALDI source. The entire surface of the human lens was examined with a raster step size of 100 µm. The laser performed 50 shots per spot with a summed spectrum collected from each spot. Mass spectra were acquired in both positive (using MBT as the matrix) and negative ion mode (using DAN as the matrix). The mass resolution at *m/z* 400 was 33000 and the mass range acquired was *m/z* 400-2000. The instrument was externally calibrated using commercially available Calmix for LTQ-Orbitrap (Sigma Aldrich, Australia) in both ion modes. MS imaging data were visualized by ImageQuest 1.0 (ThermoScientific, Australia). SM, DHSM, LacCer, Cer and DHCer were detected on lens slices in positive ion mode, with MBT as the matrix. Other classes of sphingolipids were detected in negative ion mode on adjacent lens slices using DAN. The list of *m/z* for each lipid is shown in Table S 3.1. The extracted ion count of each sphingolipid was normalized to the total ion count of the spectra

to obtain the abundance of the ions. Therefore, the abundance was compared within the same ion mode and same lens only.

3.3 Results and Discussion

3.3.1 MALDI Imaging of Sphingolipids in Human Lens

In this study, MALDI-MSI was used to analyse the sphingolipid composition and distribution of two female human lens samples from donors that were 51 and 67 years of age at the time of death. There were 51 sphingolipid species detected in the human lens based on accurate mass measurements (<3 ppm).

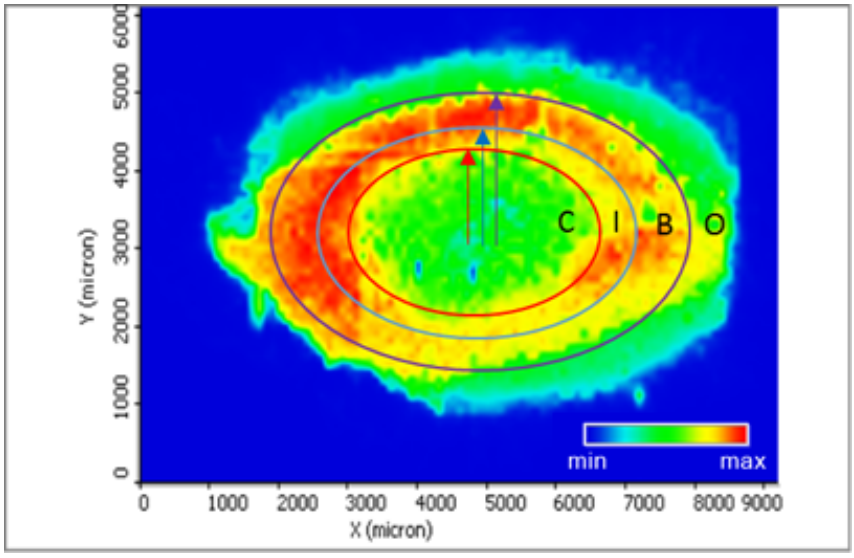

Figure 3.1: MALDI-MS image of a transverse section of a 51 year-old human lens highlighting the different regions of the lens: core (C), inner (I), barrier (B) and outer (O).

An image of SM (d18:0/16:0) in a 51 year-old lens is shown in Figure 3.1. In the image, the different regions of the lens were labelled by measuring the distance from the lens centre, as described elsewhere.[13] The nuclear region was divided into the inner and core region. The core is ~ 1 mm from the lens centre while the inner region is between 1.25 mm and 1.5 mm from the lens centre. The barrier region is located ~ 1.5 – 2 mm from the lens centre, as previously stated by Deeley *et al.*[13] The outer region refers to the region

beyond 2.5 mm from the lens centre.

Nine classes of sphingolipids with a sphinganine (d18:0) base were detected in both lenses, DHSM, DHLacCer, DHCer, dihydroceramidephosphate (DHCerP), DHSM3, DHST, dihydromonosialodihexosylganglioside (DHGM3), dihydromonosialotetrahexosylganglioside (DHGM1) and dihydrosialyl Lewis acid (DHSialyl-LeX). In contrast, only five sphingolipid classes with a sphingosine (d18:1) base were detected, *i.e*., SM, Cer, CerP, lactosylceramide sulfate (SM3) and sulfatide (ST). In comparison to previous MSI studies which only detected DHSM, DHCer, LSM, DHLacCer and DHCerP, this study includes many other classes of sphingolipids in the lens that were identified to-date. A complete distribution of all detectable lens sphingolipids is shown in the supplementary figures (see supplementary data).

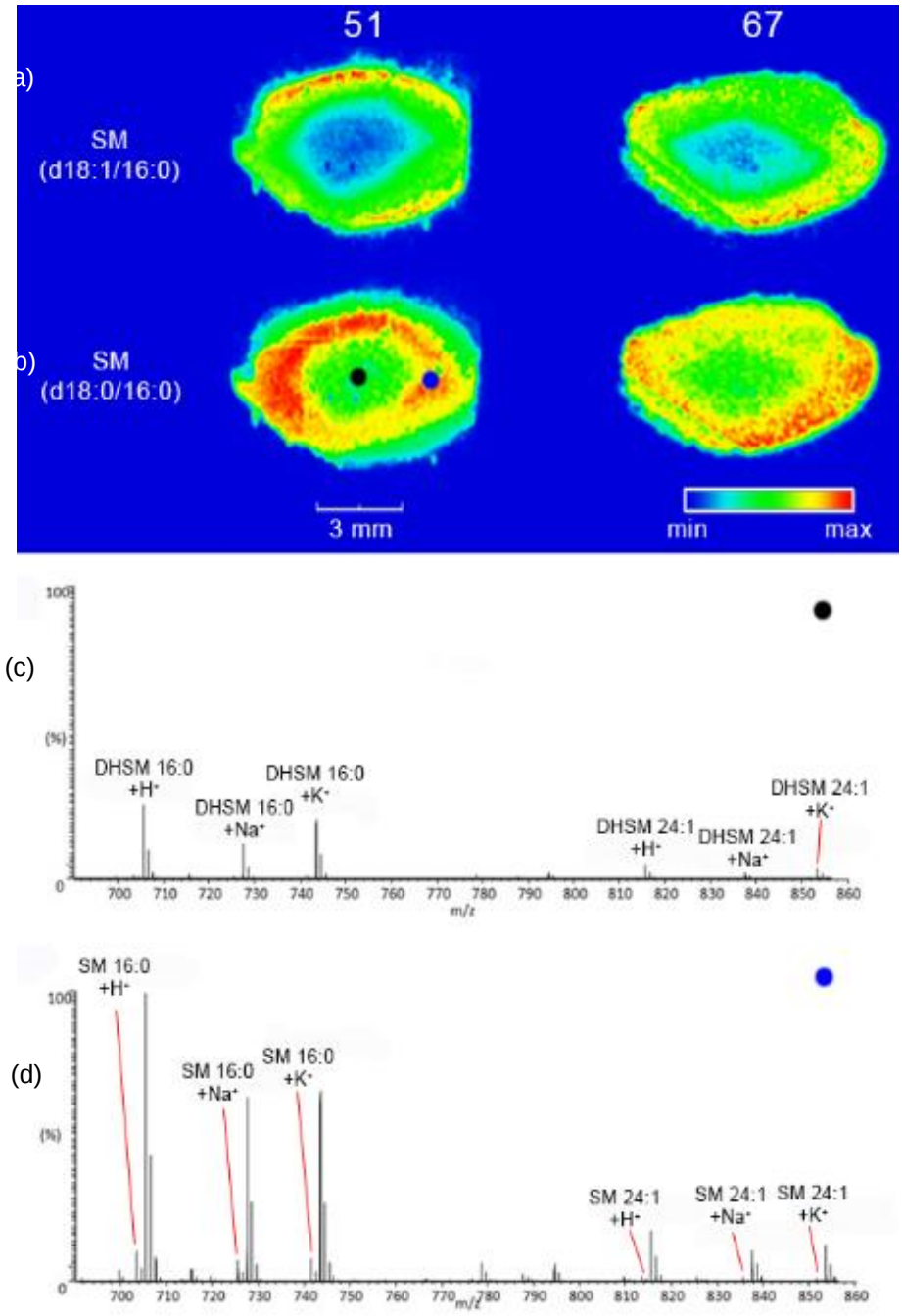

Figure 3.2: The distribution of protonated (a) SM (d18:1/16:0) (m/z 703.59), and (b) SM (d18:0/16:0) (m/z 705.59) in a 51 year-old and a 67 year-old human lens in positive ion mode using MBT as matrix. Mass spectra of SM (d18:0/16:0) detected in a 51 year-old human lens in the (c) core region as indicated by the black dot; and the (d) barrier region as indicated by the blue dot. Both spectra in (c) and (d) have been normalized to base peak m/z 705.59 in (d).

3.3.2 Sphingomyelin (SM) & Dihydrosphingomyelin (DHSM)

The distribution of SM (d18:1/16:0) and SM (d18:0/16:0) in a 51-year old and a 67 year-old human lens are shown in Figure 3.2a and b, respectively. In both lenses, SM (d18:1/16:0) was present around the cortex region, while its presence in the nucleus is negligible (Figure 3.2a). Figure 3.2c and d show the mass spectra obtained from the core (black dot) and barrier (blue dot) regions of the lens. The two most abundant fatty acyl chains in the lens sphingolipidome are 16:0 and 24:1, which is consistent across all sphingolipid subclasses.[30, 32] The masses of these fatty acyl chains are 256 Da and 366 Da, respectively, which equates to a mass difference of 110 Da. This is an important pattern used by researchers to identify different sphingolipid classes in the lens.[30] The most dominant species is SM (d18:0/16:0) at *m/z* 705, *m/z* 727 and *m/z* 743 representing its protonated, sodiated and potassiated ions respectively (Figure 3.2c and d). SM (d18:0/24:1) is present at *m/z* 815, *m/z* 837 and *m/z* 853, which correspond to proton, sodium and potassium adducts respectively. The ion intensity of DHSM is increased around the barrier region (blue dot) as shown in Figure 3.2b, forming an annular distribution around the nucleus. This agrees with previous MSI studies of human lens lipid using the same approach.[1] The ion intensity of DHSM is also higher towards the outer limits of the barrier region. This phenomenon is similar for both 51 year-old and 67 year-old lenses (Figure 3.2a & b).

We have also observed LDHSM, i.e. SM (d18:0/0:0) based on accurate mass as previously reported by Pol *et al.*[29] They were expressed almost homogeneously throughout the lens and did not show an opposite distribution trend to their parent molecule of DHSM (supplementaryFigure S 3.1) as reported by Pol and colleagues.[29] We have also not detected any LSM with a sphingosine backbone (d18:1/0:0) in our studies as we have used MBT as a matrix, which has been reported to cause more fragmentation and generates interfering ions below *m/z* 500.[33] This may explain the observed difference in LSM.

3.3.3 Ceramide (Cer), Dihydroceramide (DHCer), Ceramide Phosphate (CerP) & Dihydroceramide Phosphate (DHCerP)

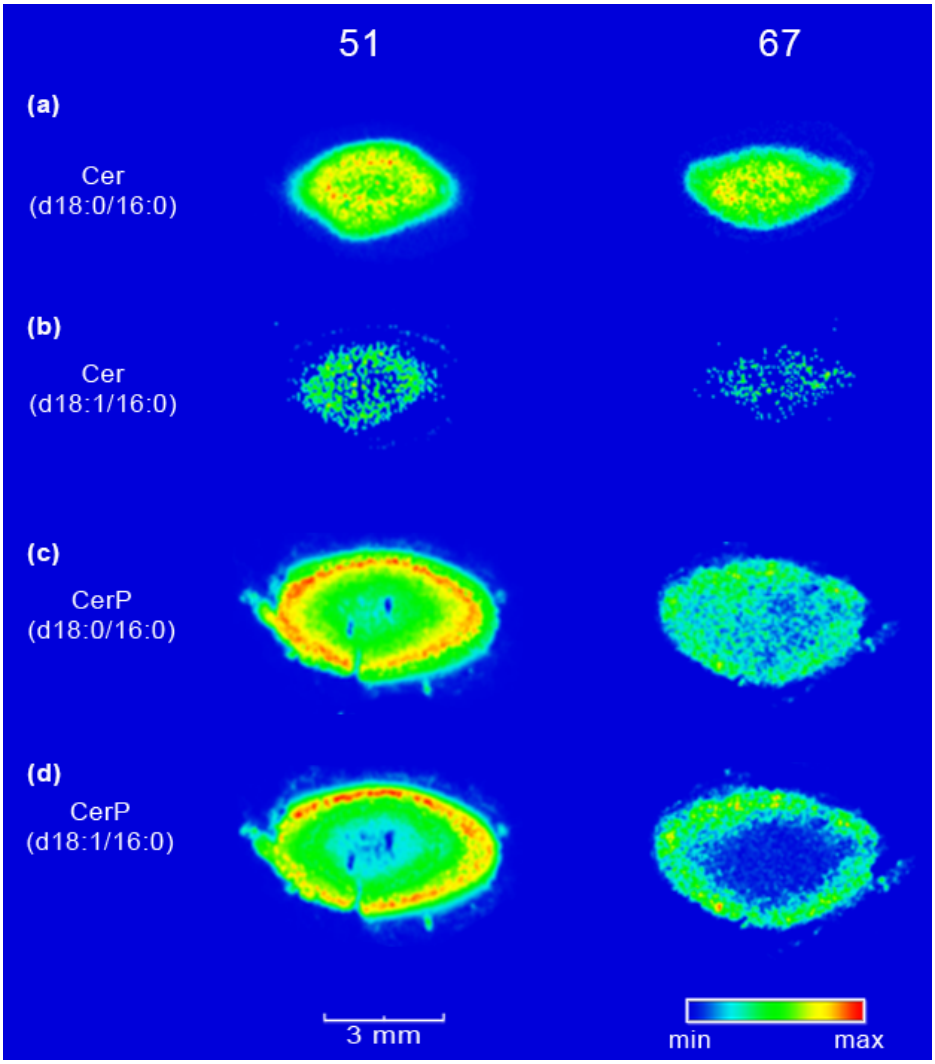

Figure 3.3: The distribution of (a) DHCer, (b) Cer, (c) DHCerP and (d) CerP in a 51 year-old (left) and a 67 year-old (right) human lens. DHCer and Cer were analysed in positive ion mode using MBT as matrix while CerP and DHCerP were analysed in negative ion mode using DAN as matrix.

Figure 3.3 shows the distribution of the most abundant Cer and CerP in a 51- and 67-year-old lens. Cer (d18:0/16:0) was observed at the highest abundance in the nuclear region of the lens as seen in Figure 3.3a. This is in agreement with previous findings by Deeley *et al* and Pol *et al.*[13, 29] Their analogues with a d18:1 backbone showed similar distribution (Figure 3.3b). CerP has almost complementary distribution to Cer, as seen in Figure 3.3c and d. That is, CerP (d18:1/16:0) and CerP (d18:0/16:0) are more abundant in the cortical

region of the lens than the nucleus. This may be due to the hydrolysis of CerP to form Cer.[9] The same distribution pattern has also been reported previously.[29] Other lipid species of CerP and DHCerP detected were shown in supplementary Figure S3.2.

3.3.4 Dihydrolactosylceramide (DHLacCer)

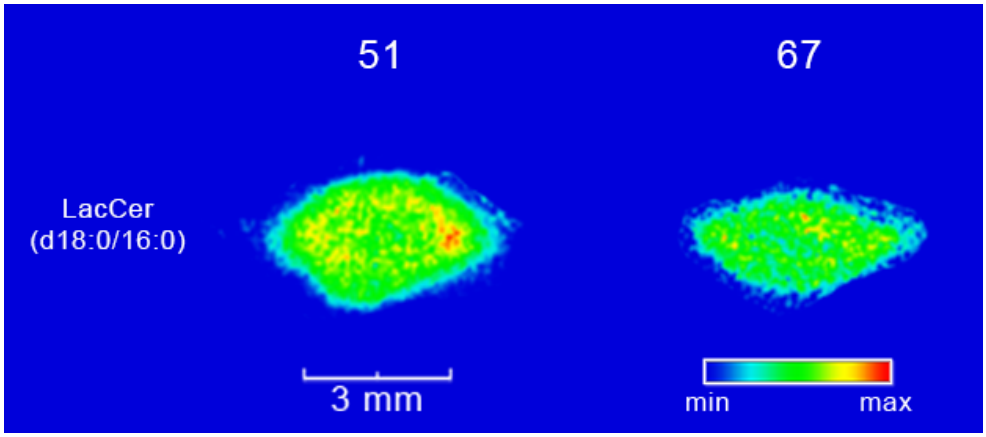

Figure 3.4: The distribution of LacCer (d18:0/16:0) in a 51 year-old and a 67 year-old human lens detected in positive ion mode using MBT as matrix.

Previous data suggest that lactosylceramide (LacCer) species in the lens are only present with a d18:0 backbone.[30] In contrast to other sphingolipid subclasses, DHLacCer with a 14:0 fatty amide was not observed, in agreement with previous findings.[30] DHLacCer has a similar distribution to DHCer. As shown in Figure 3.4, the distribution of LacCer (d18:0/16:0) was concentrated in the core and inner regions, with a negligible intensity observed in the outer region. LacCer (d18:0/16:0) and LacCer (d18:0/24:1) have an inverse relationship in their distribution in the human lens. While LacCer (d18:0/16:0) was primarily distributed around the nucleus, its analogue with a 24:1 fatty amide chain was mainly distributed around the cortex (supplementaryFigure S 3.3), as previously reported.[29]

3.3.5 Sulfatide (ST) & Dihydrosulfatide (DHST)

There is a distinct distribution of DHST and ST in both lenses, as shown in Figure 3.5a and b. They form a

circular distribution around the nucleus, primarily present in the barrier and cortex of the lens. ST have only recently been identified in the lens[30] and the data presented here are the first showing their distribution. However, we were not able to confirm if the double ring distribution is consistent across all lenses as sample was limited. Additional MSI of younger lenses showed that regardless of age, ST and DHST showed the same pattern of distribution around the lens cortex (Figure S 3.4). Other lipid species of ST and DHST detected were shown in supplementary Figure S 3.5.

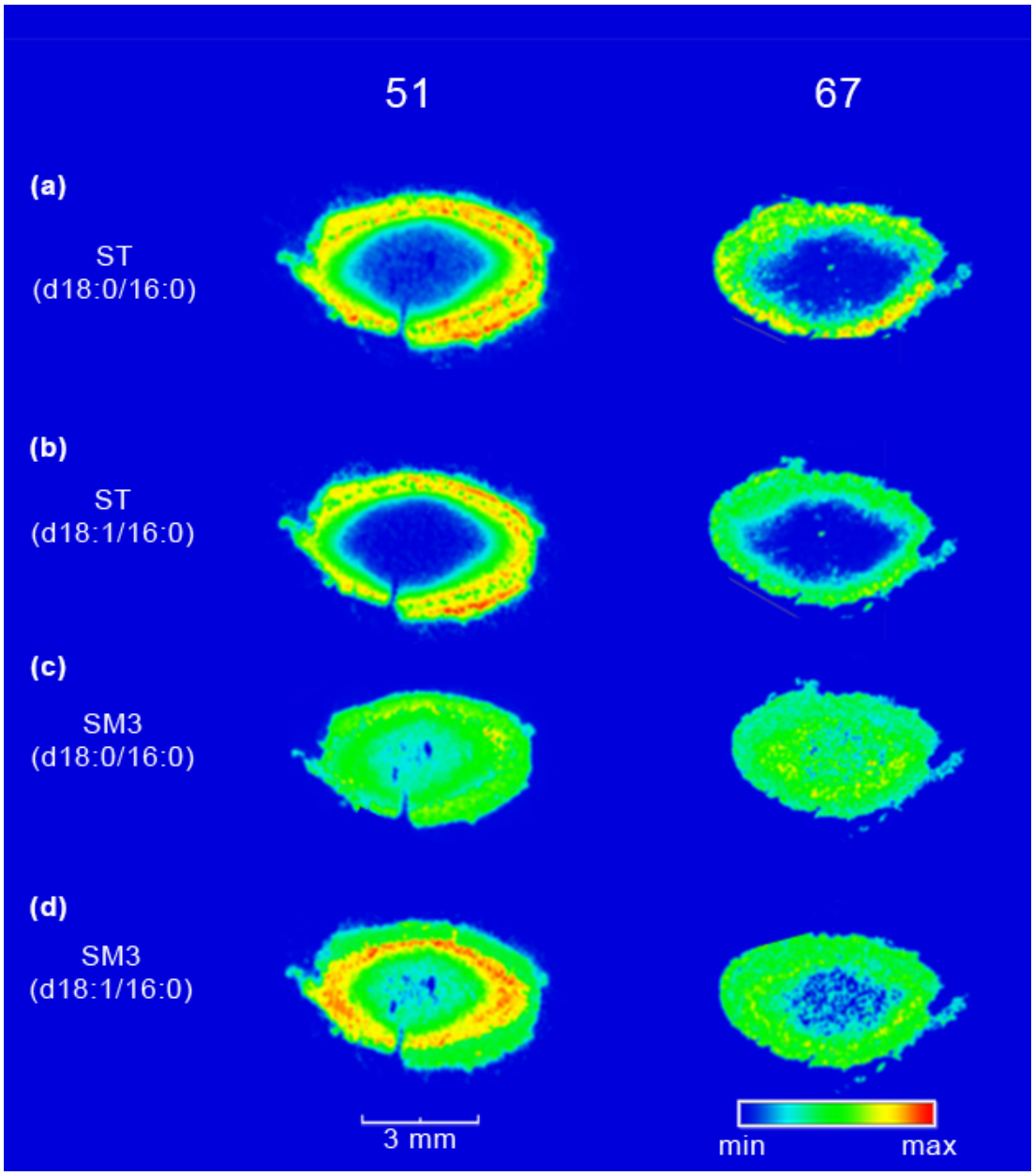

Figure 3.5: The distribution of (a) DHST, (b) ST, (c) DHSM3 and (d) SM3 in a 51 year-old and a 67 year-old human lens in negative ion mode using DAN as matrix.

3.3.6 Lactosylceramide Sulfate (SM3) & Dihydrolactosylceramide Sulfate (DHSM3)

SM3 has a similar chemical structure to ST, with SM3 having two sugar moieties attached to the

sphingolipid backbone while ST has only one. Figure 3.5c shows the distribution of SM3 (d18:0/16:0) to be relatively homogeneous across the lens in comparison to SM3 (d18:1/16:0) (Figure 5d) which shows a higher intensity of the molecule in the cortex than the nucleus. Other lipid species of SM3 and DHSM3 detected were shown in supplementary Figure S3.4.

3.3.7 Other Complex Glycosphingolipid (GSL) & Gangliosides

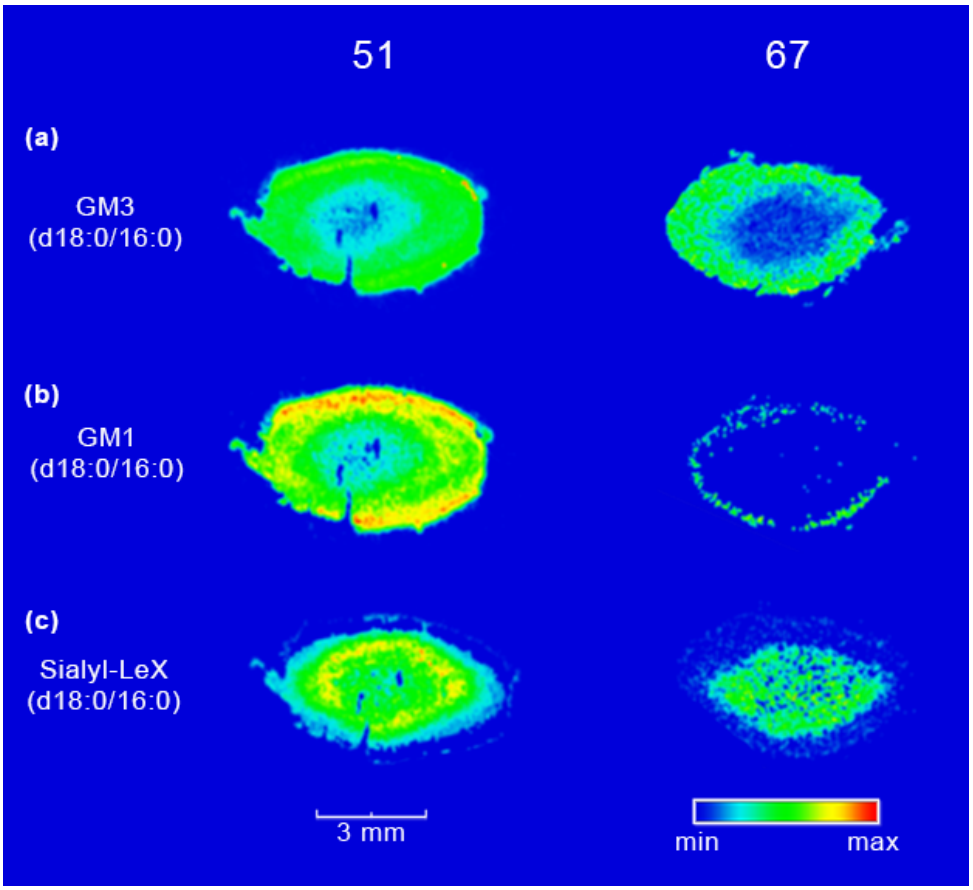

Figure 3.6: The distribution of (a) DHGM3, (b) DHGM1 and (c) DHSialyl-LeX in a 51 year-old and a 67 year-old human lens in negative ion mode using DAN as matrix.

The distribution of gangliosides such DHGM3, DHGM1 and DHSialyl-LeX were also observed in this study (Figure 3.6a, b and c). However, their analogues with a sphingosine backbone were below the limit of detection and thus not imaged. These lipids were identified based on accurate masses and their previous

characterization in the human lens.[37, 38] Previous data from lens gangliosides and GSLs show that dihydrosphingosine (d18:0) is the major base and the primary fatty amide chains are 16:0 and 24:1.[37] GM3 (d18:0/16:0) is distributed around the cortex of both lenses, with negligible presence in the nucleus as shown in Figure 3.6a. GM1 (d18:0/16:0) (Figure 3.6b) is present throughout the whole lens of the 51-year old, with a higher abundance surrounding the outer edge of the cortex. In the 67 year-old lens, GM1 (d18:0/16:0) is only observed in a faint ring around the edge of the lens. Both of the lenses showed a lower abundance of the 24:1 analogue (supplementary Figure S 3.6). In contrast to the two gangliosides, Sialyl-LeX (d18:0/16:0) is distributed primarily in the nucleus and barrier region (Figure 3.6c). The 51-year old lens showed a slightly wider distribution around the nucleus and the barrier compared to the 67 year-old lens. In contrast to the 16:0 analogue, the distribution of Sialyl-LeX (d18:0/24:1) in the 51 year-old lens is around the outer edge of the cortex (supplementary Figure S 3.6). This is only the case for the 51 year-old lens as the distribution of Sialyl-LeX (d18:0/16:0) and Sialyl-LeX (d18:0/24:1) are similar in the 67 year-old lens (Figure 3.6c).

GSLs are localised on the membrane surface of lens epithelial cells and may play an important role in epithelial differentiation and maturation.[39, 40] GSLs containing sialic acid, known as gangliosides, are involved in cell proliferation, cell-cell interaction, differentiation, oncogenic transformation and signal transduction.[41-43] Previous studies have shown that GSLs and gangliosides are higher in concentration in cataractous and ageing lenses in comparison to normal lenses.[44, 45] Ogiso *et al.* revealed that the ganglioside content in the cortical region is higher than the nuclear region in cataractous lenses.[46] Our results also showed that although these complex GSLs are distributed throughout the lens, GM3 and GM1 have a higher abundance around the outer cortex. It has been shown that gangliosides accumulate in association with ageing and cataract.[46] However, the reason and mechanism behind this increase remain unknown. It has been reported that Sialyl-LeX are expressed in cortical cells that are closer to the nuclear fibre cells, which agrees with our findings.[45] Sialyl-LeX are thought to be involved in differentiation from epithelial cells to fibre cells in mammalian lenses.[40, 45]

3.4 Conclusion

In the current study, we have used MALDI-MS to map the spatial distribution of recently identified sphingolipids in the adult human lens, including some complex GSL and gangliosides which have not been studied in detail in the last two decades. GSL such as DHST and ST showed a consistent distribution outside the nucleus regardless of age, which may suggest that DHST and ST are not required in the metabolically inactive nucleus. The functions of these lipids in the lens remain unknown, and whether they are present in the same region throughout a human's lifespan remains to be determined. Mapping of these lipids can now be extended to examine age-related changes in lipid distribution across the human lifespan. This brings us one step closer to the complete elucidation of the lens sphingolipidome and resolving the distribution of each sphingolipid, which is essential to understanding the role of lipids in the development of lens diseases such as age-related nuclear cataract and presbyopia.

Acknowledgements

This work was supported by the Australian Research Council (FT110100249). J.A.S is supported by University Postgraduate Award and International Postgraduate Research Scholarship from the University of Wollongong.

3.5 Supplementary

Table S 3.1: List of sphingolipid species detected in the human lens by MSI. All the lipids were identified by $[M+H]^+$ or $[M-H]^-$.

Sphingolipids		
	FA	*m/z* $[M+H]^+$
Sphingomyelin		
DHSM(d18:0)	14:0	677.560
	15:0	691.575
	16:0	705.591
	17:0	719.607
	18:0	733.622
	22:0	789.685
	24:1	815.701
SM(d18:1)	14:0	675.544
	15:0	689.560
	16:1	701.560
	16:0	703.575
	18:0	731.607
	22:1	785.654
	22:0	787.669
	23:0	801.685
	24:2	811.669
	24:1	813.685
Ceramide		
DHCer(d18:0)	14:0	512.504
	16:0	540.536
	22:1	622.614
	22:0	624.629
	24:1	650.645
Cer(d18:1)	14:0	510.489
	16:0	538.520
	22:1	620.598

	22:0	622.614
	24:1	648.629
Lactosylceramide		
DHLacCer(d18:0)	16:0	864.641
	22:0	948.735
	24:1	974.751
	24:0	976.766
		m/z $[M-H]^-$
Ceramide Phosphate		
DHCerP(d18:0)	16:0	618.486
	24:1	728.596
CerP(d18:1)	16:0	616.471
	24:1	726.580
Sulfatide		
DHST(d18:0)	14:0	752.498
	16:0	780.530
	24:1	890.639
ST(d18:1)	14:0	750.483
	16:0	778.514
	24:1	888.623
Lactosylceramide Sulfate		
DHSM3(d18:0)	14:0	914.551
	16:0	942.582
	24:1	1052.692
SM3(d18:1)	16:0	940.567
	22:0	1024.661
	24:1	1050.676
DHGM3		
DHGM3(d18:0)	16:0	1153.721
	24:1	1263.831
DHGM1		
DHGM1(d18:0)	16:0	1518.853
	24:1	1628.963
DHSialyl-LeX		

DHSialyl-LeX(d18:0)	16:0	1664.911
	24:1	1775.021

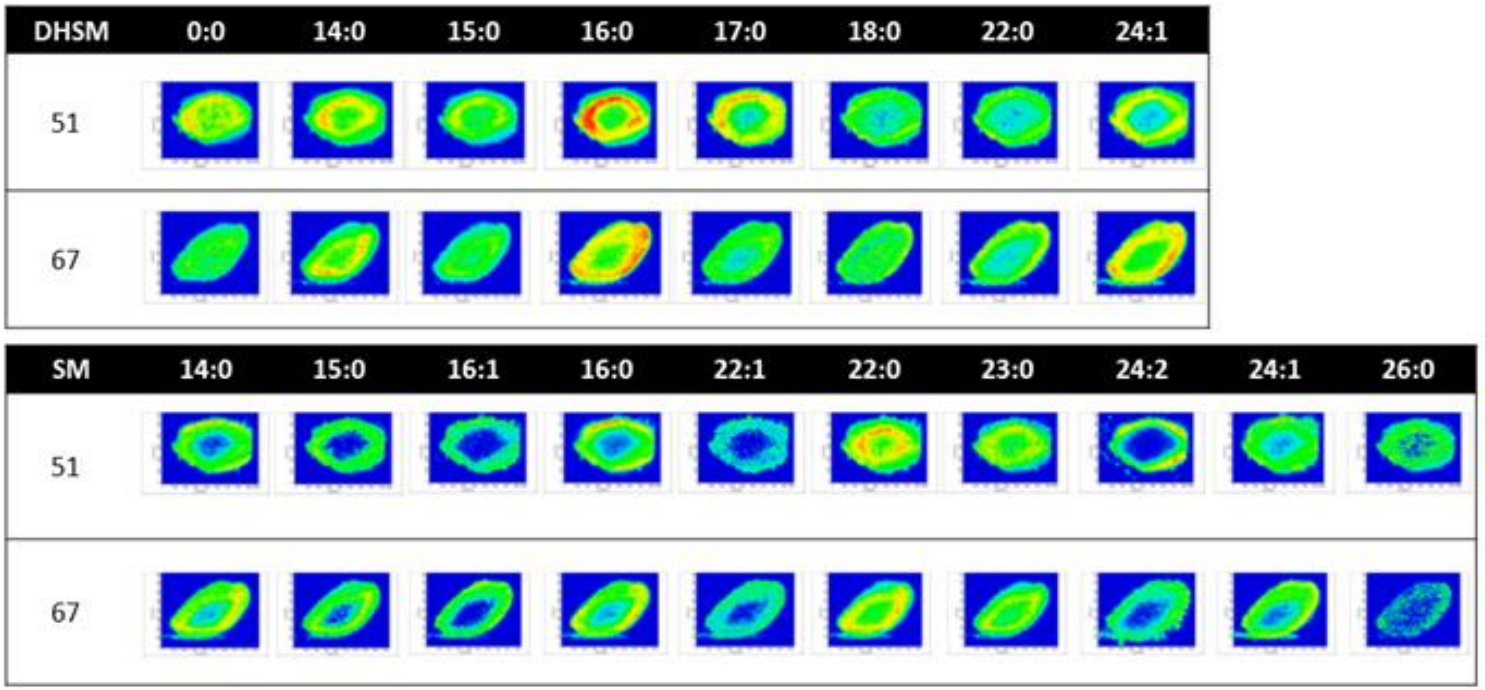

Figure S 3.1: MALDI-MS images for SM and DHSM.

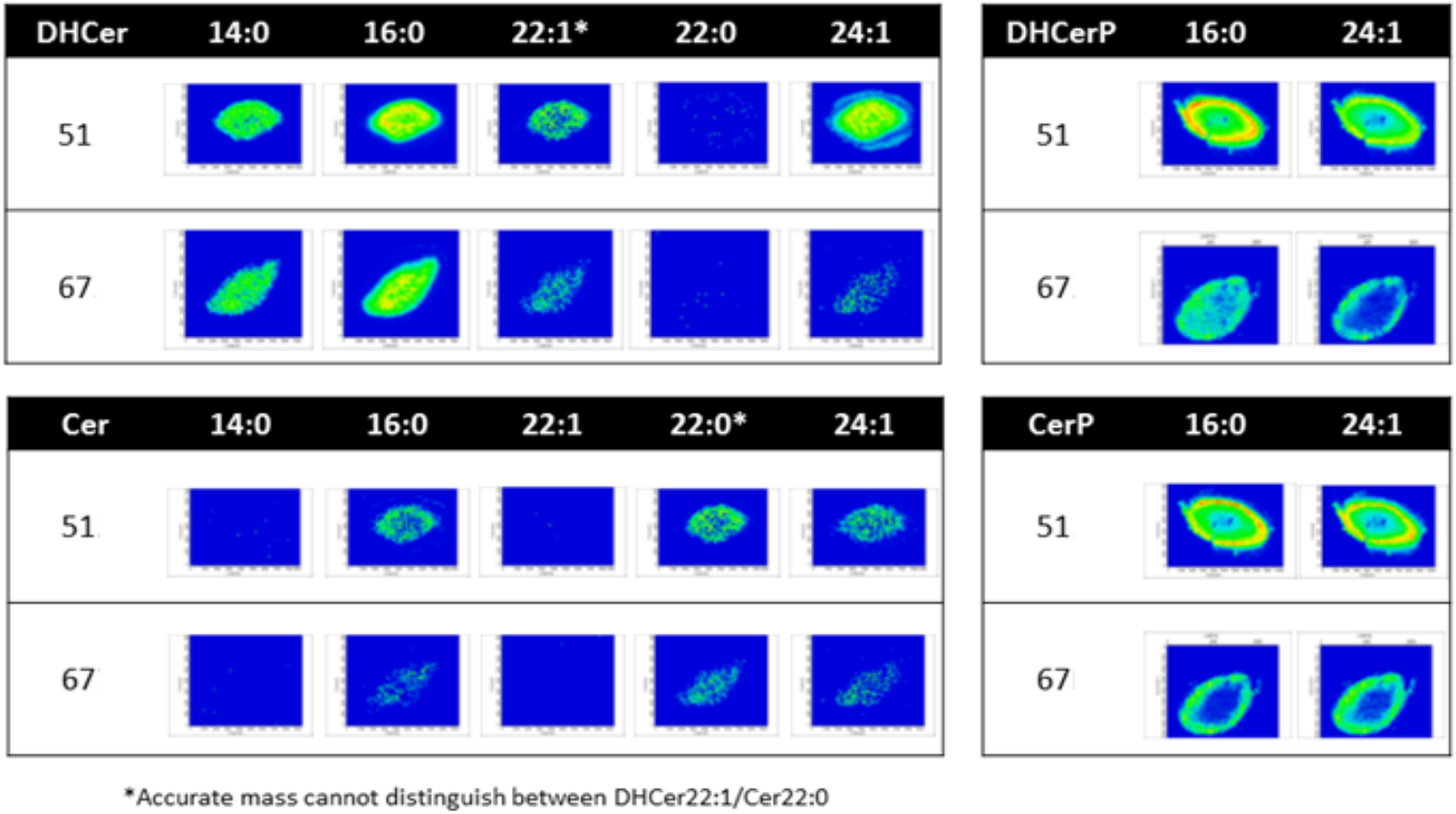

Figure S 3.2: MALDI-MS images for Cer, DHCer, CerP and DHCerP.

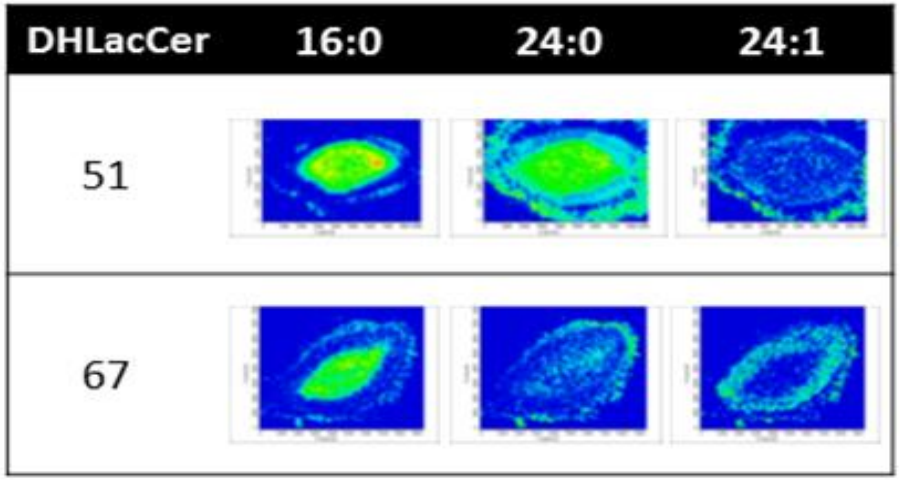

Figure S 3.3:MALDI-MS images for DHLacCer.

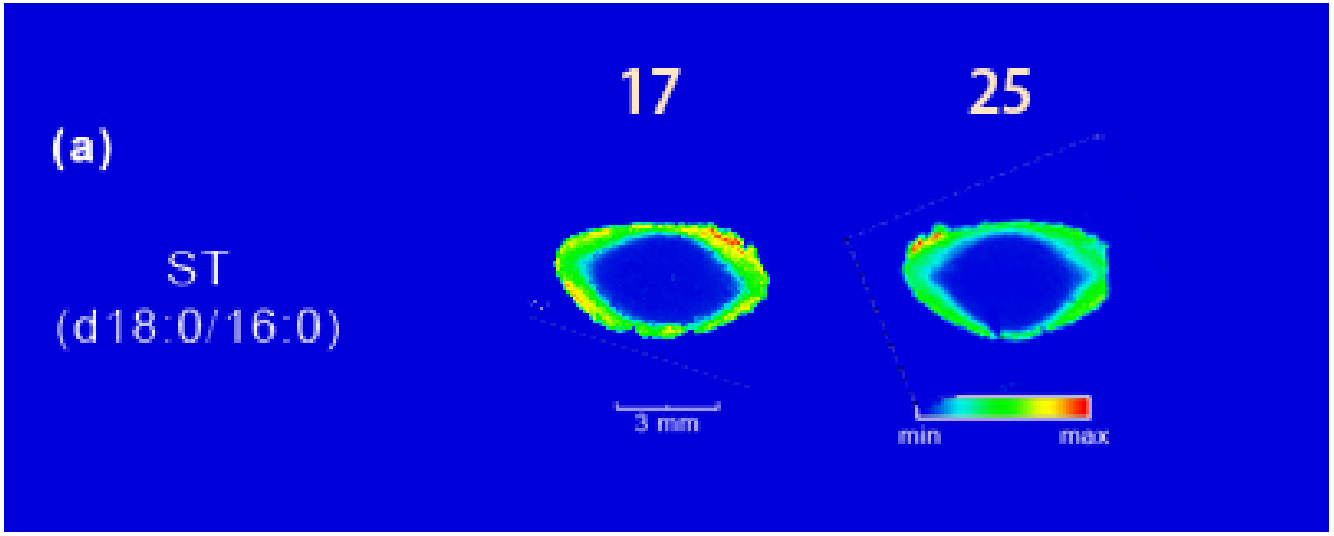

Figure S 3.4: The distribution of DHST 16:0 for 17 year-old and 25 year-old lenses.

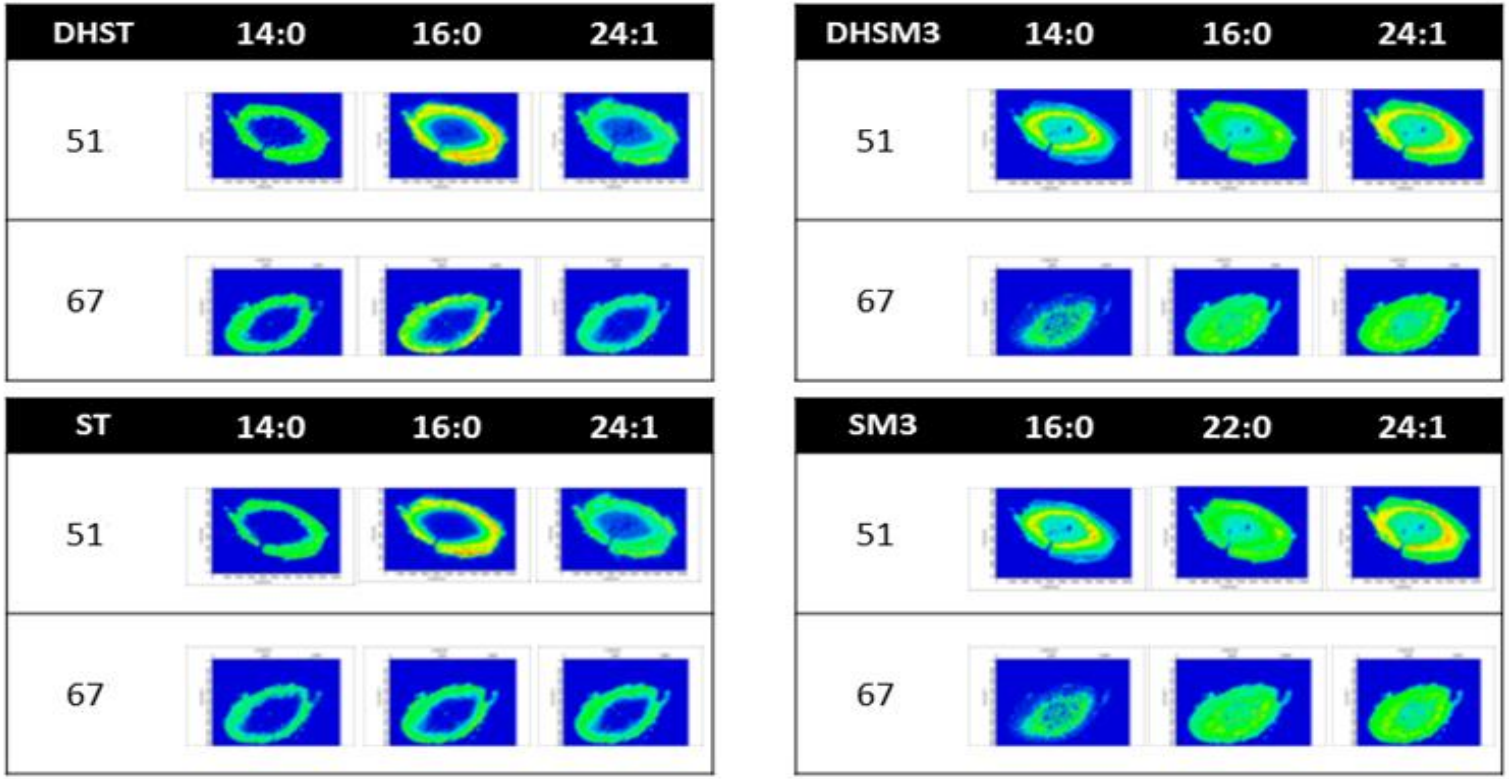

Figure S 3.5:MALDI-MS images for ST, DHST, SM3 & DHSM

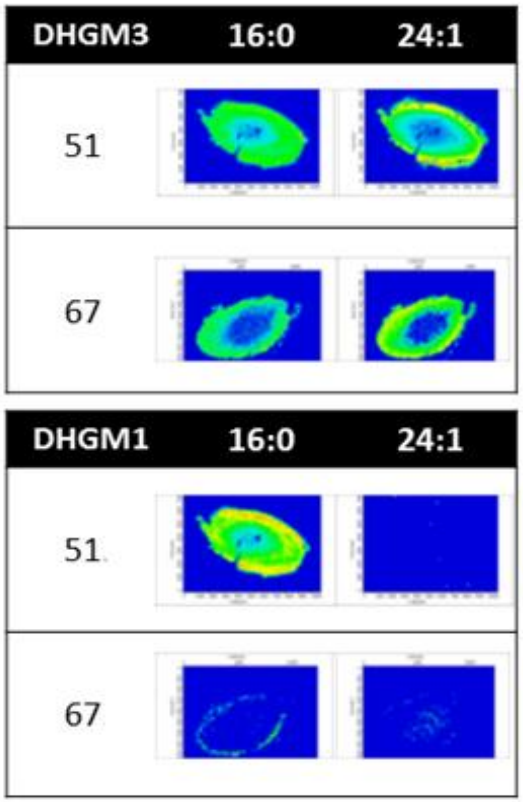

Figure S 3.6:MALDI-MS images for DHGM3, DHGM1 & DHSialyl-LeX.

3.6 References

1. Audette, D. S.; Scheiblin, D. A.; Duncan, M. K., The molecular mechanisms underlying lens fibre elongation. *Experimental Eye Research* **2017,** *156*, 41-49.

2. Borchman, D.; Yappert, M. C., Lipids and the ocular lens. *Journal of Lipid Research* **2010,** *51* (9), 2473-2488.

3. Coulombre, J. L.; Coulombre, A. J., Lens Development: Fibre Elongation and Lens Orientation. *Science* **1963,** *142* (3598), 1489.

4. Augusteyn, R. C., On the growth and internal structure of the human lens. *Experimental Eye Research* **2010,** *90* (6), 643-654.

5. Bassnett, S.; Shi, Y.; Vrensen, G. F. J. M., Biological glass: structural determinants of eye lens transparency. *Philosophical Transactions of the Royal Society B: Biological Sciences* **2011,** *366* (1568), 1250-1264.

6. Friedrich, M. G.; Truscott, R. J. W., Large-Scale Binding of α-Crystallin to Cell Membranes of Aged Normal Human Lenses: A Phenomenon That Can Be Induced by Mild Thermal Stress. *Investigative Ophthalmology & Visual Science* **2010,** *51* (10), 5145-5152.

7. Garland, D. L.; Duglas-Tabor, Y.; Jimenez-Asensio, J.; Datiles, M. B.; Magno, B., The Nucleus of the Human Lens: Demonstration of a Highly Characteristic Protein Pattern by Two-Dimensional Electrophoresis and Introduction of a New Method of Lens Dissection. *Experimental Eye Research* **1996,** *62* (3), 285-292.

8. Moffat, B. A.; Landman, K. A.; Truscott, R. J. W.; Sweeney, M. H. J.; Pope, J. M., Age-related Changes in the Kinetics of Water Transport in Normal Human Lenses. *Experimental Eye Research* **1999,** *69* (6), 663-669.

9. Sweeney, M. H. J.; Truscott, R. J. W., An Impediment to Glutathione Diffusion in Older Normal Human Lenses: a Possible Precondition for Nuclear Cataract. *Experimental Eye Research* **1998,** *67* (5), 587-595.

10. Subczynski, W. K.; Mainali, L.; Raguz, M.; O'Brien, W. J., Organization of lipids in fibre-cell plasma membranes of the eye lens. *Experimental Eye Research* **2017,** *156*, 79-86.

11. Harding, J., *Biochemistry of the Eye*. Taylor & Francis: 1998.

12. Hughes, J. R.; Levchenko, V. A.; Blanksby, S. J.; Mitchell, T. W.; Williams, A.; Truscott, R. J. W., No turnover in lens lipids for the entire human lifespan. *eLife* **2015,** *4*, e06003.

13. Deeley, J. M.; Hankin, J. A.; Friedrich, M. G.; Murphy, R. C.; Truscott, R. J. W.; Mitchell, T. W.; Blanksby, S. J., Sphingolipid distribution changes with age in the human lens. *Journal of Lipid Research* **2010,** *51* (9), 2753-2760.

14. Hughes, J. R.; Deeley, J. M.; Blanksby, S. J.; Leisch, F.; Ellis, S. R.; Truscott, R. J. W.; Mitchell, T. W., Instability of the cellular lipidome with age. *AGE* **2012,** *34* (4), 935-947.

15. Huang, L.; Grami, V.; Marrero, Y.; Tang, D.; Yappert, M. C.; Rasi, V.; Borchman, D., Human Lens Phospholipid Changes with Age and Cataract. *Investigative Ophthalmology & Visual Science* **2005,** *46* (5), 1682-1689.

16. Yappert, M. C.; Rujoi, M.; Borchman, D.; Vorobyov, I.; Estrada, R., Glycero- versus sphingo-phospholipids: correlations with human and non-human mammalian lens growth. *Experimental Eye Research* **2003,** *76* (6), 725-734.

17. Truscott, R. J. W., Age-related nuclear cataract - oxidation is the key. *Experimental Eye Research* **2005,** *80* (5), 709-725.

18. Yappert, M. C.; Borchman, D., Sphingolipids in human lens membranes: an update on their composition and possible biological implications. *Chemistry and Physics of Lipids* **2004,** *129* (1), 1-20.

19. Chaurand, P.; Schwartz, S. A.; Caprioli, R. M., Imaging mass spectrometry: a new tool to investigate the spatial organization of peptides and proteins in mammalian tissue sections. *Current Opinion in Chemical Biology* **2002,** *6* (5), 676-681.

20. Chaurand, P.; Schwartz, S. A.; Billheimer, D.; Xu, B. J.; Crecelius, A.; Caprioli, R. M., Integrating Histology and Imaging Mass Spectrometry. *Analytical Chemistry* **2004,** *76* (4), 1145-1155.

21. Chaurand, P., Imaging mass spectrometry of thin tissue sections: A decade of collective efforts. *Journal of Proteomics* **2012,** *75* (16), 4883-4892.

22. Amstalden van Hove, E. R.; Smith, D. F.; Heeren, R. M. A., A concise review of mass spectrometry imaging. *Journal of Chromatography A* **2010,** *1217* (25), 3946-3954.

23. Caprioli, R. M.; Farmer, T. B.; Gile, J., Molecular imaging of biological samples: Localization of peptides and proteins using MALDI-TOF MS. *Analytical Chemistry* **1997,** *69* (23), 4751-4760.

24. Vidová, V.; Pól, J.; Volný, M.; Novák, P.; Havlíček, V.; Wiedmer, S. K.; Holopainen, J. M., Visualizing spatial lipid distribution in porcine lens by MALDI imaging high-resolution mass spectrometry. *Journal of Lipid Research* **2010,** *51* (8), 2295-2302.

25. Ellis, S. R.; Wu, C.; Deeley, J. M.; Zhu, X.; Truscott, R. J. W.; Panhuis, M. i. h.; Cooks, R. G.; Mitchell, T. W.; Blanksby, S. J., Imaging of Human Lens Lipids by Desorption Electrospray Ionization Mass Spectrometry. *Journal of the American Society for Mass Spectrometry* **2010,** *21* (12), 2095-2104.

26. Rujoi, M.; Estrada, R.; Yappert, M. C., In situ MALDI-TOF MS regional analysis of neutral phospholipids in lens tissue. *Analytical Chemistry* **2004,** *76* (6), 1657-1663.

27. Le, C. H.; Han, J.; Borchers, C. H., Dithranol as a MALDI Matrix for Tissue Imaging of Lipids by Fourier Transform Ion Cyclotron Resonance Mass Spectrometry. *Analytical Chemistry* **2012,** *84* (19), 8391-8398.

28. Pol, J.; Vidova, V.; Hyotylainen, T.; Volny, M.; Novak, P.; Strohalm, M.; Kostiainen, R.; Havlicek, V.; Wiedmer, S. K.; Holopainen, J. M., Spatial Distribution of Glycerophospholipids in the Ocular Lens. *Plos One* **2011,** *6* (4).

29. Pol, J.; Faltyskova, H.; Krasny, L.; Volny, M.; Vlacil, O.; Hajduch, M.; Lemr, K.; Havlicek, V., Age-related changes in the lateral lipid distribution in a human lens described by mass spectrometry imaging. *European Journal of Mass Spectrometry* **2015,** *21* (3), 297-303.

30. Seng, J. A.; Ellis, S. R.; Hughes, J. R.; Maccarone, A. T.; Truscott, R. J. W.; Blanksby, S. J.; Mitchell, T. W., Characterisation of sphingolipids in the human lens by thin layer chromatography–desorption electrospray ionisation mass spectrometry. *Biochimica et Biophysica Acta (BBA) - Molecular and Cell Biology of Lipids* **2014,** *1841* (9), 1285-1291.

31. Zubarev, R. A.; Makarov, A., Orbitrap Mass Spectrometry. *Analytical Chemistry* **2013,** *85* (11), 5288-5296.

32. Michael, R.; Bron, A. J., The ageing lens and cataract: a model of normal and pathological ageing. *Philosophical Transactions of the Royal Society B: Biological Sciences* **2011,** *366* (1568), 1278-1292.

33. Gode, D.; Volmer, D. A., Lipid imaging by mass spectrometry - a review. *Analyst* **2013,** *138* (5), 1289-1315.

34. Sonnino, S.; Prinetti, A.; Nakayama, H.; Yangida, M.; Ogawa, H.; Iwabuchi, K., Role of very long fatty acid-containing glycosphingolipids in membrane organization and cell signaling: the model of lactosylceramide in neutrophils. *Glycoconjugate Journal* **2009,** *26* (6), 615-621.

35. Merrill, A. H., Sphingolipid and Glycosphingolipid Metabolic Pathways in the Era of Sphingolipidomics. *Chemical Reviews* **2011,** *111* (10), 6387-6422.

36. Farooqui, A. A.; Horrocks, L. A., On the role of sulfolipids in mammalian metabolism. *Molecular and Cellular Biochemistry* **1985,** *66* (1), 87-95.

37. Feldman, G. L.; Feldman, L. S.; Rouser, G., The isolation and partial characterization of gangliosides and ceramide polyhexosides from the lens of the human eye. *Lipids* **1966,** *1* (1), 21-26.

38. Swindell, R. T.; Harris, H.; Buchanan, L.; Bell, C.; Albers-Jackson, B., Ganglioside Composition in Human Cataractous Nuclei (With 1 color plate). *Ophthalmic Research* **1988,** *20* (4), 232-236.

39. Ogiso, M.; Irie, A.; Kubo, H.; Komoto, M.; Matsuno, T.; Koide, Y.; Hoshi, M., Characterization of neutral glycosphingolipids in human cataractous lens. *Journal of Biological Chemistry* **1993,** *268* (18), 13242-13247.

40. Kim, S.-J.; Chung, T.-W.; Choi, H.-J.; Kwak, C.-H.; Song, K.-H.; Suh, S.-J.; Kwon, K.-M.; Chang, Y.-C.; Park, Y.-G.; Chang, Hyeun W.; Kim, K.-S.; Kim, C.-H.; Lee, Y.-C., Ganglioside GM3 participates in the TGF-β1-induced epithelial–mesenchymal transition of human lens epithelial cells. *Biochemical Journal* **2012,** *449* (1), 241.

41. Hakomori, S., Glycosylation defining cancer malignancy: New wine in an old bottle. *Proceedings of the National Academy of Sciences* **2002,** *99* (16), 10231-10233.

42. Chung, T.-W.; Choi, H.-J.; Lee, Y.-C.; Kim, C.-H., Molecular mechanism for transcriptional activation of ganglioside GM3 synthase and its function in differentiation of HL-60 cells. *Glycobiology* **2005,** *15* (3), 233-244.

43. Hakomori, S.-i.; Igarashi, Y., Functional Role of Glycosphingolipids in Cell Recognition and Signaling. *The Journal of Biochemistry* **1995,** *118* (6), 1091-1103.

44. Ariga, T.; Tao, R. V.; Lee, B. C.; Yamawaki, M.; Yoshino, H.; Scarsdale, N. J.; Kasama, T.; Kushi, Y.; Yu, R. K., Glycolipid composition of human cataractous lenses. Characterization of Lewisx glycolipids. *Journal of Biological Chemistry* **1994,** *269* (4), 2667-2675.

45. Ogiso, M.; Shogomori, H.; Hoshi, M., Localization of Lewisx, sialyl-Lewisx and α-galactosyl epitopes on glycosphingolipids in lens tissues. *Glycobiology* **1998,** *8* (1), 95-105.

46. Ogiso, M.; Saito, N.; Sudo, K.; Kubo, H.; Hirano, S.; Komoto, M., Increase in lens gangliosides due to aging and cataract progression in human senile cataract. *Investigative Ophthalmology & Visual Science* **1990,** *31* (10), 2171-2179.

47. Borchman, D.; Yappert, M. C., Lipids and the ocular lens. *Journal of Lipid Research* **2010,** *51*, 2473-2488.

48. Ogiso, M.; Irie, A.; Kubo, H.; Komoto, M.; Matsuno, T.; Koide, Y.; Hoshi, M., Characterisation of Neutral Glycosphingolipids in Human Cataractous Lens. *Journal of Biological Chemistry* **1993,** *268*, 13242-13247.

49. Ogiso, M.; Komoto, M.; Okinaga, T.; Koyota, S.; Hoshi, M., Age-related changes in ganglioside composition in human lens. *Experimental Eye Research* **1995,** *60* (3), 317-323.

Chapter 4: Distribution of Glycerophospholipids in the Human Lens by Mass Spectrometry Imaging

The work presented in this chapter has been published:

***Jo Ann Seng**, Jessica R. Nealon, Stephen J. Blanksby, Todd W. Mitchell. (2018)* Distribution of Glycerophospholipids in the Human Lens by Mass Spectrometry Imaging. *Biomolecules. 8(4), 156.*

[a] School of Chemistry, Faculty of Science, Medicine and Health, University of Wollongong, NSW 2522, Australia.

[b] School of Medicine, Faculty of Science, Medicine and Health, University of Wollongong, NSW 2522, Australia.

[c] Central Analytical Research Facility, Queensland University of Technology, Brisbane, QLD 4000, Australia.

[d] Illawarra Health and Medical Institute, University of Wollongong, NSW 2522, Australia.

[*] Correspondence to: T.W. Mitchell, School of Medicine, University of Wollongong, NSW 2522, Australia. Email: toddm@uow.edu.au

Abstract

The concentration of glycerophospholipids in an adult human lens is remarkably lower than in other animal lenses. This is the result of oxidation and other deleterious events that occur over the extended human lifespan. The age of fibre cells differs across the lens, ranging from those formed before birth in the core of the lens to those formed just prior to death in the outer cortex. Therefore, the distribution of glycerophospholipids in the adult human lens should reflect this range however, limited data currently exists to confirm this hypothesis. Accordingly, this study aimed to determine the distribution of glycerophospholipids in adult human lens using mass spectrometry imaging. To achieve this 20 µm thick slices of two human lenses, aged 51 and 67 were analysed by matrix-assisted laser desorption ionisation imaging mass spectrometry. The data clearly indicate that intact glycerophospholipids such as phosphatidylethanolamine, phosphatidylserine and phosphatidic acid are mainly present in the outer cortex region, i.e. the youngest fibre cells, while lyso phosphatidylethanolamine, likely produced by the degradation of phosphatidylethanolamine is present in the nucleus (older fibre cells). This study adds further evidence to the relationship between fibre cell age and glycerophospholipid composition.

Keywords

glycerophospholipids, human lens, imaging mass spectrometry, lipidomics, phosphatidic acid, phosphatidylserine

Abbreviations

2,5-diaminonapthalene (DAN), desorption electrospray ionisation mass spectrometry (DESI-MS), glycerophospholipids (GPs), lysophosphatidylethanolamine (LPE), matrix-assisted laser desorption ionisation mass spectrometry (MALDI-MS), optimal cutting temperature (OCT), phosphatidic acid (PA), phosphatidylcholine (PC), phosphatidylethanolamine (PE), phosphatidylglycerol (PG), phosphatidylinositol (PI), phosphatidylserine (PS), total ion current (TIC).

4.1 Introduction

The lens is an ocular tissue which grows throughout a species' life span with newly differentiated fibre cells laid down upon older ones that are present from birth.[1] There is no protein[2] or lipid[3] turnover in the lens, thus structural and enzymatic proteins and lipids that are present at birth remain for the lifetime of the individual. In addition, upon fibre cell differentiation, all intracellular organelles are degraded.[4] Therefore, lens which is present from birth (known as the nucleus) is mainly composed of membranes packed with lipids and proteins.[5] Human cellular membranes are comprised of a lipid bilayer containing phospholipids and integral membrane proteins. A typical membrane consists mainly of phospholipids and glycolipids of different classes, headgroups and fatty acyl chains. Membrane fluidity is partly regulated by the degree of unsaturation of the fatty acyl chain.[5] Unlike a typical membrane, the human lens membrane is one of the most saturated and ordered membranes due to its unique lipid composition.[6] It contains a high level of cholesterol and saturated sphingolipids such as dihydrosphingolipid.[7] Also present in lens membranes are glycerophospholipids (GP), which consist of a 3-carbon glycerol backbone where two fatty acids attach at the *sn-1* and *sn-2* positions and a phosphate headgroup attached at the *sn*-3 position.[7] There are six main classes of GPs present in the human lens: phosphatidylcholine (PC), phosphatidylethanolamine (PE), phosphatidylserine (PS), phosphatidylinositol (PI), phosphatidylglycerol (PG) and phosphatidic acid (PA).[8, 9]

Phosphatidylcholine is the most abundant phospholipid in animals lenses, accounting for 31-46% of total phospholipids in rat, chicken, sheep, cow, and pig.[7] In contrast, PC in the human lens only accounts for 11% of the total phospholipidome.[7] The most abundant GP in the human lens is phosphatidylethanolamine (15%).[7, 10, 11] In the human lens, two thirds of phosphatidylethanolamine and phosphatidylserine are 1-*O*-alkyl ether-linked, contributing more than 50% and 65% of the total PE and PS content respectively in the human lens.[7, 10] They differ from the 1-*O*-alkenyl lipids only by the absence of a *cis* double bond at the 1-position.[11] These ether-linked phospholipids are believed to be associated with lens transparency, as the inhibition of their synthesis causes cataract in mice.[12] The general structures of diacyl, 1-*O*-alkenyl ether and 1-*O*-alkyl ether GPs are shown in Figure 4.1a, b and c respectively. A phospholipid with a PE head group, an alkenyl ether-linked, 16-carbon saturated radyl at the *sn*-1 position and a monounsaturated, 18-carbon radyl ester-linked at the *sn*-2 position will be named PE (16:0**p**/18:1). Alternatively, if R^1 is

substituted by an alkyl ether-linked 16-carbon long saturated radyl, it will be named PE (16:0**e**/18:1). Lyso-derivatives of GPs are also observed, which possess the *sn-1* fatty acyl chain only.[8, 10]

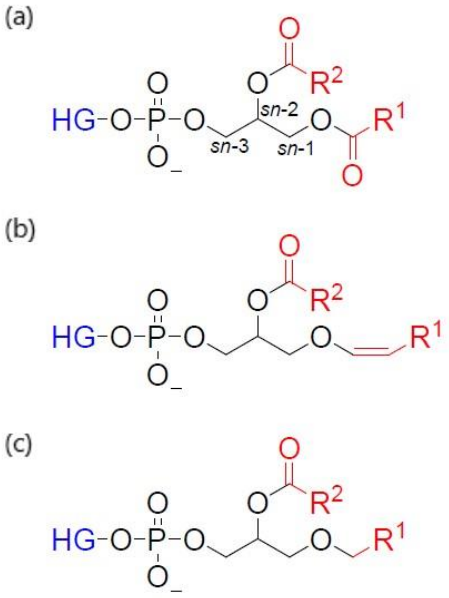

Figure 4.1: The general structures of (a) diacyl GP; (b) 1-O-alkenyl ether; (c) 1-O-alkyl ether. HG, headgroup. R^1, acyl chain at the sn-1 position; R^2, acyl chain at the sn-2 position; sn, stereospecific numbering.

GPs in the human lens have been previously identified and quantified,[7, 11, 13-16] however there is limited data on the distribution of GPs in the human lens. Ellis and colleagues imaged the human lens using desorption electrospray ionisation mass spectrometry (DESI-MS) and showed the distribution of three GPs, namely PE (18:1e/18:1), LPE (18:1e) and PS (18:1e/18:1).[17] The study did not include other classes of GPs such as PA that have been recently identified.[8, 9] In this study, we aimed to investigate the distribution of GPs in the human lens by using matrix-assisted laser desorption ionisation mass spectrometry (MALDI-MS) which provides better spatial resolution compared to DESI-MS.

4.2 Materials and Methods

4.2.1 Materials

The matrix 2,5-diaminonapthalene (DAN) was purchased from Sigma Aldrich (Castle Hill, Australia). Glass microscope slides for tissue mounting were purchased from Proscitech (Townsville, Australia). The optimal cutting temperature (OCT) compound used to adhere the lenses to the glass slides was purchased from Sakura Finetek (Torrance, USA).

4.2.2 Lenses

Human lenses were obtained from eyes donated to the NSW Lions Eye Bank at the Sydney Eye Hospital, (Sydney, Australia) within 2–6 hours of death, and were stored immediately at -80 °C until required. All work was approved by the human research ethics committee at the University of Wollongong (HE 13/401).

4.2.3 MALDI-MS

For MALDI-MS analysis, the methods are as described in Section 2.1.6 and Section 3.2. In brief, lenses were sliced in the transverse plane to produce 20 µm thick slices that were then thaw-mounted onto a glass slide and dried in a desiccator for 10 minutes prior to sublimation. Matrix was sublimed at 30 mTorr and 112 ºC for 15 minutes. Samples were analysed by an LTQ-Orbitrap XL (ThermoScientific, Australia) with a MALDI source. The laser raster step size was set to 100 µm and an average of 50 laser shots produced a spectrum from each spot. The mass spectra were acquired in negative ion mode. The mass resolution at *m/z* 400 was 33000 and the mass range acquired was *m/z* 400-2000. Lipids were identified based on accurate mass, with an error (Δ) of ± 3 ppm. MS imaging data were visualised by ImageQuest 1.0 (ThermoScientific, Australia). Images of the selected *m/z* values were normalized to the total ion current (TIC).

4.3 Results and Discussion

4.3.1 MALDI-MS Images of Phosphatidylethanolamine in Human Lens

The most abundant PEs in the human lens contain 1-*O*-alkyl ether linkages at the *sn*-1 position.[7] Figure 4.2a and b show the distribution of the lysophosphatidylethanolamine (LPE) and PE species in a 51 year-old and 67 year-old human lens, respectively. Their identities were assigned based on accurate mass and previous identification in the human lens.[7] A total of 15 species of PE (see Supplementary Figure S 4.1) and four species of LPE were detected in both human lenses.

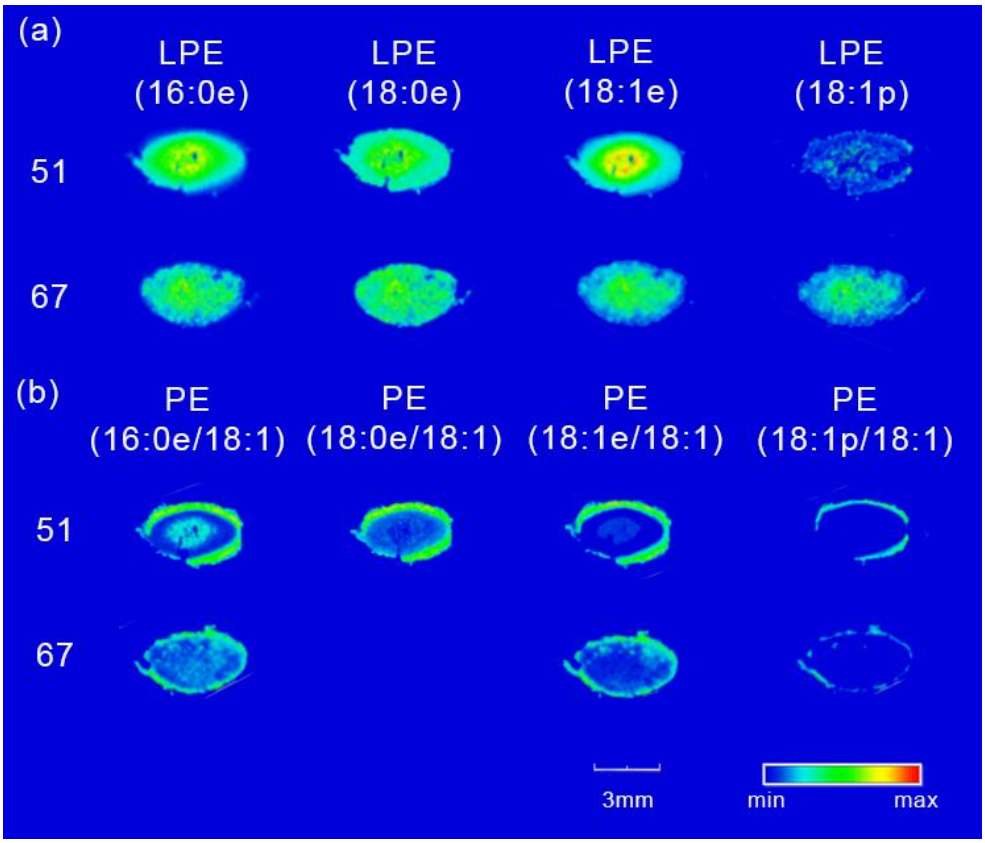

Figure 4.2: (a) Distribution of lyso-PE in a 51-year old and 67 year-old human lens. (b) Distribution of the most abundant PEs in a 51-year old and 67 year-old human lens.

Figure 4.2a shows that different species of LPEs are present in both the cortex and the nuclear regions in both lenses. Most of the LPE species have a higher relative intensity in the nucleus. This observation is more pronounced in the 51 year-old lens in comparison to the 67 year-old lens. The abundance of LPE (18:1p) in the 51-year old lens is significantly lower than the other three species in the same lens, which

was confirmed by quantification data (3% of total LPE in the lens) in Chapter 5, Table 5.3.

The diacyl PE species are located in an annular ring around the outer region of the lens (Figure 4.2b). This is in agreement with what has been observed previously in our lab.[18] PE (18:1e/18:1) is the most abundant PE in the human lens, which contributes about 40% to the total PE detected in the lens.[7] PE (18:1p/18:1), like its lyso analogue, was lower in abundance compared to other PEs. There was no PE (18:0e/18:1) detected in the 67 year-old lens. A previous study in our lab has shown that PE is approximately 1000-fold higher in intensity at the outer region in comparison to the nuclear or barrier regions.[18]

Interestingly, PE (16:0e/18:1) and PE (18:1e/18:1) and their respective LPE analogues showed a complementary distribution, *i.e.* PE were detected at higher abundance in the outer region and LPE were detected at higher abundance in the core. Previous study by Ellis *et al.* using DESI for human lens lipid imaging has obtained similar results where PE was imaged around the outer ring of the lens while LPE was detected around the inner circle of PE in the cortex area.[18] The difference in the images observed between our studies is that Ellis *et al.* did not observe LPE in the nuclear region. As the older lens nucleus contains more compact fibre cells which causes its consistency to be harder as compared to the cortex,[19] it is possible that the spray solvent used in DESI were not able to fully desorb the nuclear region resulting in less LPE to be observed in the nucleus.

4.3.2 MALDI-MS Images of Phosphatidic Acid and Phosphatidylserine in Human Lens

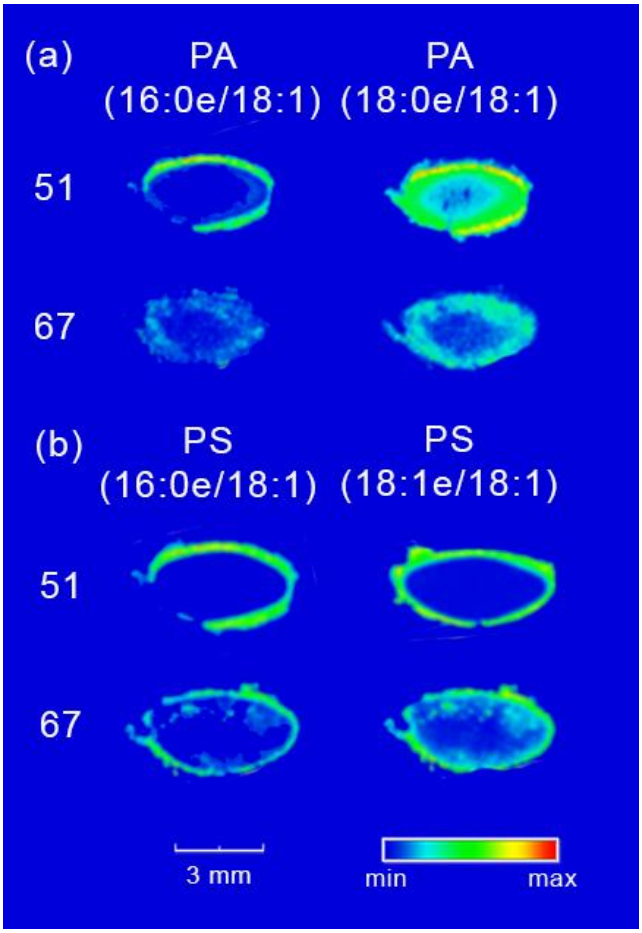

Figure 4.3: Distribution images of PA and PS in a 51-year-old and 67-year-old human lens. All the lipids were detected with $[M-H]^-$ in negative ion mode.

The distribution of PA and PS are shown in Figure 4.3. Figure 4.3a shows the distribution of PA in the human lens. PA (16:0e/18:1) showed an annular distribution around the outer region of the 51-year-old lens. The same PA species showed a similar distribution around the outer region in the 67 year-old lens, however, it does not form a distinct ring as observed in the 51 year-old lens. In contrast, PA (18:0e/18:1) showed a more homogeneous distribution in the cortex, with a higher intensity around the edge of the 51-year-old lens and a lower intensity in the nucleus. In the 67-year-old lens, the distribution of this PA lipid is similar, however it does not show as much difference in the intensity between the outer edge and the nucleus as compared to the 51-year-old lens. PA is the precursor for the biosynthesis of all phospholipids in mammals, thus the localisation of these lipids in the outer, metabolically active region of the human lens enables the potential conversion of PA to other phospholipids.[20] Previous work done in our lab using DESI-

TLC-MS has detected PA in the human lens.[9]

The distribution of seven species of PS in the human lens were obtained using this method and are shown in Supplementary Figure S 4.2. The distribution of two abundant species, PS (16:0e/18:1) and PS (18:1e/18:1),[7] is shown in Figure 4.3b. Both PS species showed a ring distribution around the outer edge of the lens in the 51 and 67 year-old lens. This agrees with the distribution pattern observed by Ellis *et al.* using DESI imaging.[18]

4.4 Conclusion

This study has demonstrated that MALDI-MS is a powerful tool that can be used to observe the localisation of different GPs in the human lens. GPs present in an adult lens were primarily detected in the cortex except for LPE. This is in agreement with previous quantitative work from our group where GPs in the nucleus were depleted in an adult lens after the age of 40.[13] LPE showed a higher relative abundance in the nucleus of the lens in comparison to its PE analogue, which agrees with work indicating that LPE concentration is 4-5 fold higher than PE in the adult lens nucleus.[13]

GPs are more susceptible to oxidation and degradation compared to sphingolipids.[21] There is no lipid turnover in the human lens nucleus,[3] a consequence of which is the degradation of GPs observed with age.[22] This increases the ratio of SL to GPs, which is known to protect against further oxidation and degradation.[21]

In combination with previous imaging studies of sphingolipids in the human lens, we have now obtained spatial distribution data for the majority of the lipids present in an adult human lens. The spatial distribution data provided by imaging mass spectrometry reveals the location of different lipids in different regions of a healthy adult human lens. This data can be used to supplement current knowledge about lens protein distribution to better understand the interaction between lens proteins and lens lipids that contribute to lens cellular function. Further studies to determine the abundance of these lipids, or the changes of their distribution with age are required in order to understand the role of these lipids in different regions of the lens.

4.5 Supplementary

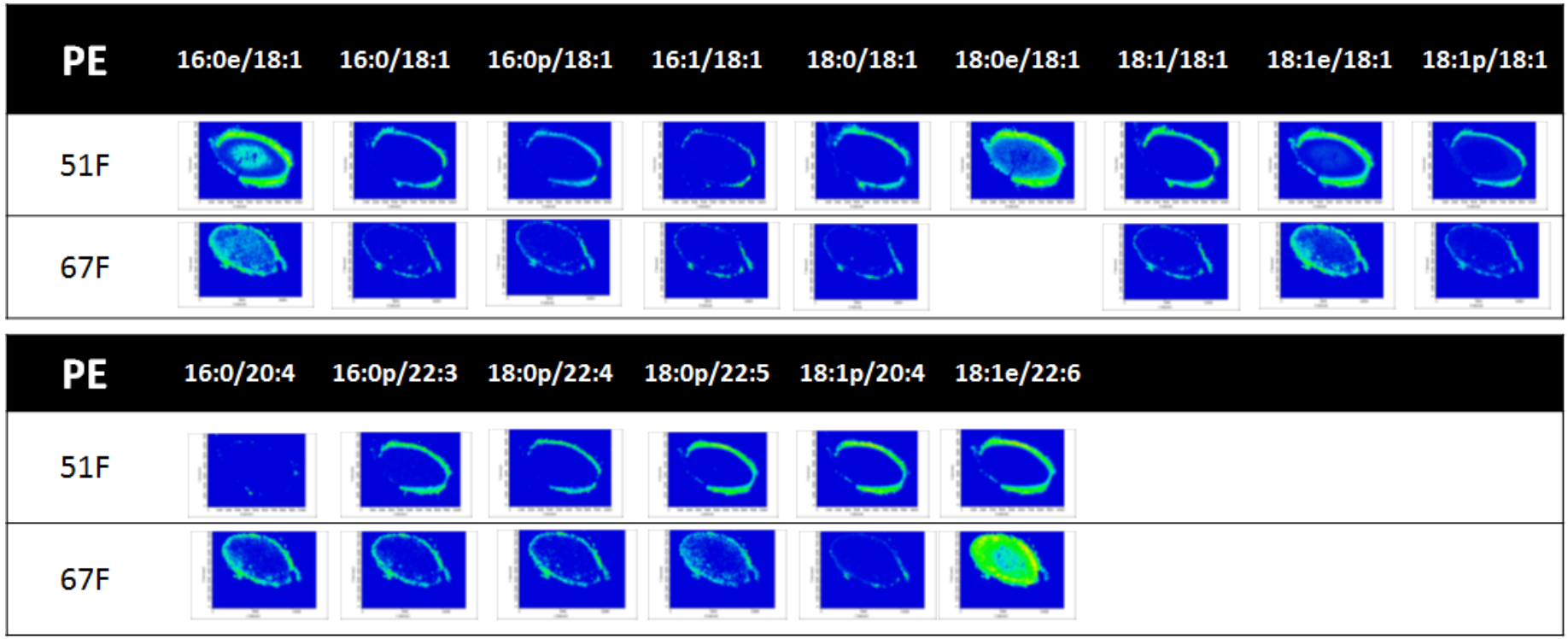

Figure S 4.1: Distribution of all PE species in a 51- and 67-year old human lens.

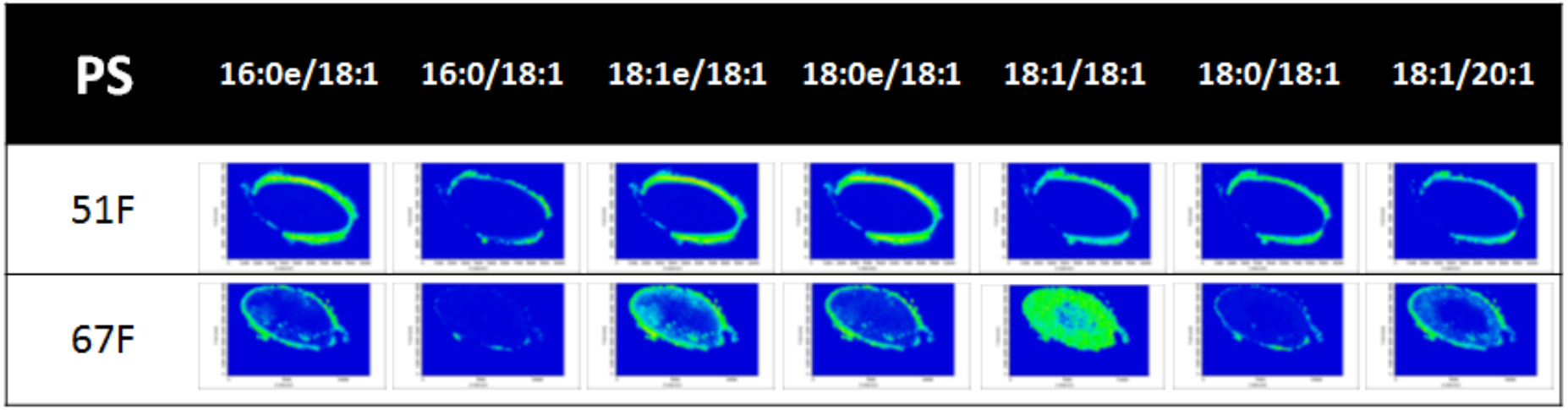

Figure S 4.2: Distribution of all PS species in a 51- and 67-year old human lens.

4.6 References

1. Harding, J., *Biochemistry of the Eye*. Taylor & Francis: 1998.

2. Heys, K. R.; Crams, S. L.; Truscott, R. J. W., Massive Increase in the Stiffness of the Human Lens Nucleus with Age: The Basis for Presbyopia? *Molecular Vision* **2004,** *10*, 956-963.

3. Hughes, J. R.; Levchenko, V. A.; Blanksby, S. J.; Mitchell, T. W.; Williams, A.; Truscott, R. J. W., No turnover in lens lipids for the entire human lifespan. *eLife* **2015,** *4*, e06003.

4. Wride, M. A., Lens fibre cell differentiation and organelle loss: many paths lead to clarity. *Philosophical Transactions of the Royal Society B: Biological Sciences* **2011,** *366* (1568), 1219-1233.

5. Borchman, D.; Yappert, M. C., Lipids and the ocular lens. *Journal of Lipid Research* **2010,** *51*, 2473-2488.

6. Berman, E. R., *Biochemistry of the Eye*. Plenum Press: New York: 1991.

7. Deeley, J. M.; Mitchell, T. W.; Wei, X.; Korth, J.; Nealon, J. R.; Blanksby, S. J.; Truscott, R. J. W., Human lens lipids differ markedly from those of commonly used experimental animals. *Biochimica et Biophysica Acta (BBA) - Molecular and Cell Biology of Lipids* **2008,** *1781* (6–7), 288-298.

8. Deeley, J. M.; Mitchell, T. W.; Xiaojia, W.; Korth, J.; Nealon, J. R.; Blanksby, S. J.; Truscott, R. J. W., Human lens lipids differ markedly from those of commonly used experimental animals. *Biochimica et Biophysica Acta* **2008,** *1781* (6-7), 288-298.

9. Seng, J. A.; Ellis, S. R.; Hughes, J. R.; Maccarone, A. T.; Truscott, R. J. W.; Blanksby, S. J.; Mitchell, T. W., Characterisation of sphingolipids in the human lens by thin layer chromatography–desorption electrospray ionisation mass spectrometry. *Biochimica et Biophysica Acta (BBA) - Molecular and Cell Biology of Lipids* **2014,** *1841* (9), 1285-1291.

10. Estrada, R.; Puppato, A.; Borchman, D.; Yappert, M. C., Reevaluation of the phospholipid composition in membranes of adult human lenses by 31P NMR and MALDI MS. *Biochimica et Biophysica Acta (BBA) - Biomembranes* **2010,** *1798* (3), 303-311.

11. Deeley, J. M.; Thomas, M. C.; Truscott, R. J. W.; Mitchell, T. W.; Blanksby, S. J., Identification of Abundant Alkyl Ether Glycerophospholipids in the Human Lens by Tandem Mass Spectrometry Techniques. *Analytical Chemistry* **2009,** *81* (5), 1920-1930.

12. Rodemer, C.; Thai, T.-P.; Brugger, B.; Kaercher, T.; Werner, H.; Nave, K.-A.; Wieland, F.; Gorgas, K.; Just, W. W., Inactivation of ether lipid biosynthesis causes male infertility, defects in eye development and optic nerve hypoplasia in mice. *Human Molecular Genetics* **2003,** *12* (15), 1881-1895.

13. Hughes, J.; Deeley, J.; Blanksby, S.; Leisch, F.; Ellis, S.; Truscott, R.; Mitchell, T., Instability of the cellular lipidome with age. *AGE* **2011,** *In Press*.

14. Borchman, D.; Byrdwell, W. C.; Yappert, M. C., Regional and age-dependent differences in the phospholipid composition of human lens membranes. *Investigative Ophthalmology & Visual Science* **1994,** *35* (11), 3938-3942.

15. Byrdwell, W. C., Dual parallel mass spectrometers for analysis of sphingolipid, glycerophospholipid and plasmalogen molecular species. *Rapid Communications in Mass Spectrometry* **1998,** *12* (5), 256-272.

16. Huang, L.; Grami, V.; Marrero, Y.; Tang, D.; Yappert, M. C.; Rasi, V.; Borchman, D., Human lens phospholipid changes with age and cataract. *Investigative Ophthalmology & Visual Science* **2005,** *46* (5), 1682-1689.

17. Ellis, S. R.; Wu, C.; Deeley, J. M.; Zhu, X.; Truscott, R. J. W.; Panhuis, M.; Cooks, R. G.; Mitchell, T. W.; Blanksby, S. J., Imaging of Human Lens Lipids by Desorption Electrospray Ionisation Mass Spectrometry. *Journal of American Society of Mass Spectrometry* **2010,** *21*, 2095-2104.

18. Ellis, S. R.; Wu, C.; Deeley, J. M.; Zhu, X.; Truscott, R. J. W.; Panhuis, M. i. h.; Cooks, R. G.; Mitchell, T. W.; Blanksby, S. J., Imaging of Human Lens Lipids by Desorption Electrospray Ionization Mass Spectrometry. *Journal of the American Society for Mass Spectrometry* **2010,** *21* (12), 2095-2104.

19. Elliott, K.; FitzSimons, D. W., *The Human Lens - in Relation to Cataract*. John Wiley & Sons: 2009.

20. Chen, Y.-L.; Montedonico, A. E.; Kauffman, S.; Dunlap, J. R.; Menn, F.-M.; Reynolds, T. B., Phosphatidylserine synthase and phosphatidylserine decarboxylase are essential for cell wall integrity and virulence in Candida albicans. *Molecular Microbiology* **2010,** *75* (5), 1112-1132.

21. Oborina, E. M.; Yappert, M. C., Effect of sphingomyelin versus dipalmitoylphosphatidylcholine on the extent of lipid oxidation. *Chemistry and physics of lipids* **2003,** *123* (2), 223-232.

22. Hughes, J. R.; Deeley, J. M.; Blanksby, S. J.; Leisch, F.; Ellis, S. R.; Truscott, R. J. W.; Mitchell, T. W., Instability of the cellular lipidome with age. *AGE* **2012,** *34* (4), 935-947.

Chapter 5: Changes in Lipids Across Different Regions of the Human Lens with Age

Jo Ann Seng [a], Jessica R. Nealon [b,e], Michael Melcher [c], Stephen J. Blanksby[d], Todd W. Mitchell [b,e*]

[a] School of Chemistry, Faculty of Science, Medicine and Health, University of Wollongong, NSW 2522, Australia.

[b] School of Medicine, Faculty of Science, Medicine and Health, University of Wollongong, NSW 2522, Australia.

[c] Institute of Applied Statistics and Computing, University of Natural Resources and Life Sciences Vienna, 1190 Vienna, Austria.

[d] Central Analytical Research Facility, Queensland University of Technology, Brisbane, QLD 4000, Australia.

[e] Illawarra Health and Medical Institute, University of Wollongong, NSW 2522, Australia.

[*] Correspondence to: T.W. Mitchell, School of Medicine, University of Wollongong, NSW 2522, Australia. Email: toddm@uow.edu.au

Abstract

The human lens consist of four regions (outer, barrier, inner and core) according to the tissue formed during different stages of life (adult, childhood, infantile, *in utero*, respectively). Previous studies examining lens lipids were performed using whole lens homogenates or lenses divided into nucleus and cortex only. However, information on the lipid composition in different regions of the lens is essential to understand the development of the barrier, which develops at the nucleus-cortex interface at middle age and prevents diffusion of molecules such as antioxidants into and out of the nucleus. In this study, lipids were quantified in each region of the lens over the human lifespan. It was revealed that the lipid composition in each lens region is different, for example, glycerophospholipids were found to have a higher abundance in the outer and barrier regions of the lens, while sphingolipids were found to have a higher abundance in the lens inner and core regions. Some lipid classes, such as dihydrolactosylceramides did not change with age whilst of those that did, glycerophospholipids decreased in concentration with age and sphingolipids increased in concentration with age. The sudden increase in ceramide and dihydroceramide levels in the nucleus after the age of 40 as previously observed was also observed in this study. Interestingly, the current data shows that this increase is consistent across all lens regions. It was also identified that age-related alterations in lipid abundances are most prevalent in the barrier region of the human lens, indicating a possible link between membrane alterations and barrier formation. This study provides the most comprehensive data describing age-related alterations to the human lens lipidome to-date. This information is essential in linking the age-related changes of other biomolecules in the lens (*e.g.* proteins) to help understand the onset of eye diseases such as cataract.

Keywords

Barrier region, electrospray ionisation mass spectrometry, glycerophospholipid, sphingolipid, human lens.

Abbreviations

butylated hydroxytoluene (BHT), ceramide (Cer), ceramide phosphate (CerP), dihydroceramide (DHCer), dihydroceramidephosphate (DHCerP), dihydrolactosylceramide (DHLacCer), dihydrolactosylceramide sulfate (DHSM3), dihydromonosialodihexosylganglioside (DHGM3), dihydrosialyl Lewis acid (DHSialyl-Le^x), dihydrosphingomyelin (DHSM), dihydrosulfatide (DHST), dihydrotrihexosylceramide

(DHTriHexCer), generalised additive models (GAM), glycerophospholipid (GP), glycosphingolipids (GSL), lactosylceramide sulfate (SM3), lysophospholipidethanolamine (LPE), methyl-tert-butyl ether (MTBE), monosialodihexosylganglioside (GM3), dihydromonosialotetrahexosylganglioside (DHGM1), monosialotetrahexosylganglioside (GM1), phosphatidic acid (PA), phosphatidylcholine (PC), phosphatidylethanolamine (PE), sphingomyelin (SM), sulfatide (ST).

5.1 Introduction

The human lens grows continuously throughout a human's life span as new fibre cells are stacked on top of the pre-existing lens at birth.[1] The lens can be divided into four regions that represent the four developmental stages of the lens i.e., the embryonic nucleus (core), infantile nucleus (inner), tissue formed in childhood (barrier), and newly synthesized cortical tissue (outer).[2-5] There is no lens fibre cell turnover once mature fibre cells are formed.[6] This is an important factor to consider when investigating the impact of ageing on the lens and the evolution of age-related nuclear cataract. Since there is a lack of protein[6] and lipid[7] turnover in the nucleus of the lens, the lens itself is a good model to investigate lipid stability over time.

Previous literature suggests that the lens lipid composition changes with age e.g., increased concentrations of lipid oxidation products[8] and complex glycosphingolipids such as gangliosides.[9, 10] The majority of these studies have used whole lens homogenates to examine age-related changes in the lens lipidome,[8, 9, 11-13] which analyses both the old and newer lipids that are synthesized after birth together. Therefore, age-related results are difficult to interpret as the "age" of a particular lipid differs greatly across regions. A recent study on age-related degradation of lipid in the lens nucleus has shown that sphingomyelin (SM) and dihydrosphingomyelin (DHSM) levels in the lens nucleus remain constant over the lifespan of an individual while ceramides (Cer) and dihydroceramides (DHCer) increase dramatically in concentration between the ages of 30 and 60.[14] The reason behind these changes remains unanswered. As there is no enzymatic activity in the lens nucleus that would synthesise ceramide,[6, 7] it is likely that this increase results from the degradation of more complex sphingolipids.

Studies performed in the 1960's have identified various glycosphingolipids (GSL) and gangliosides present in human and rhesus monkey lenses.[9, 10, 15-18] They were proposed to comprise <1% total lens lipid, but

played an important role in lens epithelial cell differentiation and maturation to fibre cells.[17] Other sphingolipids, such as lactosylceramide sulfate (SM3) and sulfatides (ST) have also been identified in the human lens recently.[19] It is clear that the previous quantification of the lens lipidome is insufficient as many other classes of glycosphingolipids such as dihydrolactosylceramide (DHLacCer) and gangliosides remain unquantified across the different regions of the lens.

Given the different age of fibre cells within each lens region and the role of age-related changes in lipid and protein composition in the development of cataract[20] and presbyopia[21] it is essential to elucidate the complete lipid profile in different regions of the lens and study their changes with age. Accordingly, the aim of this study was to characterise the changes in lipid profile in the core, inner, barrier and outer regions of the human lens with age.

5.2 Materials and Methods

5.2.1 Materials

MTBE, chloroform and methanol were HPLC grade and purchased from Thermo Scientific (Scoresby, VIC, Australia). Analytical grade butylated hydroxytoluene (BHT) and sodium hydroxide (98% minimum) where purchased from Sigma Aldrich (Sydney, NSW, Australia). Analytical grade ammonium acetate was purchased from Crown Scientific (Moorebank, NSW, Australia). Screw thread vials (4 mL) and 1.8 mL wide mouth vials (both with PTFE/silicone septa caps) were purchased from Grace Davison (Rowville, VIC, Australia). Lipid standards were synthesized by Avanti Polar Lipids (Alabaster, USA) except for deuterated monosialotetrahexosylganglioside (GM1) and monosialodihexosylganglioside (GM3), which were purchased from Matreya LLC (Pennsylvania, USA).

5.2.2 Lenses

Human lenses were obtained from eyes donated to the NSW Lions Eye Bank at the Sydney Eye Hospital, (Sydney, Australia) within 2–6 hours of death, and were stored immediately at -80 °C until required. All work was approved by the human research ethics committee at the University of Wollongong (HE 13/401). Table 5.3 shows the age and tissue weight of each region of the lenses used in this study.

Table 5.1: Age and tissue weight of each region of the lenses used in this study. O: outer region, B: barrier region, I: inner region, C: core region.

Lens age (years)	Tissue weight (mg)			
	Outer	**Barrier**	**Inner**	**Core**
8	0	60.1	21.4	29.2
9	0	48.8	18.8	61.7
16	0	43.2	16.5	37.9
19	0	3.4	19.6	25
23	0	14	22.9	33.4
27	0	32.3	30	30.2
31	0	26.4	22.3	36.9
38	9.3	25.7	22.6	35.9
43	39.6	40.6	24.5	36.8
48	3.3	26.6	25.9	57.8
50	21.6	52.5	25.4	48.7
55	38.5	27.3	20.5	43
62	5.4	15.4	23.9	33.6
66	16.2	53.4	32.6	56.1
70	30.6	53.7	13.2	34.6
74	23.5	46.2	21.6	34.5

5.2.3 Lipid Extraction

Sixteen lenses between the ages of 8 and 74 were dissected as described in Chapter 2.2.1.[3]. No technical replicates were run due to the limited sample volume extracted. Trephines with diameters of 8, 6, and 4.5 mm were used to dissect lenses into the outer (>8 mm), barrier (8–6 mm), inner (6–4.5mm), and core (4.5 mm) regions, respectively (Figure 2.10).

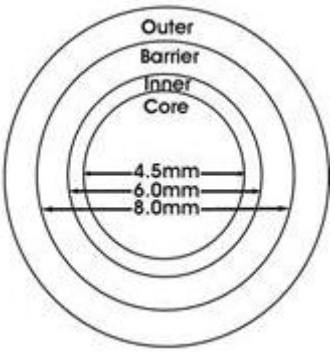

Figure 5.1: Illustration of the four regions of the lens obtained by dissection.[3]

Immediately following dissection, all regions were weighed and total lipids extracted using methyl-tert-butyl ether (MTBE) with mechanical bead homogenisation as described elsewhere.[22, 23] In brief, tissue was added to homogenisation vials (Geneworks, Hindmarsh, SA, Australia) with ceramic beads, 300 µL of methanol containing 0.01 % BHT and 50 µL of an internal standard mixture (Table 5.2). The tissue was homogenised with a mechanical bead homogenizer (FastPrep-24, MP Biomedical, Seven Hills, NSW, Australia) at 6 m/s for 40 seconds, then transferred to a glass vial. 100 µL MeOH + 0.01% BHT was used to wash the beads before combining the wash with the homogenate. 920 µL of MTBE was added to the homogenate and rotated overnight at 4 °C. Following this, 230 µL of 150 mM ammonium acetate was added to the homogenate and vortexed for 20 seconds. The homogenate was then centrifuged for 5 minutes at 2000 *g* to complete phase separation. The top phase containing MTBE and extracted lipids (~900 µL) was transferred to a new glass vial without disturbing the lower aqueous phase. Samples were dried under a stream of nitrogen at 37 °C, resuspended in 1:2 chloroform:methanol and stored at -20 °C. Prior to ESI-MS analysis, extracts were diluted 10-fold in 2:1 methanol:chloroform + 1 mM ammonium acetate.

5.2.4 Mass Spectrometry

All mass spectra were obtained using a LTQ-Orbitrap XL mass spectrometer (ThermoScientific, Australia) equipped with an electrospray ion source. Capillary voltage was set to -50 V, capillary temperature 250 °C and tube lens voltage -175 V. Sheath gas was set to 17, auxillary and sweep gas were turned off, and spray voltage was set to 4.5 kV. Multipole 00, multipole 0 and multipole 1 were set to 4 V, 4.5 V and 8 V,

respectively. Lens 0, lens 1 and gate lens voltage were set to 4.2 V, 15 V and 35 V, respectively. Multipole RF amplitude was set to 400 (V p-p) and front lens voltage was set to 5.25 V. Diluted lipid extracts were infused into the electrospray ion source at a flow rate of 5 $\mu L.min^{-1}$ with a maximum injection time of 200 ms. Mass spectra were acquired in negative mode with an average of 50 microscans with mass resolution of 100,000. Lipids were identified according to accurate mass (< 3 ppm) with a signal to noise ratio of 5:1. However, sugar groups were not specifically characterised in this study with GSL identities assigned based on previous identification in the human lens.[15, 16, 24] All lipids were detected as $[M+Cl]^-$ or $[M-H]^-$ ions (See supplementary Table S 5.1 and Table S 5.2 for details).

Lipids were quantified by averaging 50 MS scans in negative ion mode and the peak intensity of each lipid was obtained. Following isotope correction, the ion abundance for each lipid was normalised to the appropriate internal standard (Table 5.2), and multiplied by the known concentration of that internal standard (nmol.g $(tissue)^{-1}$). Lipid classes with no commercially available standard were quantified using an internal standard with the closest chemical properties. The internal standard used for each lipid class is shown in Table 5.2. All lipid species were summed to give a total lipid of each class in the different regions of the lens.

Table 5.2: Lipid standard used to quantify each lipid class and its concentration in the internal standard mixture.

Lipid Class	Lipid Standard	Concentration (μM)
LPE	LPE 14:0	20
PA	PA (17:0/17:0)	20
PE	PE (17:0/17:0)	20
PC	PC (19:0/19:0)	30
SM	DHSM 12:0	85
DHSM		
Cer	Cer 12:0	25
DHCer	DHCer 12:0	25
CerP	CerP 12:0	30
DHCerP		
DHLacCer	LacCer 12:0	30
DHTriHexCer		
ST	ST 12:0	30
DHST		
SM3		
DHSM3		
DHGM3	GM3 17:0-CD3	20
DHGM1	GM1 17:0-CD3	30
DHSialyl-Le^x	GM3 17:0-CD3	20

LPE: lysophospholipidethanolamine, PA: phosphatidic acid, PE: phosphatidylethanolamine, PC: phosphatidylcholine, SM: sphingomyelin, DHSM: dihydrosphingomyelin, Cer: ceramide, DHCer: dihydroceramide, CerP: ceramide phosphate, DHCerP: dihydroceramidephosphate, DHLacCer: dihydrolactosylceramide, DHTriHexCer: dihydrotrihexosylceramide, ST: sulfatide, DHST: dihydrosulfatide, SM3: lactosylceramide sulfate, DHSM3: dihydrolactosylceramide sulfate, DHGM3: dihydromonosialodihexosylganglioside, DHGM1: monosialotetrahexosylganglioside, DHSialyl-Le^x: dihydrosialyl Lewis acid.

5.2.5 Nomenclature

In this paper glycerophospholipids (GPs) and sphingolipids will adopt the abbreviations of Fahy *et al.*[25] 1-*O*-alkyl ether and 1-*O*-alkenyl ether lipids will have the abbreviation of "O-" before the fatty acyl chains.

5.2.6 Statistical Analysis

As the change in concentration with age was nonlinear for most lipids, generalised additive models (GAM) were fit to the data. GAM is an extension of generalised linear models with a smoothing function.[26] It helps to predict a model that is not totally linear by applying a smoothing term. The solid line in all figures corresponds to the GAM fit while dashed lines show the 95% confidence interval for the fit. All

computations were performed using R version 3.4.10 (R Core Team 2009) with extension package mgcv.

5.3 Results and Discussion

In this study 94 lipids species were detected in the human lens using ESI-MS. This includes 6 classes of SL, 9 classes of GSLs and 4 classes of GPs. A full list of individual lipids detected is shown in Supplementary tables S 5.1 and S 5.2. A comparison of the percentage distribution of each lipid class in the core, inner, barrier and outer region of human lenses is shown in Table 5.3.

Table 5.3: Comparison of the percentage distribution of lipid classes in the core, inner, barrier and outer region of human lenses. Data are presented as mean ± SEM. n=16 for the core, inner and barrier regions, n=10 for the outer region.

Lipid Class		Percentage of total lipid (%)											
		Core			Inner			Barrier			Outer		
GP	LPE	5.78	±	0.50	4.53	±	0.35	3.28	±	0.24	3.04	±	0.39
	PA	0.46	±	0.13	0.59	±	0.18	1.00	±	0.20	0.89	±	0.27
	PE	13.1	±	2.99	21.8	±	3.33	25.06	±	2.28	28.19	±	2.45
	PC	1.30	±	0.38	3.70	±	0.86	6.95	±	1.63	9.05	±	2.28
	Total	20.64	±	2.89	30.62	±	4.79	36.29	±	5.47	41.17	±	6.21
SL	SM	6.54	±	0.46	8.18	±	0.62	8.54	±	0.52	8.77	±	0.76
	DHSM	34.35	±	1.45	35.41	±	1.87	30.55	±	1.12	30.01	±	2.60
	Cer	2.73	±	0.74	1.33	±	0.43	0.48	±	0.18	0.65	±	0.37
	DHCer	8.79	±	2.20	3.74	±	1.12	0.93	±	0.34	0.6	±	0.21
	CerP	2.48	±	0.44	1.91	±	0.50	2.52	±	0.48	2.46	±	0.75
	DHCerP	10.34	±	1.69	7.22	±	1.89	7.80	±	1.43	6.14	±	1.32
	Total	65.23	±	4.87	57.8	±	5.68	50.81	±	4.63	48.62	±	4.57
GSL	DHLacCer	4.19	±	0.25	2.27	±	0.19	1.25	±	0.09	0.85	±	0.08
	DHTriHexCer	0.73	±	0.11	0.49	±	0.06	0.41	±	0.05	0.36	±	0.09
	ST	0.02	±	0.01	0.04	±	0.01	0.05	±	0.01	0.07	±	0.02
	DHST	0.06	±	0.01	0.10	±	0.01	0.12	±	0.01	0.13	±	0.02
	SM3	0.06	±	0.01	0.07	±	0.01	0.07	±	0.01	0.07	±	0.02
	DHSM3	0.24	±	0.02	0.24	±	0.03	0.23	±	0.02	0.21	±	0.02
	DHGM3	7.13	±	0.91	5.83	±	0.65	8.51	±	1.00	6.73	±	0.55
	DHGM1	1.49	±	0.49	2.36	±	0.91	2.14	±	0.68	1.75	±	0.41
	DHSialyl-LeX	0.20	±	0.04	0.18	±	0.05	0.11	±	0.03	0.05	±	0.02
	Total	14.13	±	0.83	11.58	±	0.65	12.9	±	0.92	10.21	±	0.72

LPE: lysophospholipidethanolamine, PA: phosphatidic acid, PE: phosphatidylethanolamine, PC: phosphatidylcholine, SM: sphingomyelin, DHSM: dihydrosphingomyelin, Cer: ceramide, DHCer: dihydroceramide, CerP: ceramide phosphate, DHCerP: dihydroceramidephosphate, DHLacCer: dihydrolactosylceramide, DHTriHexCer: dihydrotrihexosylceramide, ST: sulfatide, DHST: dihydrosulfatide, SM3: lactosylceramide sulfate, DHSM3: dihydrolactosylceramide sulfate, DHGM3:

dihydromonosialodihexosylganglioside, DHGM1: monosialotetrahexosylganglioside, DHSialyl-Le^x: dihydrosialyl Lewis acid

5.3.1 Core Region

Phosphatidylethanolamine (PE) was the most abundant GP class in the human lens core, contributing 13.1% of total lipid and 63.5% of total GP (Table 5.3). As shown in Table 2, lysophosphatidylethanolamine (LPE) was also a major GP class in the lens core (28% of total GP), with phosphatidylcholine (PC) and phosphatidic acid (PA) detected at much lower levels. Of the molecular phospholipids in the core PE (O-36:2) was the most abundant species contributing 7.6% of total GP (Supplementary Table S 5.1). These findings agree with previous studies for the most part,[14, 27, 28] however, data from Hughes *et al.* suggests that LPE levels are considerably higher at almost 50% of total GP.[14] Nevertheless, the current LPE data is in agreement with another previous study,[29] which suggests that the correction factor used by Hughes and colleagues to adjust for differences in fragmentation between LPE and the PE internal standard may have been overestimated.

The most abundant SL class in the human lens core was DHSM, which contributed 34.4% of total lipid measured in the core (Table 5.3). As shown in Table 5.3, dihydroceramide phosphate (DHCerP) (10.3%) and DHCer (8.8%) were also a major SLs in the lens core, with their analogues comprising a sphingosine backbone at much lower levels. Of the SLs in the core, DHSM 16:0 was the most abundant SL which accounts for 58% of total DHSM followed by DHSM 24:1 (30%) (Table 5.2). This agrees with previous studies and applies for all the SL in the lens where the two most abundant species are those with a sphinganine backbone and a 16:0 or 24:1 fatty amide.[14, 19, 27, 30]). Interestingly, both DHLacCer 16:0 and DHLacCer 24:1 were very similar in abundance (~ 49% and ~ 40% of total DHLacCer, respectively), which was different from other SL classes mentioned previously, where the 16:0 analogue had a higher abundance than the 24:1 analogue. For example DHSM 16:0 was approximately 28% higher in abundance than DHSM 24:1 while DHCer 16:0 was approximately 25% higher in abundance than DHCer 24:1.

Total GSLs in the core comprised about 14.1% of total lipid (Table 5.3). Dihydromonosialodihexosylganglioside (DHGM3) (7.1%) was the most abundant GSL class in the core region, followed by DHLacCer (4.2%) and dihydromonosialotetrahexosylganglioside (DHGM1) (1.5%). As shown in Table 5.3, the rest of the GSLs were of very low abundance in the lens core, with sulfo-GSLs

such as ST abundance being as low as 0.02%.

5.3.2 Inner Region

The inner region of the lens is comprised of fibre cells that were laid down immediately after birth.[3, 31, 32] Total GP in inner region of the human lens was 30.6%. PE was the most abundant GP class in the inner region accounting for 21.8% of total lipid, followed by LPE at 4.5% and PC at 3.7%. PA was the least abundant GP class at 0.6%.

Total SL in the inner region of the lens was 57.8% of total lipid. DHSM was the most abundant SL (35.4%) in the inner region of the lens (Table 5.3). Cer and DHCer accounted for 1.3% and 3.7% of total lipid in the inner region of the lens, respectively (Table 5.3). Meanwhile, ceramide phosphate (CerP) and DHCerP levels in the inner region were around 1.9% and 7.2% of total lipid, respectively (Table 5.3).

DHGM3 (5.8%) was the most abundant GSL, followed by DHGM1 (2.4%) and DHLacCer (2.3%). Dihydrotrihexosylceramide (DHTriHexCer) and dihydrosialyl Lewis acid (DHSialyl-Le^x) comprised 0.5% and 0.2% of total lipid in the inner region. The sulfo-GSLs such as SM3, dihydrosulfatide (DHST), and ST had negligible abundance in total lipid with less than 0.1% each except for dihydrolactosylceramide sulfate (DHSM3) (0.2%).

5.3.3 Barrier Region

The barrier region is part of the lens cortex, with its cells laid down during childhood years. The GP content in the barrier region is 36.3% as shown in Table 5.3. PE was the most abundant GP in the barrier region at 25.1% of total lipid, followed by PC (6.9%), LPE (3.3%) and PA (1%). The most abundant PC in the lens was PC (34:1), which contributed ~ 35% to total PC. This is in agreement with previous quantification by Deeley *et al.* and Hughes *et al.* where the most abundant PC is assigned as PC (16:0/18:1).[14, 27]

The most abundant SL in the barrier region of the human lens was DHSM (30.6%), as shown in Table 5.3. It was followed by SM (8.5%), DHCerP (7.8%) and CerP (2.5%). Cer and DHCer in the barrier region were less than 1% each. DHGM3 (8.5%) was the most abundant GSL class followed by DHGM1 (2.1%) and DHLacCer (1.3%) (Table 5.3). Total sulfo-GSLs (ST+ DHST+SM3+DHSM3) in the barrier region was 0.5%, with DHTriHexCer accounted for 0.4% and DHSialyl-Le^x at 0.1% of total lipid.

5.3.4 Outer Region

There were only 10 samples in the outer region as the young lenses were relatively smaller in size (not more than 8mm), thus there was no outer region tissue obtained for lenses from age 8 to 30). PE was the most abundant GP class in the outer region of human lens, contributing 28.2% of total lipid and 68.5% of total GP (Table 5.3). As shown in Table 5.2, PC was also a major GP class in the lens outer region (21.9% of total GP), with LPE and PA detected at much lower levels.

The most abundant SL in the outer region was DHSM (30.0%) as shown in Table 5.3. This is followed by SM and DHCerP which accounted for 8.8% and 6.1% of total lipid in the outer region, respectively. Cer and DHCer had the lowest abundance in this region (< 1%). GSLs in the outer region accounted for 10.2% of total lipid. DHGM3 was the most abundant GSL class, contributing 6.7% of total lipid followed by DHGM1 (1.8%). The rest of the GSLs were less than 1% each.

5.3.5 Comparison Across Lens Regions

This is the first study to quantify some of the SLs (CerP and DHCerP) and GSLs (DHLacCer, DHTriHexCer, ST, DHST, SM3 and DHSM3) in different lens regions. This work demonstrates that the lipid composition of different regions in the lens can vary. The outer region was comprised of the highest percentage of GPs at 41.2% of total lipid in all regions of the lens (Table 5.3). It was observed that the GP content decreases as the lens fibre cells get older (from cortex to nucleus). This may be due to the lack of metabolic pathways in the lens core. Subsequently, this lack of repair mechanisms results in the degradation of GPs over time.[33-35] PA remained as the GP with the lowest abundance in all regions. PE was the most abundant lipid class of all GPs across each region of the lens. Total PE levels were twice as high in the outer region compared to core of the lens (28.2% vs. 13.1%). The relative percentage of PE increased from the core towards the outer region, in contrast to the percentage of LPE, which decreased from the core towards the outer region. This is contrary to previous observations of LPE abundance by DESI-MSI, which was higher in the barrier/inner cortex region of the human lens than in the nucleus.[36] However, the data obtained from imaging an individual lens slice may not be a true representation of the lipid abundance of an entire region. The abundance of PC was also highest in the outer region at 9.1% of total lipid.

SL levels were highest in the lens core and lowest in the outer region of the lens. This may be due to the

low oxidative susceptibility of SLs in the lens nucleus.[6, 7] DHSM represented the most abundant lipid in all regions of the lens. Both Cer and DHCer percentages decreased gradually from the core towards the outer region. In the barrier and outer regions, both of these lipids abundances were less than 1%. This is in agreement with our previous imaging data (Chapter 3, Figure 3.3) where the distribution of Cer and DHCer were concentrated in the lens nucleus only.

The most abundant GSL in all regions of the lens was DHGM3. Both DHLacCer and DHTriHexCer showed a decrease in percentage from the lens core towards the outer region. DHLacCer abundance in the inner region was about half its abundance in the core (2.3% and 4.2% respectively). DHSM3 and SM had similar relative abundances across all regions of the lens, while the percentage of both ST and DHST increased from the core towards the outer region. DHST 16:0 was more abundant than DHST 24:1, however, for ST, SM3 and DHSM3, their 24:1 analogue was more abundant than their 16:0 analogues. As opposed to DHST, DHSialyl-Le^x showed a decrease in relative abundance from the core towards the outer region. This is in agreement with our previous imaging data (Chapter 3, Figure 3.5), which showed that both ST and DHST were present in the outer region of the lens where as DHSialyl-Le^x was present in the nucleus. The gangliosides in the lens were predominated by 16:0 and 24:1 fatty acids, which agreed with previous literature.[37] In our study, all gangliosides in the lens had a higher abundance of long chain monounsaturated 24:1 analogues in comparison to their 16:0 analogue. This is in agreement with previous observation by Tao and co-workers.[38]

5.3.6 Age-related Changes in Lipids

5.3.6.1 Core Region

As shown in Figure 5.2a, PE decreased in abundance in adolescent lenses and started to plateau around 30-50 years of age before declining again as observed previously.[14] Conversely, no age-related changes were observed for LPE, PA or PC (see Supplementary Figure S 5.1). This is in contrast to a previous observation of decreases in PC and LPE abundance with age by Hughes et al.[14] This may be due to a smaller number of samples below the age of 20 in our experiment, which contained a higher abundance of PC and high variability in lipid concentration between lenses.

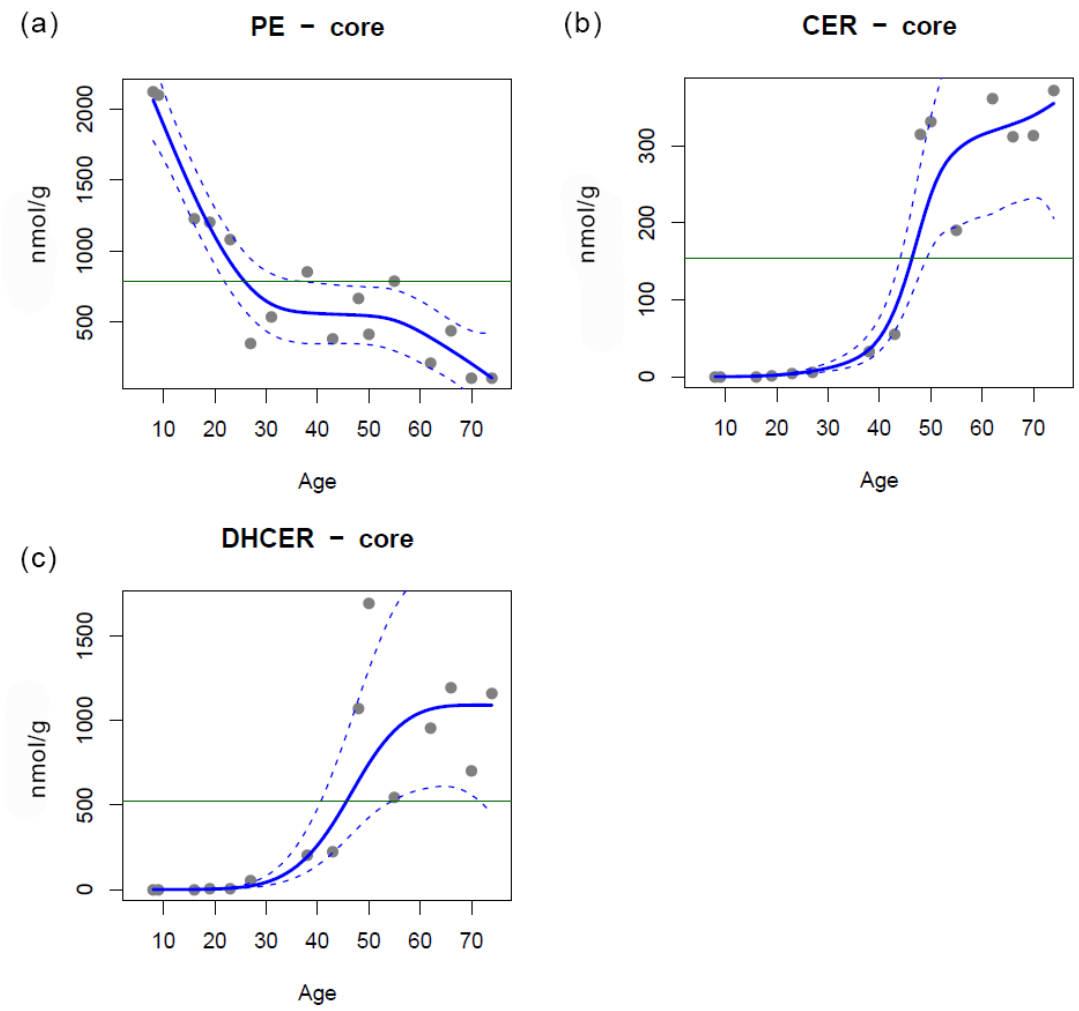

Figure 5.2: Total (a) PE; (b) Cer and (c) DHCer present in the core region of human lenses of different ages. All values are expressed in nmol/g tissue wet weight. The solid line is a generalised additive model fit; the dashed lines give a 95% confidence band. The green line corresponds to the mean of the data. PE: phosphatidylethanolamine, Cer: ceramide, DHCer: dihydroceramide.

Data from the current study regarding changes to Cer and DHCer concentrations with age demonstrates similar patterns to previous reports.[14] It was observed that Cer and DHCer that were almost undetectable in the adolescent lens (0-6 nmol/g) increased suddenly in concentration from age 40 onwards (Figure 5.2b and c). DHCer increased 1100-fold (~1100 nmol/g) from adolescence whereas Cer increased approximately 350-fold (~350 nmol/g) from adolescence. The reason for this pronounced change remains unkown. No age-related changes in DHSM, SM, CerP or DHCerP were observed in the lens core (Supplementary Figure S 5.2). While age-related changes in CerP and DHCerP levels have not previously been investigated the DHSM and SM data agree with previous findings.[14]

Regardless of age, the presence of the same GSL classes in the lens core was observed. This is in agreement with an age-related study by Ogiso *et al.* where they observed that the ganglioside composition was constant for whole human lens homogenates between 16 – 80 years.[10] Our data also suggest that there are no age-related changes in any GSL class in the core region of the lens (see Supplementary Figure S 5.3). Although Ogiso *et al.* observed that DHGM3 and DHGM1 levels accumulated with ageing and cataract progressing lenses, this may be due to their study using whole lenses and therefore cannot be compared to the lens core where there is no lipid turnover.[7, 10]

5.3.6.2 Inner Region

Like the core region, most GP classes such as LPE, PA and PC showed no age-related effects changes in concentration (Supplementary Figure S 5.4). The only GP that displayed a different age-related effect to its core is PE, where it showed a more pronounced linear decrease in concentration with age (Figure 5.3a) in comparison to its core, where the decrease plateaus around middle age (Figure 5.2a). The total PE in the inner region decreased from approximately 3500 nmol/g at adolescent years to approximately 500 nmol/g at 70 years of age.

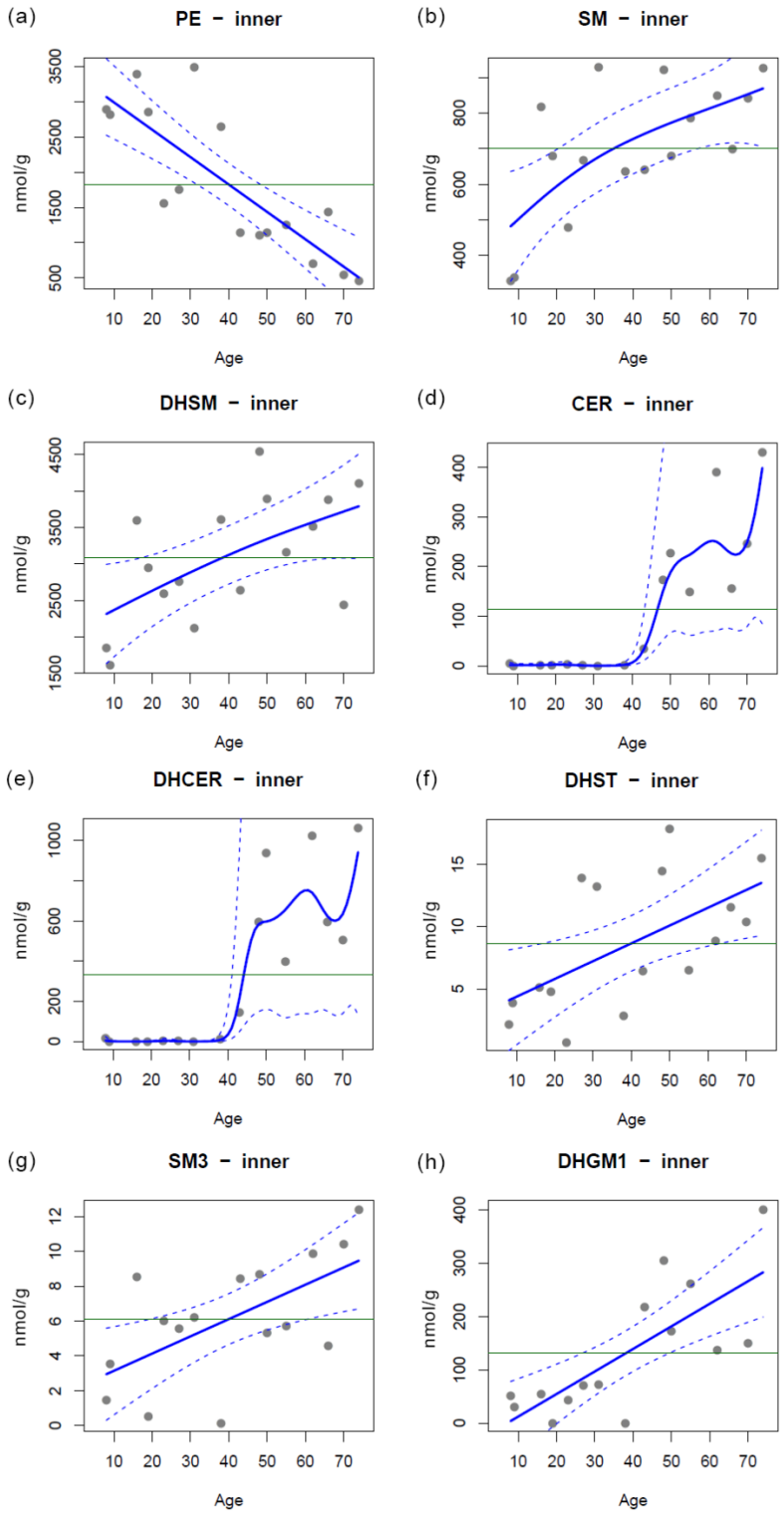

Figure 5.3: Total (a) PE; (b) SM, (c) DHSM, (d) Cer, (e) DHCer, (f) DHST, (g) SM3 and (h) DHGM1 present in the inner region of human lenses of different ages. All values are expressed in nmol/g tissue wet weight. The solid line is a generalised additive model fit; the dashed lines give a 95% confidence band. The green line corresponds to the mean of the data. PE: phosphatidylethanolamine, SM: sphingomyelin, DHSM: dihydrosphingomyelin, Cer: ceramide, DHCer: dihydroceramide, DHST: dihydrosulfatide, SM3: lactosylceramide sulfate, DHGM1: monosialotetrahexosylganglioside.

Figure 5.3b and c show the age effect on the total concentration of SM and DHSM in the inner region of human lenses, respectively. An increase in the total concentration was observed for both SL with age in contrary to the core where no age-related change was observed. The relationship between Cer and DHCer with age is shown in Figure 5.3d and e, respectively. The trend for both Cer and DHCer is similar to what was observed in the lens core, where no traces of these lipids were found in adolescent lenses, but a sharp increase was observed after the age of 40 until old age. The amplitude of increase is also similar to the core, ~ 400 nmol/g for Cer and ~ 1000 nmol/g for DHCer. No age-dependent effect on the concentration of CerP and DHCerP was observed (see Supplementary Figure S 5.4).

SM3, DHST and DHGM1 abundance increased linearly with age, as shown in Figure 5.3f, g and h, respectively. No other GSLs displayed age-related changes in concentration in the inner region of the lens (Supplementary Figure S 5.5).

5.3.6.3 Barrier Region

Figure 5.4a and b show an age-related effect for total PE and PC abundance in the barrier region of human lenses, respectively. It was observed that PE concentration decreased with age in the barrier region, but this decrease was not as pronounced as that observed in the core and inner regions. The total abundance of PC decreased non-linearly with age as opposed to the lens nucleus (core and inner regions) where no age-related effect was observed. PC decreased from ~1200 nmol/g to ~600 nmol/g from a young age until 40 years and then plateaued. Other GPs such as LPE and PA did not show any changes with age (Supplementary Figure S 5.6).

Figure 5.4c and d show that SM and DHSM levels increased in the barrier region with age, respectively. SM abundance increased until 20 years, then plateaued from 20 to 40 years before increasing again. Meanwhile, DHSM increased linearly with age in the human lens barrier. This is in agreement with a previous study that reported an increase of DHSM in the barrier region of older lens.[30]

Similar to the core and inner region, Cer and DHCer were negligible in young lenses but showed a sharp increase after the age of 40 (as shown in Figure 5.4e and f, respectively). However, the increase is not as pronounced as that observed in the lens core and inner regions (250-fold and 400-fold vs. 1000-fold). CerP abundance increased linearly with age (Figure 4g) whereas its sphinganine analogue, DHCerP, did not show

any age-related changes in abundance (Supplementary Figure S 5.6).

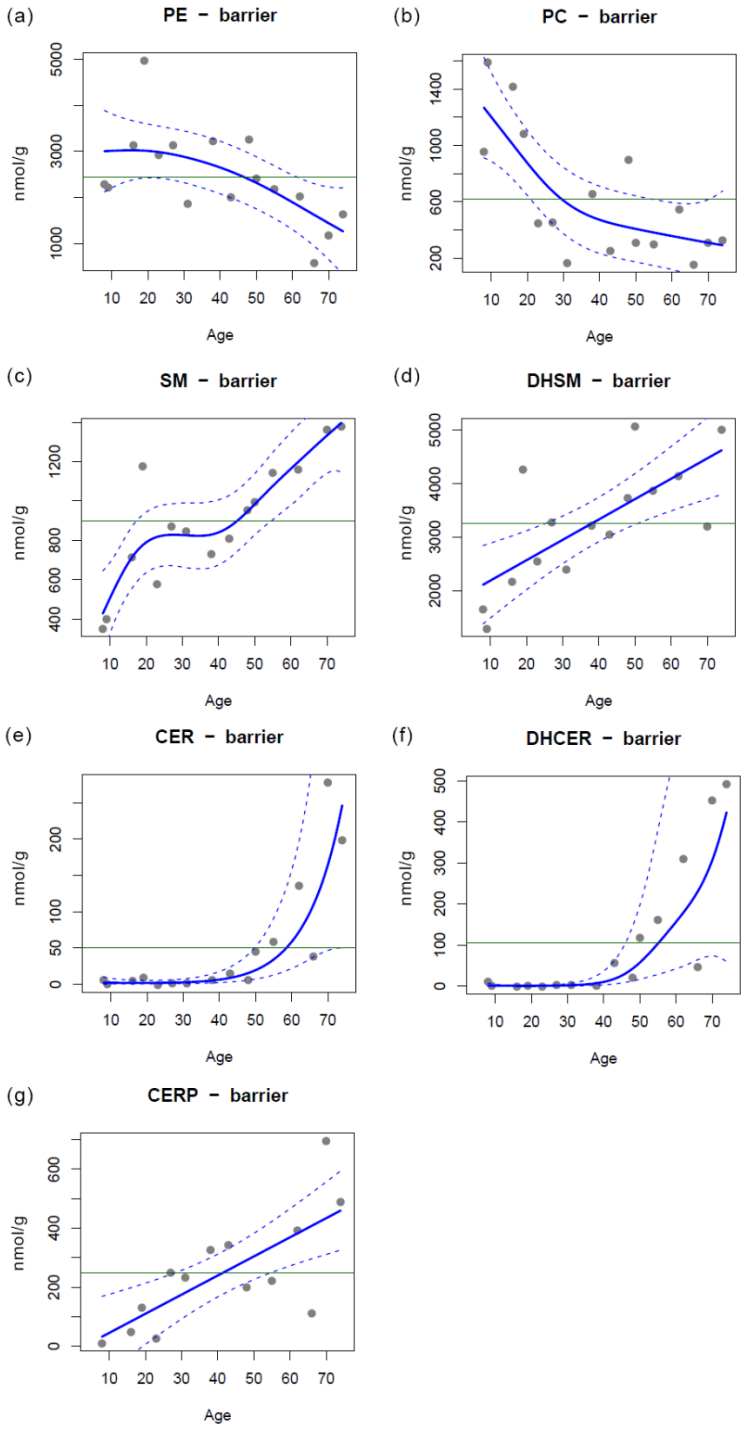

Figure 5.4: Total (a) PE; (b) PC, (c) SM, (d) DHSM, (e) Cer, (f) DHCer, (g) CerP present in the barrier region of human lenses of different ages. All values are expressed in nmol/g tissue wet weight. The solid line is a generalised additive model fit; the dashed lines give a 95% confidence band. The green line corresponds to the mean of the data. PE: phosphatidylethanolamine, PC: phosphatidylcholine, SM: sphingomyelin, DHSM: dihydrosphingomyelin, Cer: ceramide, DHCer: dihydroceramide, CerP: ceramide phosphate.

Of the GSLs, only sulfo-GSLs displayed age-related changes in the barrier region of the lens. A linear increase was observed for ST (Figure 5.5a) and DHST (Figure 5.5b) with age. ST increased from ~0 nmol/g to ~10 nmol/g from young to old age where DHST increased from ~5nmol/g to 20 nmol/g. SM3 and DHSM3 also increased in total abundance from young to old age (Figure 5.5c and d). Other GSLs did not show any age-related changes in abundance (see Supplementary Figure S 5.6).

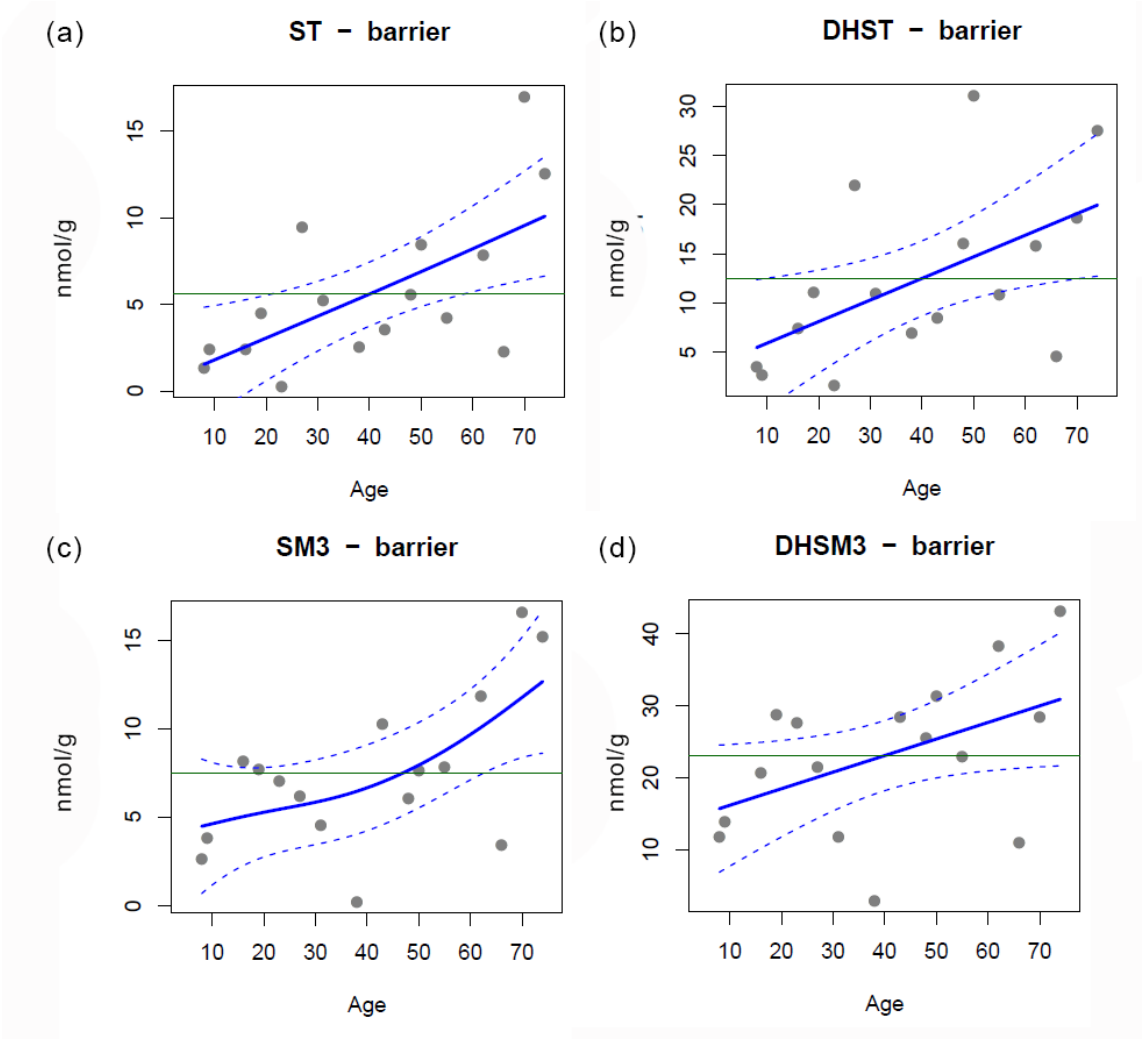

Figure 5.5: Total (a) ST; (b) DHST, (c) SM3, (d) DHSM3 present in the barrier region of human lenses of different ages. All values are expressed in nmol/g tissue wet weight. The solid line is a generalised additive model fit; the dashed lines give a 95% confidence band. The green line corresponds to the mean of the data. ST: sulfatide, DHST: dihydrosulfatide, SM3: lactosylceramide sulfate, DHSM3: dihydrolactosylceramide sulfate.

5.3.6.4 Outer Region

There were no age-related changes observed in any GP class in the outer region (See Supplementary Figure S 5.7). Age-related effects on the total abundance of SM and DHCer are shown in Figure 5.6a and b, respectively. SM levels increased by approximately 400 nmol/g in lenses aged 50 and above (Figure 5.6a). On the other hand, DHCer levels gradually increased from age 50 to 70 by approximately 100 nmol/g. Due to the small sample size, many of the age-related effects on other SLs were difficult to determine (see Supplementary Figure S 5.7).

Age-related effects on total ST and DHST abundance are shown in Figure 5.6c and d, respectively. Both ST and DHST abundance increased linearly from the age of 30. Similarly, age-related increases in SM3 (Figure 5.6e) and DHSM3 (Figure 5.6f) were also observed. Although they are of relatively low abundance (~ 2 to 30 nmol/g) in comparison to other GSLs, these sulfo-GSLs showed a consistent age-related increase in abundance in the cortical cells of human lenses.

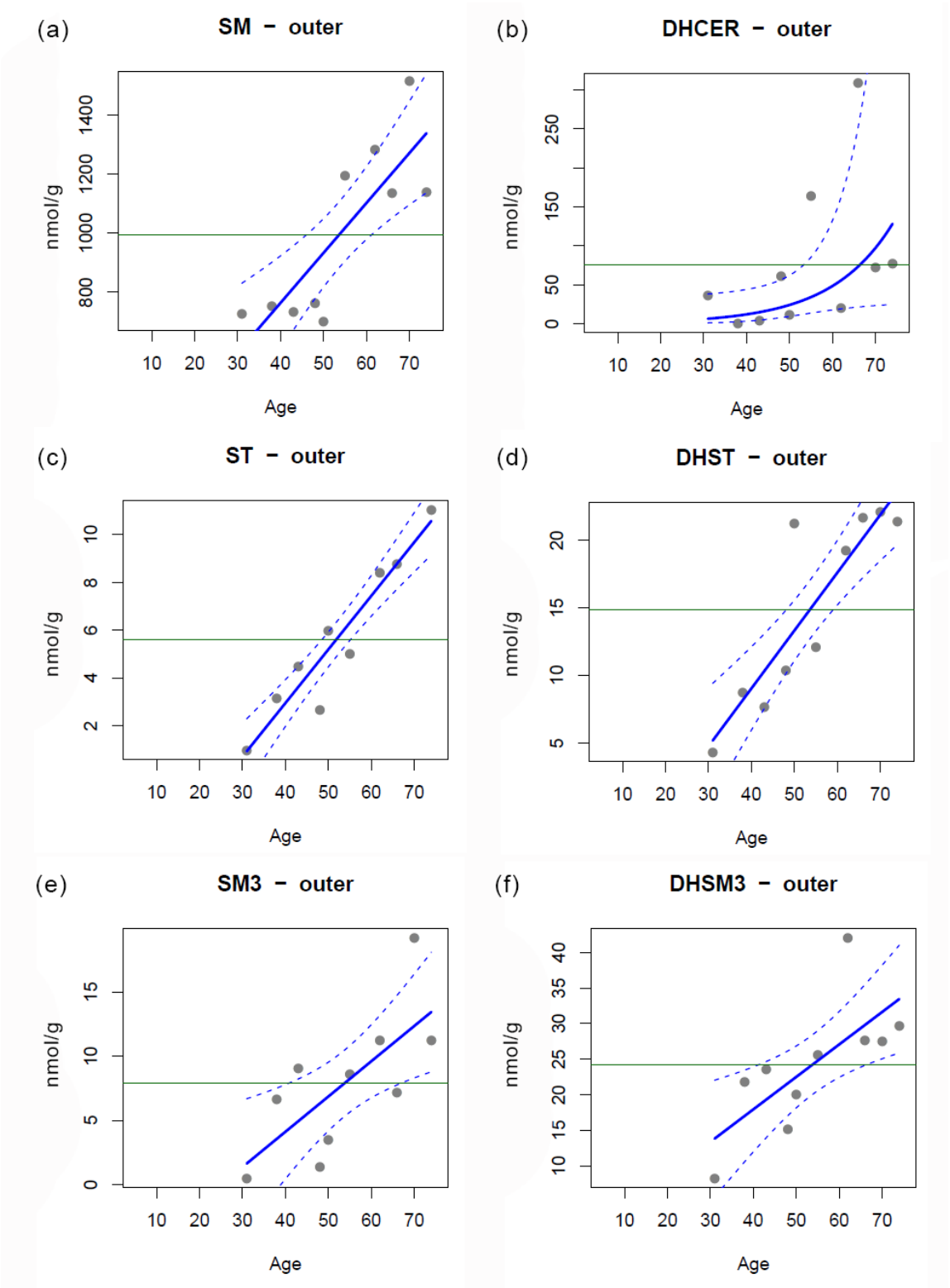

Figure 5.6: Total (a) SM; (b) DHCer; (c) ST; (d) DHST, (e) SM3, (f) DHSM3 present in the barrier region of human lenses of different ages. All values are expressed in nmol/g tissue wet weight. The solid line is a generalised additive model fit; the dashed lines give a 95% confidence band. The green line corresponds to the mean of the data. SM: sphingomyelin, DHCer: dihydroceramide, ST: sulfatide, DHST: dihydrosulfatide, SM3: lactosylceramide sulfate, DHSM3: dihydrolactosylceramide sulfate.

In this study, we demonstrated that the GP and SL composition in older human lenses varies from that of

younger individuals. Some classes of GPs and SLs remained constant throughout a human's lifespan, whereas other GP classes decreased in concentration with age while some SL classes increased in abundance with age. With increasing age, an increase in total lipid content was observed in all regions (except the outer region where there is not enough data to make a comparison between young and old lenses). As there is no turnover of lipid,[7] this may be due to the central compaction of lens fibre cells with age that leads to the alteration in packing density and membrane topology.[39, 40] The core region has the least change in total wet weight of tissue, from 6.3 mg to 6.7 mg, whereas the inner region increases from 8.4 mg to 9.0 mg. The largest increase in wet weight of lens tissue occurs in the barrier region from 9.1 mg to 11.2 mg. A previous study has shown that age-related changes affecting the composition of lipid can be used as an oxidative stress marker.[41] As the lens is packed with cholesterol, oxysterol levels in the lens increased with oxidative stress.[41] Age-related compaction of fiber cells may also lead to higher oxidative stress in the lens.[2] In this study, the presence of any oxidised lipids were not investigated as standards were not commercially available.

Our observation of age-related changes in the lens core is similar to what has been observed previously.[14] Although the inner region is also a part of the lens nucleus, ageing affects more lipid classes in this region as compared to the core where only PE, Cer and DHCer changed with age. In addition to these three lipid classes, SM, DHSM, DHST, SM3 and DHGM1 also showed an increase with age in the inner region. The most age-related changes in lipid class abundance occurred in the barrier region. On the other hand, only six SLs showed an age-related effect in the outer region of the lens.

In 1999, Moffat *el al.* observed a reduction in the amount of water entering the lens nucleus via the cortex and epithelium.[42] This phenomenon could be due to the development of a barrier to the diffusion of water between the nucleus and cortex. Alterations to the diffusion of metabolic substances, nutrients, antioxidants and reactive molecules can cause antioxidants such as glutathione to be lower in concentration than the reactive species in the nucleus.[20, 43] The formation of this barrier occurs around middle-age (around the age of 40),[20, 42] where some GP classes were observed to have been depleted while SLs levels were increased. GPs and SLs are known to change either the water permeability of cell membranes,[44] or the structure and function of important lens membrane proteins such as water or ion channels[45] that may facilitate lens metabolite movement. Alterations to the lipid composition of fibre cell membranes with age may therefore,

play a role in the development of this functional barrier.

Although the literature suggests that gangliosides accumulate in conjunction with ageing and senile cataract progression,[10] the current study found an increase of only one class of gangliosides, DHGM1, in the inner region. There are other gangliosides such as GD1a, III^{3}FucnLc4 and other globo- and neolacto- species in the lens that were not detected and quantified in our study. Therefore, the increase of gangliosides in the previous study cannot be directly compared to the current work.[9] Sulfo-GSLs such as ST, DHST, SM3 and DHSM3 showed a linear increase in all regions of the lens except the core. The age-related changes in GSLs may modify the cell-to-cell interactions induced by cell surface sugar chains, leading to the initiation and progression of cataract.[46]

Although we have successfully quantified the majority of known lipids in different regions of the lens and examined their change in abundance with age, the reason behind the sharp rise in Cer and DHCer levels in all of the regions the lens remains unknown. None of the SL classes that are biosynthetically related to Cer and DHCer are large enough in abundance to account for the increase in these two lipid classes. In fact, most of the ceramide conjugates such as DHCerP and CerP also increased with age. Therefore, the hypothesis that the dramatic increase Cer and DHCer concentration were caused by the hydrolysis of other more complex sphingolipids must be rejected.

5.4 Conclusion

In summary, this study has produced several findings: (i) the lipid membrane composition is different in each region of the lens, (ii) GP content increases in abundance from the core towards the outer region, in contrast to SL abundance which decreases, (iii) the increase in Cer and DHCer after the age of 40 occurs in all regions of the lens, and (iv) most of the lipid classes were affected by age in the barrier region as compared to other regions. In addition, the most abundant SL molecule of each detected class were those with a 16:0 fatty acyl chain. For GSLs, however, their 24:1 analogues were of higher abundance (except DHST). This study provides the first insight into the composition of lens lipids categorised into three main groups of GP, SL and GSL in the four regions of the lens. If an age-related change was observed for any lipid class, that lipid class always displayed the same change (*i.e.*, consistently increased or decreased) irrespective of the region. Although the best effort was put into elucidating and quantifying the full lens

sphingolipidome, some gangliosides that were previously identified such as GD1a were not included which may be due to its low abundance. However, this work has provided insight into the possibility of quantifying very low abundance GSLs (some were less than 0.1% of total lipid), and therefore future work may aim at optimising the quantification methods for these low abundance lipids that exist at a higher mass range.

5.5 Supplementary

Table S 5.1: List of phospholipid species detected in the human lens with their chemical formula and exact mass (neutral). All the lipids were identified by $[M+Cl]^-$ or $[M-H]^-$.

Glycerophospholipids			
	FA	Chemical Formula	*m/z* $[M+Cl]^-$
Phosphatidylcholine			
PC	30:0	C38H76NO8P	740.4997
	31:0	C39H78NO8P	754.5154
	32:1	C40H78NO8P	766.5154
	32:0	C40H80NO8P	768.5310
	O-34:0	C42H84NO7P	780.5674
	34:2	C42H80NO8P	792.5310
	34:1	C42H82NO8P	794.5467
	O-36:2	C44H86NO7P	806.5830
	36:4	C44H80NO8P	816.5310
	36:3	C44H82NO8P	818.5467
	36:2	C44H84NO8P	820.5623
	36:1	C44H86NO8P	822.5780
	38:5	C46H82NO8P	842.5467
	38:4	C46H84NO8P	844.5623
Phosphatidylethanolamine			*m/z* $[M-H]^-$
PE	O-34:2	C39H76NO7P	700.5281
	O-34:1	C39H78NO7P	702.5438
	34:2	C39H74NO8P	714.5074
	34:1	C39H76NO8P	716.5230
	O-36:3	C41H78NO7P	726.5438
	O-36:2	C41H80NO7P	728.5594
	O-36:1	C41H82NO7P	730.5751
	36:4	C41H74NO8P	738.5074
	36:2	C41H78NO8P	742.5387
	36:1	C41H80NO8P	744.5543

	O-38:6	C43H76NO7P	748.5281
	O-38:5	C43H78NO7P	750.5438
	O-38:4	C43H80NO7P	752.5594
	38:5	C43H76NO8P	764.5230
	38:4	C43H78NO8P	766.5387
	O-40:8	C45H78NO7P	774.5438
	O-40:6	C45H80NO7P	776.5594
	O-40:5	C45H82NO7P	778.5751
Phosphatidic Acid			*m/z* [M-H]$^-$
PA	O-34:1	C37H73O7P	659.5016
	O-36:1	C39H77O7P	687.5329
Lyso lipids			
Phosphatidylethanolamine			*m/z* [M-H]$^-$
LPE	16:0e	C21H46NO6P	438.2985
	16:0	C21H44NO7P	452.2777
	18:1p	C23H46NO6P	462.2985
	18:1e	C23H48NO6P	464.2777
	18:0e	C23H50NO6P	466.3298

Table S 5.2: List of sphingolipid species detected in the human lens with their chemical formula and exact mass (neutral). All the lipids were identified by $[M+Cl]^-$ or $[M-H]^-$.

Sphingolipids			
	FA	Chemical Formula	*m/z* $[M+Cl]^-$
Sphingomyelin			
DHSM(d18:0)	14:0	C37H77N2O6P	711.5208
	15:0	C38H79N2O6P	725.5364
	16:0	C39H81N2O6P	739.5521
	17:0	C40H83N2O6P	753.5677
	18:0	C41H85N2O6P	767.5834
	22:0	C45H93N2O6P	823.6460
	24:1	C47H95N2O6P	849.6616
SM(d18:1)	14:0	C37H75N2O6P	709.5051
	15:0	C38H77N2O6P	723.5208
	16:1	C39H77N2O6P	735.5208
	16:0	C39H79N2O6P	737.5364
	18:0	C41H83N2O6P	765.5677
	22:1	C45H89N2O6P	819.6147
	22:0	C45H91N2O6P	821.6303
	23:0	C46H93N2O6P	835.6460
	24:2	C47H91N2O6P	845.6303
	24:1	C47H93N2O6P	847.6460
Ceramide			*m/z* $[M+Cl]^-$
DHCer(d18:0)	14:0	C32H65NO3	546.4653
	16:0	C34H69NO3	574.4966
	22:1	C40H79NO3	656.5748
	22:0	C40H81NO3	658.5905
	24:1	C42H83NO3	684.6061
Cer(d18:1)	14:0	C32H63NO3	544.4496
	16:0	C34H67NO3	572.4809
	22:1	C40H77NO3	654.5592
	22:0	C40H79NO3	656.5748
	24:1	C42H81NO3	682.5905
Ceramide Phosphate			*m/z* $[M-H]^-$
DHCerP(d18:0)	16:0	C34H70NO6P	618.4863
	24:1	C42H84NO6P	728.5958

CerP(d18:1)	16:0	C34H68NO6P	616.4706
	24:1	C42H82NO6P	726.5802
Lactosylceramide			*m/z* $[M+Cl]^-$
DHLacCer(d18:0)	16:0	C46H89NO13	898.6022
	22:0	C52H101NO13	982.6961
	24:1	C54H103NO13	1008.7118
	24:0	C54H105NO13	1010.7274
DHTrihexosylceramide (d18:0)	16:0	C52H99NO18	1060.6551
	24:1	C60H113NO18	1170.7646
Sulfatide			*m/z* $[M-H]^-$
DHST(d18:0)	14:0	C38H75NO11S	752.4983
	16:0	C40H79NO11S	780.5296
	24:1	C48H93NO11S	890.6391
ST(d18:1)	14:0	C38H73NO11S	750.4826
	16:0	C40H77NO11S	778.5139
	24:1	C48H91NO11S	888.6235
Lactosylceramide Sulfate			*m/z* $[M-H]^-$
DHSM3(d18:0)	14:0	C44H85NO16S	914.5511
	16:0	C46H89NO16S	942.5824
	24:1	C54H103NO16S	1052.6919
SM3(d18:1)	16:0	C46H87NO16S	940.5667
	22:0	C52H99NO16S	1024.6606
	24:1	C54H101NO16S	1050.6763
DHGM3			*m/z* $[M-H]^-$
DHGM3(d18:0)	16:0	C57H106N2O21	1153.7210
	24:1	C65H120N2O21	1263.8305
DHGM1			*m/z* $[M-H]^-$
DHGM1(d18:0)	16:0	C71H129N3O31	1518.8532
	24:1	C79H143N3O31	1628.9627
DHSialyl-LeX			*m/z* $[M-H]^-$
DHSialyl-LeX(d18:0)	16:0	C77H139N3O35	1664.9111
	24:1	C85H153N3O35	1775.0206

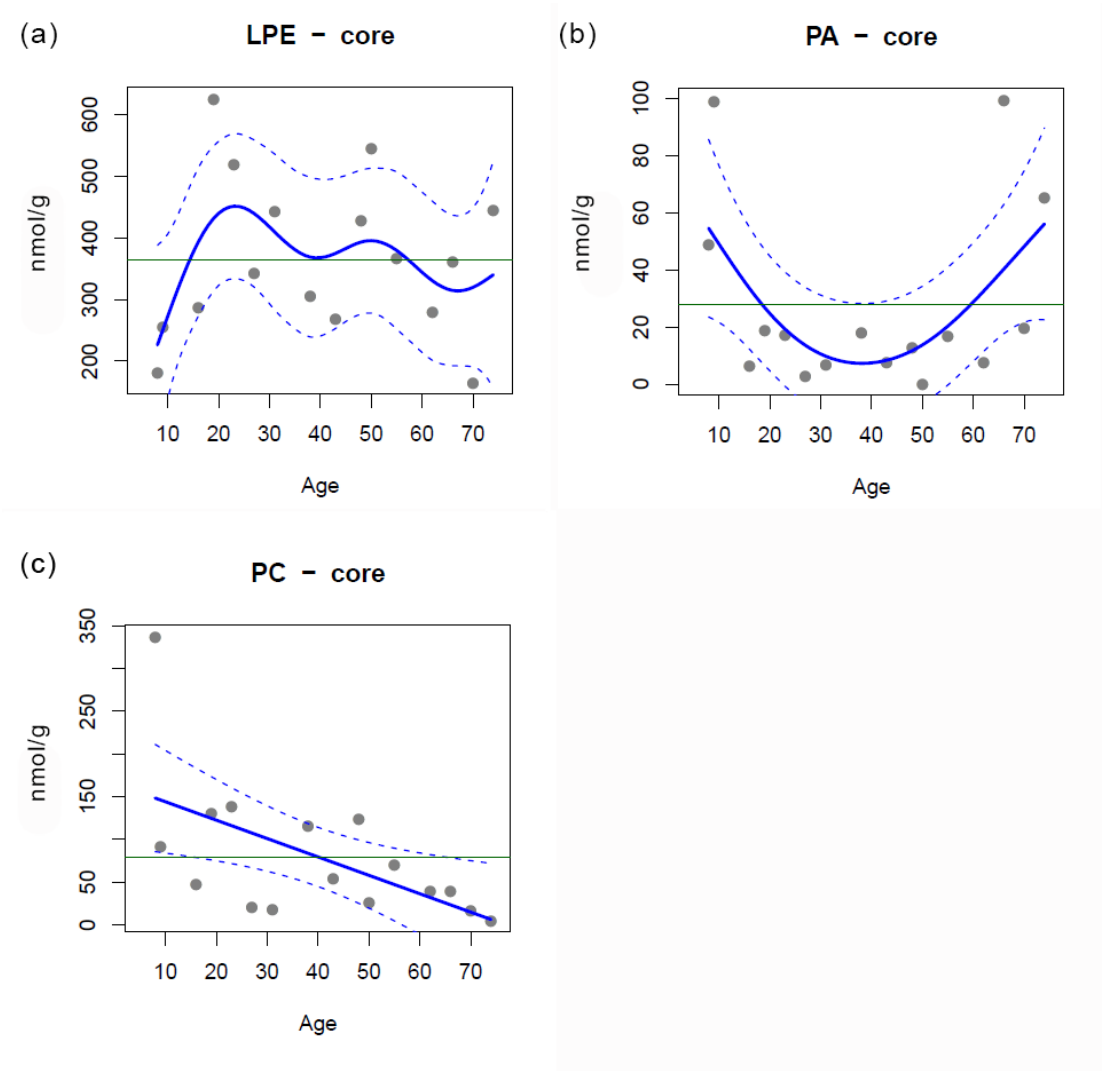

Figure S 5.1: Total glycerophospholipid present in the core region of human lenses of different ages; (a) lyosophosphatidylethanolamine; (b) phosphatidic acid; (c) phosphatidylcholine. All values are expressed in nmol/g tissue wet weight. The solid line is a generalised additive model fit; the dashed lines give a 95% confidence band. The green line corresponds to the mean of the data and if the mean line is in between the 95% confidence band, the null hypothesis of no change with age cannot be rejected. LPE: lysophospholipidethanolamine, PA: phosphatidic acid, PC: phosphatidylcholine.

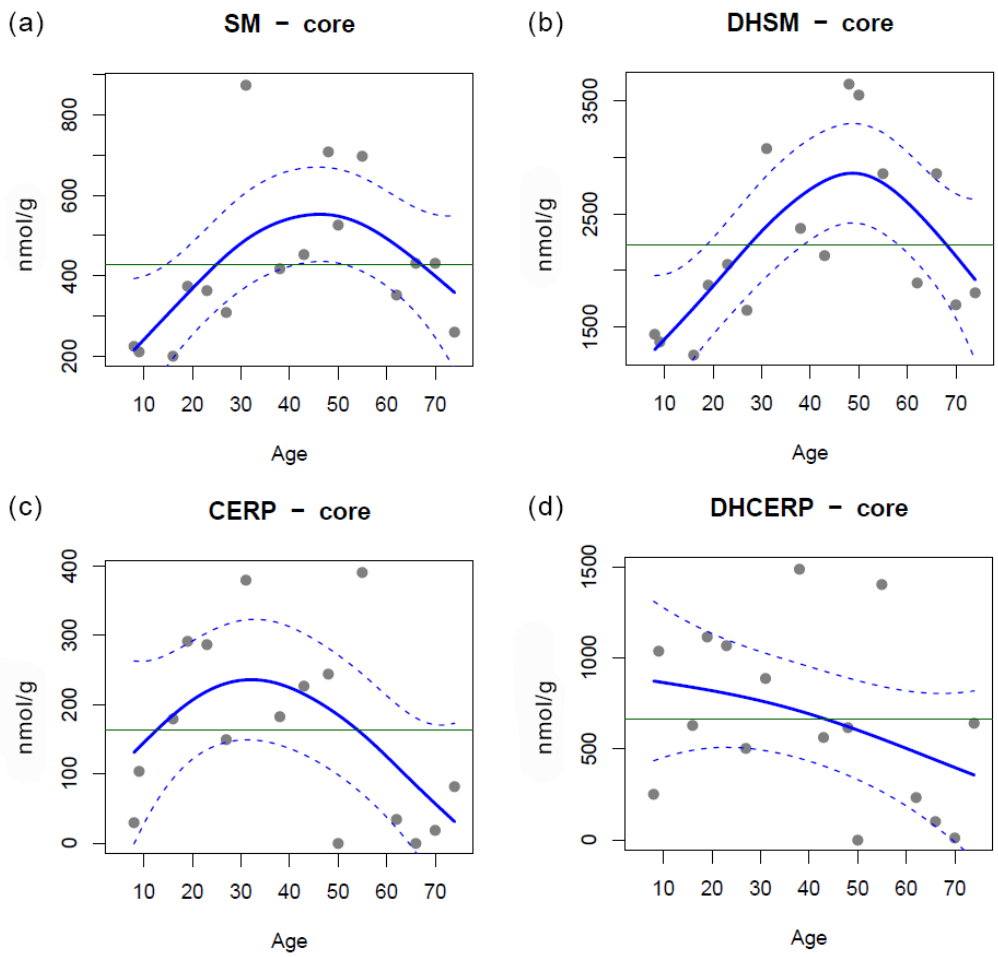

Figure S 5.2: Total sphingolipid present in the core region of human lenses of different ages; (a) sphingomyelin; (b) dihydrosphingomyelin; (c) ceramide phosphate; and (d) dihydroceramidephosphate. All values are expressed in nmol/g tissue wet weight. The solid line is a generalised additive model fit; the dashed lines give a 95% confidence band. The green line corresponds to the mean of the data and if the mean line is in between the 95% confidence band, the null hypothesis of no change with age cannot be rejected. SM: sphingomyelin, DHSM: dihydrosphingomyelin, CerP: ceramide phosphate, DHCerP: dihydroceramidephosphate.

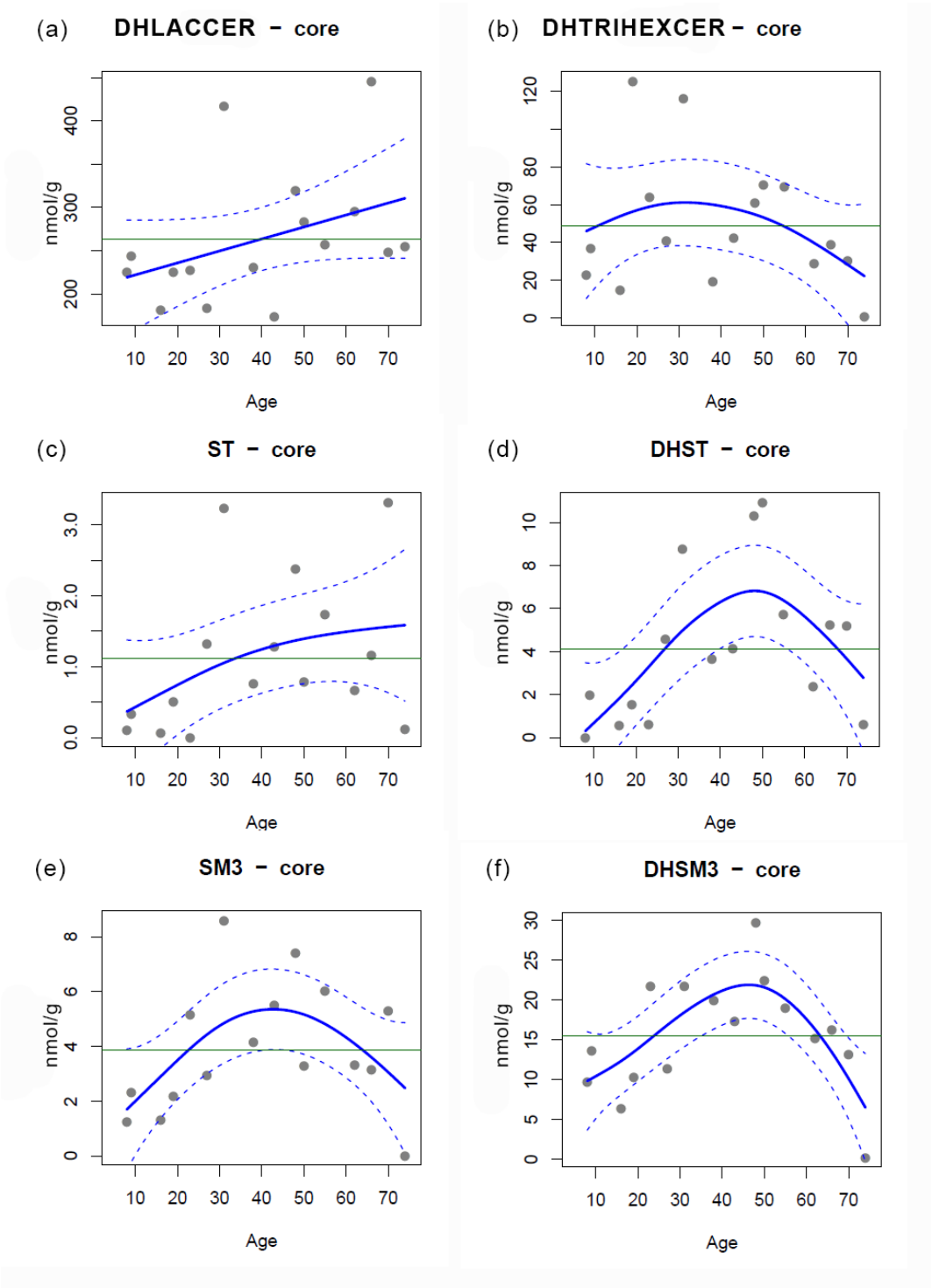

Figure S 5.3: Total glycosphingolipids present in the core region of human lenses of different ages; (a) sphingomyelin; (b) dihydrosphingomyelin; (c) ceramide; (d) dihydroceramide; (e) ceramide phosphate; (f) dihydroceramide phosphate. All values are expressed in nmol/g tissue wet weight. The solid line is a generalised additive model fit; the dashed lines give a 95% confidence band. The green line corresponds to the mean of the data and if the mean line is in between the 95% confidence band, the null hypothesis of no change with age cannot be rejected. DHLacCer: dihydrolactosylceramide, DHTriHexCer: dihydrotrihexosylceramide, ST: sulfatide, DHST: dihydrosulfatide, SM3: lactosylceramide sulfate, DHSM3: dihydrolactosylceramide sulfate.

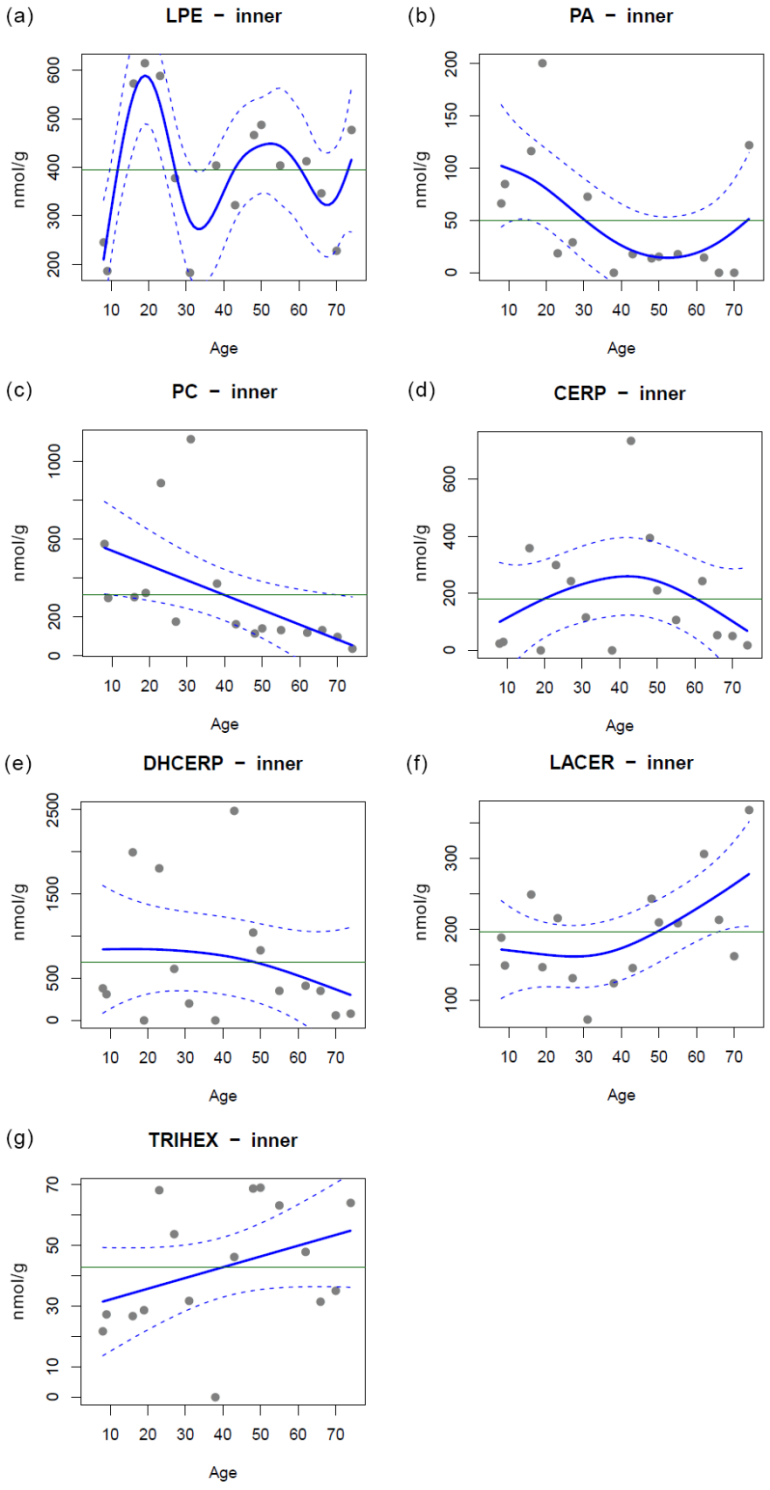

Figure S 5.4: Total lipids present in the inner region of human lenses of different ages; (a) LPE; (b) PA; (c) PC; (d) CerP; (e) DHCerP; (f) DHLacCer; (g) DHTriHexCer. All values are expressed in nmol/g tissue wet weight. The solid line is a generalised additive model fit; the dashed lines give a 95% confidence band. The green line corresponds to the mean of the data and if the mean line is in between the 95% confidence band, the null hypothesis of no change with age cannot be rejected. LPE: lysophospholipidethanolamine, PA: phosphatidic acid, PC: phosphatidylcholineCerP: ceramide phosphateDHLacCer: dihydrolactosylceramide, DHTriHexCer: dihydrotrihexosylceramide.

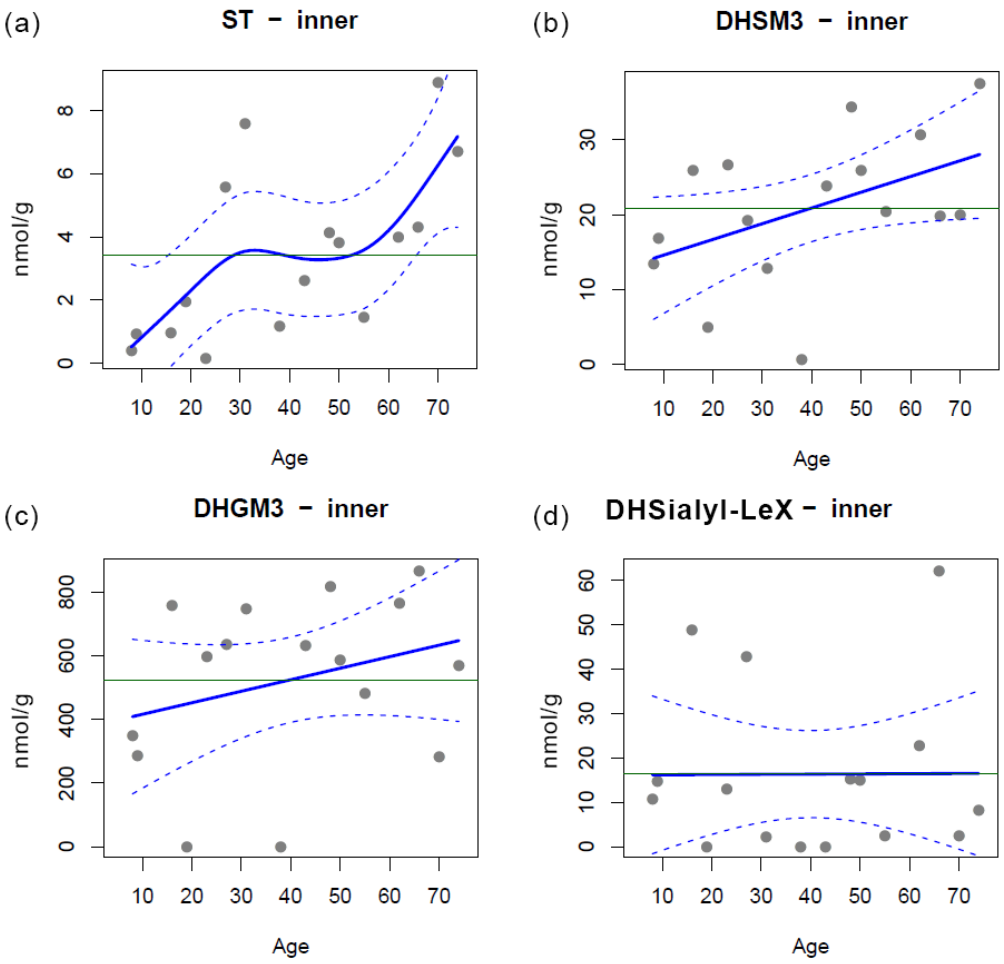

Figure S 5.5: Total lipids present in the inner region of human lenses of different ages; (a) ST; (b) DHSM3; (c) DHGM3; (d) DHSialyl-Le^x. All values are expressed in nmol/g tissue wet weight. The solid line is a generalised additive model fit; the dashed lines give a 95% confidence band. The green line corresponds to the mean of the data and if the mean line is in between the 95% confidence band, the null hypothesis of no change with age cannot be rejected. ST: sulfatide, DHSM3: dihydrolactosylceramide sulfate, DHGM3: dihydromonosialodihexosylganglioside, DHSialyl-Le^x: dihydrosialyl Lewis acid.

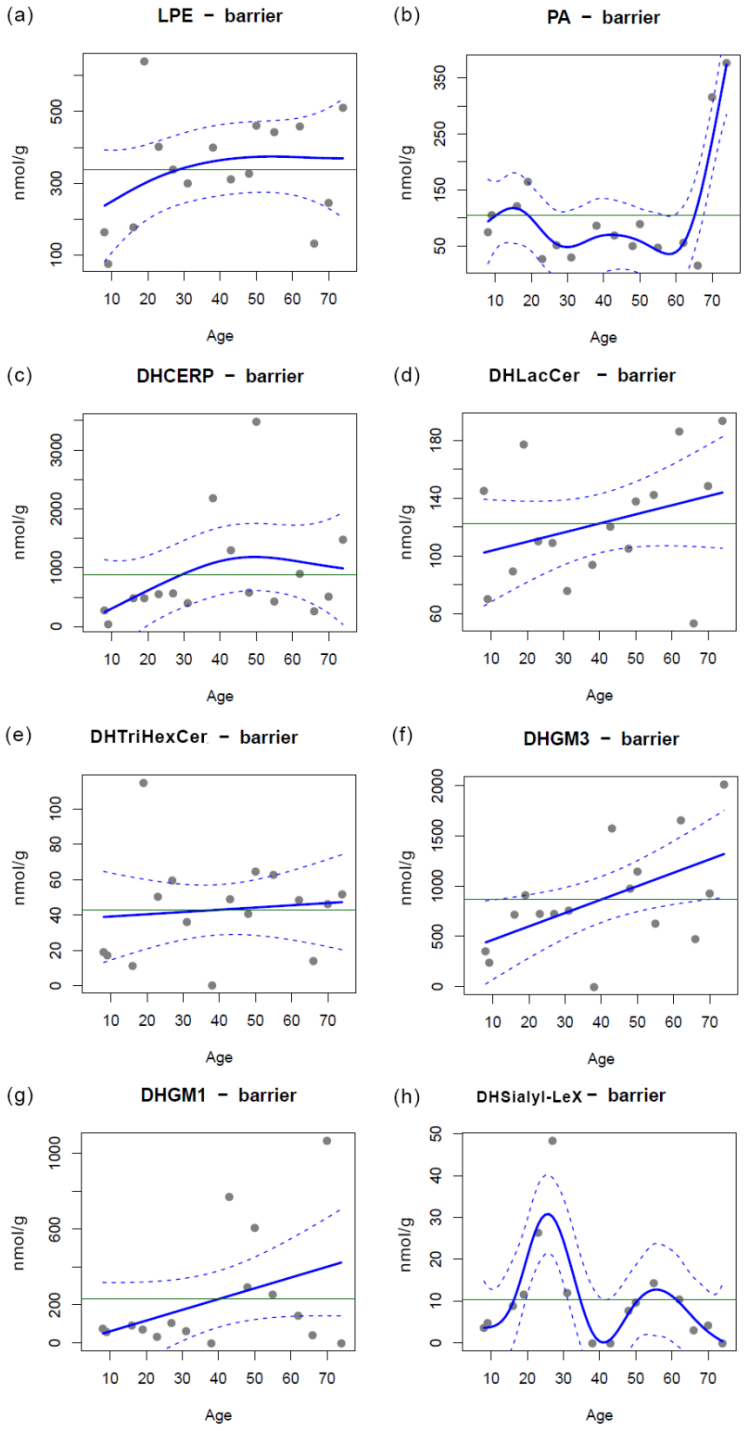

Figure S 5.6:Total lipids present in the barrier region of human lenses of different ages; (a) LPE; (b) PA; (c) DHCERP; (d) DHLacCer; (e) DHTriHexCer; (f) DHGM3; (g) DHGM1, (h) DHSialyl-le^x. All values are expressed in nmol/g tissue wet weight. The solid line is a generalised additive model fit; the dashed lines give a 95% confidence band. The green line corresponds to the mean of the data and if the mean line is in between the 95% confidence band, the null hypothesis of no change with age cannot be rejected. LPE: lysophospholipidethanolamine, PA: phosphatidic acid, DHCerP: dihydroceramidephosphate, DHLacCer: dihydrolactosylceramide, DHTriHexCer: dihydrotrihexosylceramide, DHGM3: dihydromonosialodihexosylganglioside, DHGM1: monosialotetrahexosylganglioside, DHSialyl-Le^x: dihydrosialyl Lewis acid.

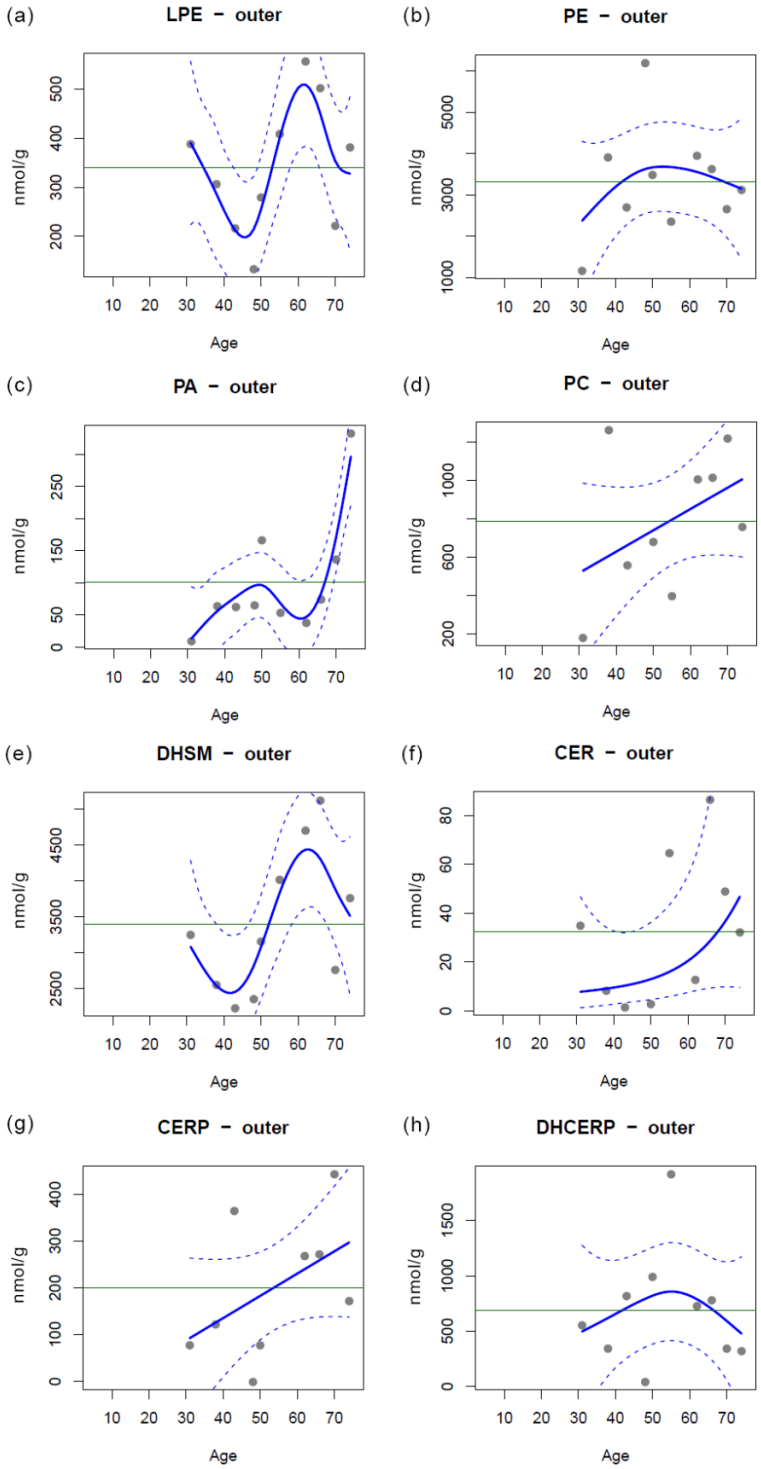

Figure S 5.7: Total lipids present in the outer region of human lenses of different ages; (a) LPE; (b) PE; (c) PA; (d) PC; (e) DHSM; (f) Cer; (g) CerP, (h) DHCerP. All values are expressed in nmol/g tissue wet weight. The solid line is a generalised additive model fit; the dashed lines give a 95% confidence band. The green line corresponds to the mean of the data and if the mean line is in between the 95% confidence band, the null hypothesis of no change with age cannot be rejected. LPE: lysophospholipidethanolamine, PE: phosphatidylethanolamine, PC: phosphatidylcholine, DHSM: dihydrosphingomyelin, Cer: ceramide, CerP: ceramide phosphate, DHCerP: dihydroceramidephosphate.

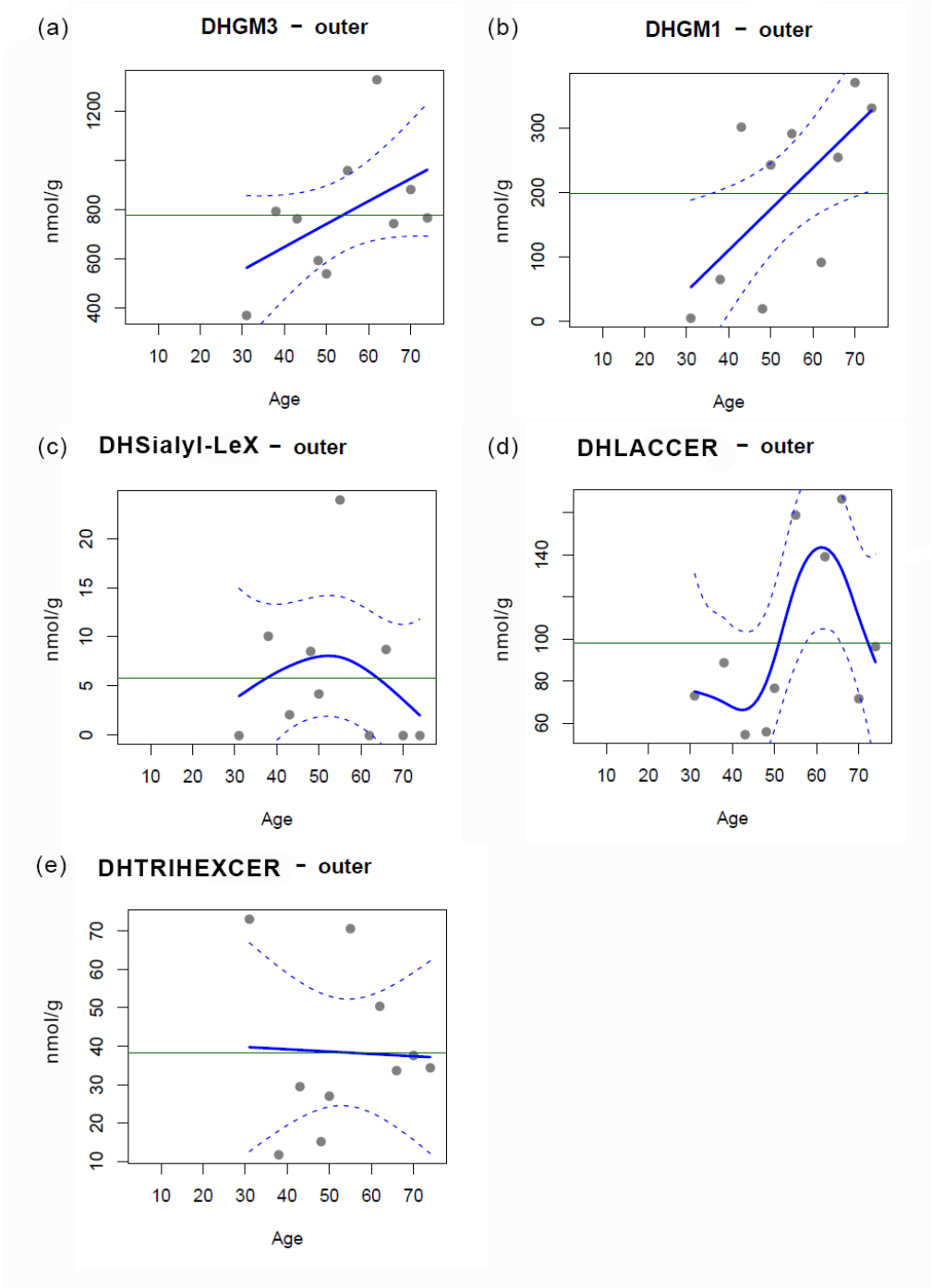

Figure S 5.8: Total glycosphingolipids present in the outer region of human lenses of different ages; (a) DHGM3; (b) DHGM1; (c) DHSialyl-Le^x; (d) DHLacCer; (e) DHTriHexCer. All values are expressed in nmol/g tissue wet weight. The solid line is a generalised additive model fit; the dashed lines give a 95% confidence band. The green line corresponds to the mean of the data and if the mean line is in between the 95% confidence band, the null hypothesis of no change with age cannot be rejected. DHGM3: dihydromonosialodihexosylganglioside, DHGM1: monosialotetrahexosylganglioside, DHSialyl-Le^x: dihydrosialyl Lewis acid, DHLacCer: dihydrolactosylceramide, DHTriHexCer: dihydrotrihexosylceramide.

5.6 References

1. Yappert, M. C.; Rujoi, M.; Borchman, D.; Vorobyov, I.; Estrada, R., Glycero- versus sphingo-phospholipids: correlations with human and non-human mammalian lens growth. *Experimental Eye Research* **2003,** *76* (6), 725-734.

2. Augusteyn, R. C., On the contribution of the nucleus and cortex to human lens shape and size. *Clinical and Experimental Optometry* **2018,** *101* (1), 64-68.

3. Friedrich, M. G.; Truscott, R. J. W., Large-Scale Binding of α-Crystallin to Cell Membranes of Aged Normal Human Lenses: A Phenomenon That Can Be Induced by Mild Thermal Stress. *Investigative Ophthalmology & Visual Science* **2010,** *51* (10), 5145-5152.

4. Kuszak, J. R., The development of lens sutures. *Progress in Retinal and Eye Research* **1995,** *14* (2), 567-591.

5. Garland, D. L.; Duglas-Tabor, Y.; Jimenez-Asensio, J.; Datiles, M. B.; Magno, B., The Nucleus of the Human Lens: Demonstration of a Highly Characteristic Protein Pattern by Two-Dimensional Electrophoresis and Introduction of a New Method of Lens Dissection. *Experimental Eye Research* **1996,** *62* (3), 285-292.

6. Lynnerup, N.; Kjeldsen, H.; Heegaard, S.; Jacobsen, C.; Heinemeier, J., Radiocarbon Dating of the Human Eye Lens Crystallines Reveal Proteins without Carbon Turnover throughout Life. *PLOS ONE* **2008,** *3* (1), e1529.

7. Hughes, J. R.; Levchenko, V. A.; Blanksby, S. J.; Mitchell, T. W.; Williams, A.; Truscott, R. J. W., No turnover in lens lipids for the entire human lifespan. *eLife* **2015,** *4*, e06003.

8. Borchman, D.; Yappert, M. C., Age-related lipid oxidation in human lenses. *Investigative ophthalmology & visual science* **1998,** *39* (6), 1053-1058.

9. Ogiso, M.; Saito, N.; Sudo, K.; Kubo, H.; Hirano, S.; Komoto, M., Increase in lens gangliosides due to aging and cataract progression in human senile cataract. *Investigative Ophthalmology & Visual Science* **1990,** *31* (10), 2171-2179.

10. Ogiso, M.; Komoto, M.; Okinaga, T.; Koyota, S.; Hoshi, M., Age-related changes in ganglioside composition in human lens. *Experimental Eye Research* **1995,** *60* (3), 317-323.

11. Broekhuyse, R., Phospholipids in tissues of the eye: III. Composition and metabolism of phospholipids in human lens in relation to age and cataract formation. *Biochimica et Biophysica Acta (BBA)-Lipids and Lipid Metabolism* **1969,** *187* (3), 354-365.

12. Merchant, T.; Lass, J.; Meneses, P.; Greiner, J.; Glonek, T., Human crystalline lens phospholipid analysis with age. *Investigative ophthalmology & visual science* **1991,** *32* (3), 549-555.

13. Huang, L.; Grami, V.; Marrero, Y.; Tang, D.; Yappert, M. C.; Rasi, V.; Borchman, D., Human Lens Phospholipid Changes with Age and Cataract. *Investigative Ophthalmology & Visual Science* **2005,** *46* (5), 1682-1689.

14. Hughes, J. R.; Deeley, J. M.; Blanksby, S. J.; Leisch, F.; Ellis, S. R.; Truscott, R. J. W.; Mitchell, T. W., Instability of the cellular lipidome with age. *AGE* **2012,** *34* (4), 935-947.

15. Ogiso, M.; Okinaga, T.; Ohta, M.; Komoto, M.; Hoshi, M., Identification and synthetic pathway of sialyl-Lewisx-containing neolacto-series gangliosides in lens tissues. l. Characterisation of gangliosides in human senile cataractous lens. *Biochimica et Biophysica Acta (BBA) - Lipids and Lipid Metabolism* **1995,** *1256* (2), 166-174.

16. Ogiso, M.; Irie, A.; Kubo, H.; Komoto, M.; Matsuno, T.; Koide, Y.; Hoshi, M., Characterization of neutral glycosphingolipids in human cataractous lens. *Journal of Biological Chemistry* **1993,** *268* (18), 13242-13247.

17. Ogiso, M., Implication of glycolipids in lens fiber development. *Acta Biochimica Polonica* **1998,** *45* (2), 501-507.

18. Ogiso, M.; Shogomori, H.; Hoshi, M., Localization of Lewisx, sialyl-Lewisx and α-galactosyl epitopes on glycosphingolipids in lens tissues. *Glycobiology* **1998,** *8* (1), 95-105.

19. Seng, J. A.; Ellis, S. R.; Hughes, J. R.; Maccarone, A. T.; Truscott, R. J. W.; Blanksby, S. J.; Mitchell, T. W., Characterisation of sphingolipids in the human lens by thin layer chromatography–desorption electrospray ionisation mass spectrometry. *Biochimica et Biophysica Acta (BBA) - Molecular and Cell Biology of Lipids* **2014,** *1841* (9), 1285-1291.

20. Sweeney, M. H. J.; Truscott, R. J. W., An impediment to glutathione diffusion in older normal human lenses: a possible precondition for nuclear cataract. *Experimental Eye Research* **1998,** *67* (5), 587-595.

21. Heys, K. R.; Cram, S. L.; Truscott, R. J., Massive increase in the stiffness of the human lens nucleus with age: the basis for presbyopia? *Molecular Vision* **2004,** *16* (10), 956-963.

22. Abbott, S. K.; Jenner, A. M.; Mitchell, T. W.; Brown, S. H. J.; Halliday, G. M.; Garner, B., An Improved High-Throughput Lipid Extraction Method for the Analysis of Human Brain Lipids. *Lipids* **2013,** *48* (3), 307-318.

23. Matyash, V.; Liebisch, G.; Kurzchalia, T. V.; Shevchenko, A.; Schwudke, D., Lipid extraction by methyl-tert-butyl ether for high-throughput lipidomics. *Journal of Lipid Research* **2008,** *49* (5), 1137-1146.

24. Ariga, T.; Tao, R. V.; Lee, B. C.; Yamawaki, M.; Yoshino, H.; Scarsdale, N. J.; Kasama, T.; Kushi, Y.; Yu, R. K., Glycolipid composition of human cataractous lenses. Characterization of Lewisx glycolipids. *Journal of Biological Chemistry* **1994,** *269* (4), 2667-2675.

25. Fahy, E.; Subramaniam, S.; Murphy, R. C.; Nishijima, M.; Raetz, C. R. H.; Shimizu, T.; Spener, F.; van Meer, G.; Wakelam, M. J. O.; Dennis, E. A., Update of the LIPID MAPS comprehensive classification system for lipids. *Journal of Lipid Research* **2009,** *50* (Supplement), S9-S14.

26. Schimek, M. G.; Turlach, B. A., Additive and Generalized Additive Models. In *Smoothing and Regression*, 2000.

27. Deeley, J. M.; Mitchell, T. W.; Xiaojia, W.; Korth, J.; Nealon, J. R.; Blanksby, S. J.; Truscott, R. J. W., Human lens lipids differ markedly from those of commonly used experimental animals. *Biochimica et Biophysica Acta* **2008,** *1781* (6-7), 288-298.

28. Deeley, J. M.; Thomas, M. C.; Truscott, R. J. W.; Mitchell, T. W.; Blanksby, S. J., Identification of Abundant Alkyl Ether Glycerophospholipids in the Human Lens by Tandem Mass Spectrometry Techniques. *Analytical Chemistry* **2009,** *81* (5), 1920-1930.

29. Cotlier, E.; Obara, Y.; Toffness, B., Cholestrol and phospholipids in protein fractions of human lens and senile cataract. *Biochimica et Biophysica Acta* **1978,** *530* (2), 267-278.

30. Deeley, J. M.; Hankin, J. A.; Friedrich, M. G.; Murphy, R. C.; Truscott, R. J. W.; Mitchell, T. W.; Blanksby, S. J., Sphingolipid distribution changes with age in the human lens. *Journal of Lipid Research* **2010,** *51* (9), 2753-2760.

31. Friedrich, M. G.; Truscott, R. J. W., Membrane Association of Proteins in the Aging Human Lens: Profound Changes Take Place in the Fifth Decade of Life. *Investigative Ophthalmology & Visual Science* **2009,** *50* (10), 4786-4793.

32. Heys, K. R.; Friedrich, M. G.; Truscott, R. J. W., Free and Bound Water in Normal and Cataractous Human Lenses. *Investigative Ophthalmology & Visual Science* **2008,** *49* (5), 1991-1997.

33. Dovrat, A.; Gershon, D., Rat lens superoxide dismutase and glucose-6-phosphate dehydrogenase: studies on the catalytic activity and the fate of enzyme antigen as a function of age. *Experimental eye research* **1981,** *33* (6), 651-661.

34. Dovrat, A.; Scharf, J.; Gershon, D., Glyceraldehyde 3-phosphate dehydrogenase activity in rat and human lenses and the fate of enzyme molecules in the aging lens. *Mechanisms of Ageing and Development* **1984,** *28* (2-3), 187-191.

35. Scharf, J.; Dovrat, A.; Gershon, D., Defective superoxide-dismutase molecules accumulate with age in human lenses. *Graefe's Archive for Clinical and Experimental Ophthalmology* **1987,** *225* (2), 133-136.

36. Ellis, S. R.; Wu, C.; Deeley, J. M.; Zhu, X.; Truscott, R. J. W.; Panhuis, M.; Cooks, R. G.; Mitchell, T. W.; Blanksby, S. J., Imaging of Human Lens Lipids by Desorption Electrospray Ionisation Mass Spectrometry. *Journal of American Society of Mass Spectrometry* **2010,** *21*, 2095-2104.

37. Feldman, G. L.; Feldman, L. S.; Rouser, G., The isolation and partial characterization of gangliosides and ceramide polyhexosides from the lens of the human eye. *Lipids* **1966,** *1* (1), 21-26.

38. Tao, R. V. P.; Yu-Wei, S.; Kovathana, N.; Cotlier, E., A new family of fucose-containing gangliosides isolated from human senile cataracts. *Biochimica et Biophysica Acta (BBA) - Lipids and Lipid Metabolism* **1983,** *753* (1), 89-96.

39. Augusteyn, R. C., On the growth and internal structure of the human lens. *Experimental Eye Research* **2010,** *90* (6), 643-654.

40. Al-khudari, S.; Donohue, S. T.; Al-Ghoul, W. M.; Al-Ghoul, K. J., Age-related compaction of lens fibers affects the structure and optical properties of rabbit lenses. *BMC Ophthalmology* **2007,** *7* (1), 19.

41. Borchman, D.; Yappert, M. C., Lipids and the ocular lens. *Journal of Lipid Research* **2010,** *51* (9), 2473-2488.

42. Moffat, B. A.; Landman, K. A.; Truscott, R. J. W.; Sweeney, M. H. J.; Pope, J. M., Age-related Changes in the Kinetics of Water Transport in Normal Human Lenses. *Experimental Eye Research* **1999,** *69* (6), 663-669.

43. Pescosolido, N.; Barbato, A.; Giannotti, R.; Komaiha, C.; Lenarduzzi, F., Age-related changes in the kinetics of human lenses: prevention of the cataract. *International Journal of Ophthalmology* **2016,** *9* (10), 1506-1517.

44. Tong, J.; Canty, J. T.; Briggs, M. M.; McIntosh, T. J., The water permeability of lens aquaporin-0 depends on its lipid bilayer environment. *Experimental Eye Research* **2013,** *113*, 32-40.

45. Rujoi, M.; Borchman, D.; DuPré, D. B.; Yappert, M. C., Interactions of Ca(2+) with sphingomyelin and dihydrosphingomyelin. *Biophysical journal* **2002,** *82* (6), 3096-3104.

46. Saito, M.; Sugiyama, K., Gangliosides of rat eye lens: A severe reduction in the content of C-series gangliosides following streptozotocin treatment. *Life Sciences* **2000,** *67* (15), 1891-1899.

Chapter 6: Conclusions

The work performed in this thesis focused on investigating the lipidome in each region of the human lens. Most of the lens lipid composition studies done to-date were based solely on whole lens homogenates or lenses split into cortical and nuclear regions only. In addition, most work has been completed on adult lenses, or lenses of a similar age. Deeley *et al.* observed changes to the lens DHSM distribution in the barrier region with age.[1] Moreover, Hughes *et al.* reported significant increases in DHCer and Cer concentration in the nucleus of the human lens after the age of 40.[2] Therefore, it is important that our study included all four regions of the lens, which develop at different stages across the lifespan and included lenses of different ages to observe any age-related changes. By applying MALDI-MS to human lens tissue sections and ESI-MS to lens lipid extracts, new insights into the distribution and composition of human lens lipids were revealed.

The aims of this thesis were to study the distribution and age-related changes of lipids in the different regions of the human lens. This involved:

i. Development and optimisation of MALDI imaging methods for the imaging of human lenses including tissue preparation and matrix application methods (Chapter 2)

ii. Study of the distribution of sphingolipids in the human lens by MALDI-MS (Chapter 3)

iii. Study of the distribution of phospholipids in the human lens by MALDI-MS (Chapter 4)

iv. Quantification of age-related changes in lipid composition in four different regions of the lens, i.e. the outer, barrier, inner and core by ESI-MS (Chapter 5)

In order to image human lens lipids, tissue preparation and matrix application methods were optimised and developed (Chapter 2). Previous studies involving the imaging of lipids in the human lens were limited,[1, 3, 4] as most of the studies were done on other animal lenses, which are larger in size than a human lens.[5-7] Furthermore, the lipid composition of the human lens is different to those of animals,[8] which may require a different tissue preparation technique. The lens is also a very delicate tissue and tends to disintegrate during the process of slicing and mounting.[6] Therefore, our study involved optimsing the mounting of tissue

onto a glass slide which plays a role in preserving the spatial resolution of the image. Although alternative landing techniques, such as ethanol-assisted soft landing were developed for the imaging of lens proteins,[9, 10] we have found that the soft landing of tissue directly on a glass slide and thaw-mounting the tissue with a finger pressed at the back of the glass slide to be the simplest and most effective way. For a tissue to undergo MALDI-MSI analysis, the application of a layer of homogenous matrix is essential. Previous MALDI-MSI studies of lens lipids have utilised ImagePrep™ or sublimation as the matrix application technique.[1, 3] However, our work to develop a matrix application by ImagePrep™ has shown that it is not suitable for lens lipid analysis as it requires matrices that are soluble in a limited range of organic solvents. Furthermore, the ImagePrep™ matrix application technique produces large crystals and does not form a homogeneous layer of matrix, resulting in poor spatial resolution. Sublimation was also tested as it requires a shorter preparation time (~15 mins) compared to the ImagePrep™ method (~90 mins) and produces a more homogeneous layer of crystals. Previous studies used CHCA[3] or DHB[1] as the matrix for lipid imaging but no GSLs were imaged. As the range of lipids we have imaged involved many GSLs in the higher mass range, we tested other matrices such as MBT and DAN in different ion modes in order to image the highest number of lipid species possible. This thesis demonstrated that sublimation is the best matrix application method for human lenses, with MBT and DAN being the most suitable matrices for lipid imaging in positive and negative ion modes, respectively.

This thesis utilised MALDI-MS to map the spatial distribution of recently identified sphingolipids in the adult human lens (Chapter 3). While numerous classes of SLs and GSLs have been identified in the human lens[11-16] an understanding of their distribution across the different regions of the lens is limited.[17] In this chapter, the distribution of many sphingolipids was revealed for the first time in the adult lens and we have observed that certain sphingolipids are only present in specific lens regions. For example, DHST and ST are only present in the cortex, not the nucleus, whilst DHLacCer, Cer and DHCer are found in the nucleus and are absent in the cortex. The different distribution of various sphingolipids in the adult human lens raises intriguing questions as to the role of these lipids within the human lens.

This thesis also determined the distribution of GPs in the adult human lens, including PA that was imaged for the first time in the adult human lens (Chapter 4). The majority of GPs such as PE, PS and PA were found to be mainly present around the cortex, except for LPE, which is present in the nucleus. Combining

these data with the previous chapter, we have now gained spatial information for most of the lipids identified to-date in the human lens.

Quantification of the lipids in different regions of the human lens was also undertaken in this thesis (Chapter 5). Previous quantification of lens lipids in the core region of human lens published by Hughes *et al.* only included GPs and four classes of SLs.[2] In our study, we have included the quantification of 15 classes of SLs and GSLs. Previous studies that have quantified human lens lipids were only performed on whole lenses, or lens nuclear and cortical regions.[2, 8, 18, 19] As the lens nucleus is synthesised before birth and has no lipid turnover,[20] its lipid composition can be very different from the cortex, particularly with the development of the barrier region around middle age.[21, 22] Our data from previous imaging experiments (Chapter 3 and 4) have also shown that lipids can have very different distributions in the lens, thus it is important to quantify lipids in each region of the lens. Our data has shown that the lipid composition in each region of the lens can vary. For example, the lens core and inner region have a higher percentage of SL in comparison to the barrier and outer regions, whereas GPs were most abundant in the outer region and lowest in concentration in the core. Many events occur around middle age (40-45) in the lens such as the formation of a barrier to the diffusion of antioxidants,[21, 22] an increase in lens stiffness and presbyopia,[23-25] a sudden increase in Cer and DHCer levels[2] and the increase of cation permeability[26]. Thus, it is also essential that age-related changes to the lens lipid composition be studied in detail across all regions of the lens. We have observed that some lipids like PA and DHLacCer did not show any age-related changes in all regions. For those that did, GP levels decreased with age while SL levels increased with age in all regions. The sudden increase in DHCer levels around the age of 40 also occurs in all regions. Another interesting finding is that the barrier has the most lipid classes that were altered in abundance with age.

The lens is a unique model for studying age-related changes in the human body as it contains both old and new fibre cells that were synthesised throughout a human's lifespan. This thesis showed that lens lipids were localised to specific regions of the lens. Each region was composed of a different lipid composition and it was shown that ageing can affect the abundance of lipids in the region. This is important, particularly as the unique composition of the lens lipid bilayer is vital in various homeostatic functions such as resisting oxidation[27] and regulating water permeability.[28] As the biosynthesis of fatty acids and cholesterol in the lens does not appear to change significantly throughout a human's lifespan,[29] our observation of the relative

increase in SL levels and the decrease of PL levels in the lens nucleus may be the consequence of non-enzymatic degradation. Our observations of lipid changes around middle age matches with previous identification of a key transition point where changes in lipid composition and also lens stiffness were observed.[20, 23] It was hypothesised by Borchman *et al.* that during one's lifespan, a threshold of lipid oxidation may be exceeded that causes a cascade of lipid and protein changes, leading to age-related nuclear cataract.[30]

The imaging and quantification studies done in this thesis are aimed to complement each other so that a thorough overview of changes in distribution and abundance of lipids with age can be investigated. Our results comparing the images obtained in Chapter 3 and 4 with the abundance data in Chapter 5 have shown that the results obtained with ESI-MS matched with the results obtained with MALDI-MSI. For example, DHSM showed an annular distribution around the nucleus region for a lens of 51-year old. Quantification studies also showed that DHSM has the highest abundance in the barrier region around the age of 51. However, there were limited samples used in the imaging studies, where only lenses older than the age of 40 were imaged. As mentioned, middle age is the key transition point for changes to occur in the lens, therefore, future work may aim to image lenses of different ages to see if their distribution changes matches with the results observed in Chapter 5. This thesis showed that MALDI-MSI may be used as a quick analysis tool to study the changes of lipids in the lens with age. Methods of obtaining absolute abundance of a lipid directly off a tissue slice without the need of lengthy extraction and quantification procedure may be developed in the future for more efficient analysis. As mentioned in Chapter 5, some gangliosides such as GD1a were not detected or quantified in this study. Therefore, more work is required to fully elucidate and quantify the GSLs in the lens. A previous study by Friedrich and Truscott found that with age, denatured crystallins interact with fibre cell membranes.[31] However, studies of this nature show the effect of increased protein on protein-lipid interaction instead of investigating the effect of increased lipid on protein-lipid interaction. It is unknown whether alterations in membrane lipids alters lens function, or if lipids are increased as a consequence of other ageing processes in the lens. The information of lens lipid alteration with age can be combined with the information of lens protein or other age-related lens studies to see if there is any link between the changes in lipid composition with other age-related changes in the lens. This may perhaps help to understand their role in the human lens and if they are involved in the enzymatic activities in the outer region of the lens, or play a role in anti-oxidation or anti-ageing in the lens nucleus.

6.1 References

1. Deeley, J. M.; Hankin, J. A.; Friedrich, M. G.; Murphy, R. C.; Truscott, R. J. W.; Mitchell, T. W.; Blanksby, S. J., Sphingolipid distribution changes with age in the human lens. *Journal of Lipid Research* **2010,** *51* (9), 2753-2760.

2. Hughes, J. R.; Deeley, J. M.; Blanksby, S. J.; Leisch, F.; Ellis, S. R.; Truscott, R. J. W.; Mitchell, T. W., Instability of the cellular lipidome with age. *AGE* **2012,** *34* (4), 935-947.

3. Pol, J.; Faltyskova, H.; Krasny, L.; Volny, M.; Vlacil, O.; Hajduch, M.; Lemr, K.; Havlicek, V., Age-related changes in the lateral lipid distribution in a human lens described by mass spectrometry imaging. *European Journal of Mass Spectrometry* **2015,** *21* (3), 297-303.

4. Ellis, S. R.; Wu, C.; Deeley, J. M.; Zhu, X.; Truscott, R. J. W.; Panhuis, M.; Cooks, R. G.; Mitchell, T. W.; Blanksby, S. J., Imaging of Human Lens Lipids by Desorption Electrospray Ionisation Mass Spectrometry. *Journal of American Society of Mass Spectrometry* **2010,** *21*, 2095-2104.

5. Pol, J.; Vidova, V.; Hyotylainen, T.; Volny, M.; Novak, P.; Strohalm, M.; Kostiainen, R.; Havlicek, V.; Wiedmer, S. K.; Holopainen, J. M., Spatial Distribution of Glycerophospholipids in the Ocular Lens. *Plos One* **2011,** *6* (4).

6. Vidová, V.; Pól, J.; Volný, M.; Novák, P.; Havlíček, V.; Wiedmer, S. K.; Holopainen, J. M., Visualizing spatial lipid distribution in porcine lens by MALDI imaging high-resolution mass spectrometry. *Journal of Lipid Research* **2010,** *51* (8), 2295-2302.

7. Le, C. H.; Han, J.; Borchers, C. H., Dithranol as a MALDI Matrix for Tissue Imaging of Lipids by Fourier Transform Ion Cyclotron Resonance Mass Spectrometry. *Analytical Chemistry* **2012,** *84* (19), 8391-8398.

8. Deeley, J. M.; Mitchell, T. W.; Xiaojia, W.; Korth, J.; Nealon, J. R.; Blanksby, S. J.; Truscott, R. J. W., Human lens lipids differ markedly from those of commonly used experimental animals. *Biochimica et Biophysica Acta* **2008,** *1781* (6-7), 288-298.

9. Han, J.; Schey, K. L., MALDI tissue Imaging of ocular lens alpha-crystallin. *Investigative Ophthalmology & Visual Science* **2006,** *47* (7), 2990-2996.

10. Grey, A. C.; Schey, K. L., Age-Related Changes in the Spatial Distribution of Human Lens alpha-Crystallin Products by MALDI Imaging Mass Spectrometry. *Investigative Ophthalmology & Visual Science* **2009,** *50* (9), 4319-4329.

11. Ariga, T.; Tao, R. V.; Lee, B. C.; Yamawaki, M.; Yoshino, H.; Scarsdale, N. J.; Kasama, T.; Kushi, Y.; Yu, R. K., Glycolipid composition of human cataractous lenses. Characterization of Lewisx glycolipids. *Journal of Biological Chemistry* **1994,** *269* (4), 2667-2675.

12. Ogiso, M.; Irie, A.; Kubo, H.; Komoto, M.; Matsuno, T.; Koide, Y.; Hoshi, M., Characterization of neutral glycosphingolipids in human cataractous lens. *Journal of Biological Chemistry* **1993,** *268* (18), 13242-13247.

13. Ogiso, M.; Komoto, M.; Okinaga, T.; Koyota, S.; Hoshi, M., Age-related changes in ganglioside composition in human lens. *Experimental Eye Research* **1995,** *60* (3), 317-323.

14. Ogiso, M.; Saito, N.; Sudo, K.; Kubo, H.; Hirano, S.; Komoto, M., Increase in lens gangliosides due to aging and cataract progression in human senile cataract. *Investigative Ophthalmology & Visual Science* **1990,** *31* (10), 2171-2179.

15. Ogiso, M.; Okinaga, T.; Ohta, M.; Komoto, M.; Hoshi, M., Identification and synthetic pathway of sialyl-Lewisx-containing neolacto-series gangliosides in lens tissues. l. Characterisation of gangliosides in human senile cataractous lens. *Biochimica et Biophysica Acta (BBA) - Lipids and Lipid Metabolism* **1995,** *1256* (2), 166-174.

16. Ogiso, M.; Shogomori, H.; Hoshi, M., Localization of Lewisx, sialyl-Lewisx and α-galactosyl epitopes on glycosphingolipids in lens tissues. *Glycobiology* **1998,** *8* (1), 95-105.

17. Seng, J. A.; Ellis, S. R.; Hughes, J. R.; Maccarone, A. T.; Truscott, R. J. W.; Blanksby, S. J.; Mitchell, T. W., Characterisation of sphingolipids in the human lens by thin layer chromatography–

desorption electrospray ionisation mass spectrometry. *Biochimica et Biophysica Acta (BBA) - Molecular and Cell Biology of Lipids* **2014,** *1841* (9), 1285-1291.

18. Borchman, D.; Byrdwell, W. C.; Yappert, M. C., Regional and age-dependent differences in the phospholipid composition of human lens membranes. *Investigative Ophthalmology & Visual Science* **1994,** *35* (11), 3938-3942.

19. Yappert, M. C.; Rujoi, M.; Borchman, D.; Vorobyov, I.; Estrada, R., Glycero- versus sphingo-phospholipids: correlations with human and non-human mammalian lens growth. *Experimental Eye Research* **2003,** *76* (6), 725-734.

20. Hughes, J. R.; Levchenko, V. A.; Blanksby, S. J.; Mitchell, T. W.; Williams, A.; Truscott, R. J. W., No turnover in lens lipids for the entire human lifespan. *eLife* **2015,** *4*, e06003.

21. Sweeney, M. H. J.; Truscott, R. J. W., An impediment to glutathione diffusion in older normal human lenses: a possible precondition for nuclear cataract. *Experimental Eye Research* **1998,** *67* (5), 587-595.

22. Moffat, B. A.; Landman, K. A.; Truscott, R. J. W.; Sweeney, M. H. J.; Pope, J. M., Age-related Changes in the Kinetics of Water Transport in Normal Human Lenses. *Experimental Eye Research* **1999,** *69* (6), 663-669.

23. Heys, K. R.; Cram, S. L.; Truscott, R. J., Massive increase in the stiffness of the human lens nucleus with age: the basis for presbyopia? *Molecular Vision* **2004,** *16* (10), 956-963.

24. Weale, R. A., Evolution, age and ocular focus. *Mechanisms of Ageing and Development* **1990,** *53* (1), 85-89.

25. Ostrin, L. A.; Glasser, A., Accommodation measurements in a prepresbyopic and presbyopic population. *Journal of Cataract & Refractive Surgery* **2004,** *30* (7), 1435-1444.

26. DUNCAN, G.; WORMSTONE, I. M.; DAVIES, P. D., The aging human lens: structure, growth, and physiological behaviour. *British Journal of Ophthalmology* **1997,** *81* (10), 818-823.

27. Borchman, D.; Yappert, M. C.; Afzal, M., Lens lipids and maximum lifespan. *Experimental Eye Research* **2004,** *79* (6), 761-768.

28. Tong, J.; Canty, J. T.; Briggs, M. M.; McIntosh, T. J., The water permeability of lens aquaporin-0 depends on its lipid bilayer environment. *Experimental Eye Research* **2013,** *113*, 32-40.

29. de Vries, A. C. J.; Vermeer, M. A.; Hendriks, A. L. A. M.; Bloemendal, H.; Cohen, L. H., Biosynthetic capacity of the human lens upon aging. *Experimental Eye Research* **1991,** *53* (4), 519-524.

30. Borchman, D.; Yappert, M. C., Lipids and the ocular lens. *Journal of Lipid Research* **2010,** *51* (9), 2473-2488.

31. Michael G. Friedrich, Roger J. W. Truscott; Membrane Association of Proteins in the Aging Human Lens: Profound Changes Take Place in the Fifth Decade of Life. Invest. Ophthalmol. Vis. Sci. 2009;50(10):4786-4793. doi: 10.1167/iovs.09-3588.